INSTITUTO POTOSINO DE INVESTIGACIÓN CIENTÍFICA Y TECNOLÓGICA, A.C.

POSGRADO EN NANOCIENCIAS Y MATERIALES

"Growth of *Trichoderma atroviride* and importance of the nano-motor Kinesin-1 in its development"

Tesis que presenta

Gamaliel Sánchez Orellana

Para obtener el grado de

Doctor en Nanociencias y Materiales

Director de la Tesis:

Dr. Braulio Gutiérrez Medina

San Luis Potosí, S.L.P., Febrero del 2019

IPICYT

Constancia de aprobación de la tesis

La tesis ***"Growth of Trichoderma atroviride and importance of the nano-motor Kinesin-1 in its development"*** presentada para obtener el Grado de Doctor en Nanociencias y Materiales fue elaborada por **Gamaliel Sánchez Orellana** y aprobada el **primero de marzo de dos mil diecinueve** por los suscritos, designados por el Colegio de Profesores de la División de Materiales Avanzados del Instituto Potosino de Investigación Científica y Tecnológica, A.C.

Dr. Braulio Gutiérrez Medina
Director de la tesis

Dra. Olga Araceli Patrón Soberano
Miembro del Comité Tutoral

Dr. Miguel Avalos Borja
Miembro del Comité Tutoral

Dra. Meritxell Riquelme Pérez
Miembro del Comité Tutoral

Créditos Institucionales

Esta tesis fue elaborada en el Laboratorio de Biofísica de la División de Materiales Avanzados del Instituto Potosino de Investigación Científica y Tecnológica, A.C, bajo la dirección del Dr. Braulio Gutiérrez Medina y en el laboratorio de Genómica Funcional y Comparativa del Dr. J. Sergio Casas Flores.

Durante la realización del trabajo el autor recibió una beca académica del Consejo Nacional de Ciencia y Tecnología (No. de registro 346135) y del Instituto Potosino de Investigación Científica y Tecnológica, A. C. Así como también una beca proporcionada por el proyecto CONACYT-Fronteras de la Ciencia (Clave: 1144).

Instituto Potosino de Investigación Científica y Tecnológica, A.C.

Acta de Examen de Grado

El Secretario Académico del Instituto Potosino de Investigación Científica y Tecnológica, A.C., certifica que en el Acta 010 del Libro Primero de Actas de Exámenes de Grado del Programa de Doctorado en Nanociencias y Materiales está asentado lo siguiente:

En la ciudad de San Luis Potosí a los 1 días del mes de marzo del año 2019, se reunió a las 12:10 horas en las instalaciones del Instituto Potosino de Investigación Científica y Tecnológica, A.C., el Jurado integrado por:

Dr. Miguel Avalos Borja	**Presidente**	**IPICYT**
Dra. Olga Araceli Patrón Soberano	**Secretaria**	**IPICYT**
Dr. Braulio Gutiérrez Medina	**Sinodal**	**IPICYT**
Dra. Meritxell Riquelme Pérez	**Sinodal externo**	**CICESE**

a fin de efectuar el examen, que para obtener el Grado de:

DOCTOR EN NANOCIENCIAS Y MATERIALES

sustentó el C.

Gamaliel Sánchez Orellana

sobre la Tesis intitulada:

Growth of Trichoderma atroviride and importance of the nano-motor Kinesin-1 in its development

que se desarrolló bajo la dirección de

Dr. Braulio Gutiérrez Medina

El Jurado, después de deliberar, determinó

APROBARLO

Dándose por terminado el acto a las 13:42 horas, procediendo a la firma del Acta los integrantes del Jurado. Dando fe el Secretario Académico del Instituto.

A petición del interesado y para los fines que al mismo convengan, se extiende el presente documento en la ciudad de San Luis Potosí, S.L.P., México, a los 1 días del mes de marzo de 2019.

Dr. Horacio Flores Zúñiga
Secretario Académico

Mtra. Ivonne Lizette Cuevas Vélez
Jefa del Departamento del Posgrado

Dedicated to my parents,
Bertha Alicia Orellana & Pedro Luis Sánchez

Acknowledgements

Thank to all the friends and family that supported me throughout all these years. Thanks to my advisor for his support and teachings. Also, thanks to all my tutorial committee for their teachings.

Thanks to IPICyT for allowing me to be part of this great community.

Table of Contents

Chapter 3. Kinesin-1 on *Trichoderma atroviride* growth

Chapter 4. Final Comments

List of Figures

Appendixes

List of abbreviations

BFM	Bright Field Microscopy
MT	Micro-Tubules
WT	Wild Type
PDA	Potato Dextrose Agar
LED	Light Emitting Diode
2D	Two Dimensional
3D	Three Dimensional
Px	Pixel
ROI	Region Of Interest
CCD	Charge-Coupled Device
L_p	Persistence Length
PCR	Polymerase Chain Reaction
bp	base pair

Abstract

The vegetative growth of filamentous fungi comprises cell elongation and branching. This complex process involves Intracellular transport of molecules, vesicles and organelles within the cell interior, assisted by motor proteins, which, under the study of Nanosciences, are considered the smallest motors. Here, the growth process of *Trichoderma atroviride* was studied. First, a novel tool for automated tracking of growth in fungal cells (called hyphae) is introduced. This tool allows performing quantitative analysis of growth rate and morphology. An image-processing routine that detects in real-time the tip of a hypha and tracks it as the hypha elongates was developed. Tracking records allowed to determine that *T. atroviride* hyphae grow with characteristic elongation rates of ~ 0.07 μm/s. Prior to the occurrence of an apical branching event the parental hypha stopped growing during a few minutes. From tracking data, it was found that the persistence length (a measure of filament extension before presenting a change in direction) associated to *T. atroviride* hyphae is 362 μm. Second, the absence of Kinesin-1, one of the main nano-motors transporters of essential growth vesicles (reported for other filamentous fungi), and how it affects hyphal elongation, branching and morphology of *T. atroviride* was studied. By developing a Kinesin-1 deletion mutant strain it was shown that *T. atroviride* elongation rate drops up to ~ 60%, while branching highly increases. Several experiments following *T. atroviride* growth stages were carried out (germination, vegetative growth and conidiation) and determined that: The absence of Kinesin-1 modifies *T. atroviride* germination resulting in delayed conidia germination times. Also, about 50% of conidia presented bipolar germination. Vegetative growth was highly reduced with characteristic elongation rates of ~ 0.03 μm/s. Conidiation was also reduced in ΔKinesin-1 producing ~$30x10^8$ conidia vs ~$8x10^8$ WT. Altogether, these preliminary results show how integration of image analysis and computer control enable quantitative microscopic observations of fungal hyphae dynamics and how the absence of the nano-motor protein Kinesin-1 results in severe modifications of hyphal elongation, branching, conidiation and morphology.

Resumen

El crecimiento vegetativo de los hongos filamentosos se define por el alargamiento y la ramificación celular. Este crecimiento es un proceso complejo que involucra el transporte intracelular de moléculas, vesículas y organelos, mediado principalmente por nano-motores. En este proyecto, se estudió el proceso de crecimiento de *Trichoderma atroviride* en dos aspectos principales: Primero, se presenta una herramienta para el seguimiento automático del crecimiento de células de hongos filamentosos (llamadas hifas) para realizar un análisis cuantitativo de la tasa de crecimiento y aspectos de su morfología. Se desarrolló una rutina de procesamiento de imágenes que detecta en tiempo real la punta de una hifa y la rastrea a medida que la hifa se alarga. Los registros de seguimiento permitieron determinar que las hifas de *T. atroviride* crecen con tasas de elongación características de ~ 0.07 µm / s. Se encontró que antes de que ocurriera un evento de ramificación apical, la hifa parental detiene su crecimiento durante unos minutos. Finalmente, se determinó que la longitud de persistencia (una medida de la extensión del filamento antes de presentar un cambio en la dirección) asociada a las hifas de *T. atroviride* es de 362 µm. Segundo, se estudió que la ausencia de la Cinesina-1, uno de los principales nano-motores transportadores de vesículas de crecimiento esenciales (reportados para otros hongos filamentosos), afecta la elongación de las hifas, la ramificación y la morfología de *T. atroviride*. Al desarrollar en el laboratorio una cepa mutante ΔCinesina-1, se observó que la tasa de elongación de *T. atroviride* disminuye hasta en un 60%, mientras que la ramificación aumenta considerablemente. Se llevaron a cabo varios experimentos morfológicos siguiendo las etapas de crecimiento de *T. atroviride* (germinación, crecimiento vegetativo y conidiación) y se encontró que: la ausencia de la Cinesina-1 afectó la germinación de *T. atroviride* dando como resultado que el ~ 50% de los conidios presentan germinación bipolar. El crecimiento vegetativo se vió altamente disminuido con tasas de elongación características de ~ 0.03 µm/s. El proceso de conidiación también se vió

afectado en la cepa ΔCinesina-1 produciendo ~ $30x10^8$ conidias vs ~ $8x10^8$ en la cepa silvestre. En conjunto, estos resultados preliminares muestran cómo la integración del análisis de imágenes y el control por computadora permiten realizar observaciones microscópicas cuantitativas de la dinámica de las hifas de los hongos y cómo la ausencia de la proteína nano-motora Cinesina-1 produce modificaciones en la elongación de hifas, la ramificación, la conidiación y la morfología.

Chapter 1. Introduction

The growth of filamentous fungi is more complex than that of unicellular bacteria and yeasts. The basic vegetative structure of growth consists of a tubular filament known as hypha that originates from the germination of a single reproductive spore (conidia). Spore germination is an essential stage in the development of filamentous fungi. It is divided into two main stages: 1) Activation of a resting spore in response to environmental conditions and 2) Swelling growth characterized by the absorbance of water and activation of fungal metabolism, followed by the emergence of a germ tube (d'Enfert 1997).

After spore germination there is a vegetative growth phase defined by an initial phase of discontinuous tip production, then followed by a phase of 'continuous' tip production (Trinci, n.d.). Vegetative growth involves two components, an increase in volume which results from tip extension and an increase in protoplasmic contents. These involve a complex interaction of biosynthesis of macromolecules and their subsequent organisation into physical structures. The latter aspect of growth occurs over long distances within an individual hypha. As the hypha continues to grow, it frequently branches repeatedly to form a mass of hyphal filaments referred to as a mycelium (Peberdy 1980).

Under appropriate conditions, the vegetative mycelium gives rise to a reproductive mycelium that supports the production of reproductive spores. This process involves specialized cellular differentiation, regulation of gene expression, and cellular communication. Asexual conidiospores (conidia), are formed from the apex of conidiogenous cells (phialides) through mitosis followed by repeated asymmetric division (Park and Yu 2012).

A fungal hypha may be up to several hundred microns long and is typically 3-10 μm in diameter (Oliver and Trinci 1985). Its characteristic type of growth enables the organism to expand while maintaining a constant surface to volume ratio, making fungi well adapted to colonization of solid substrates.

In order to sustain continuous hyphal elongation and branching, filamentous fungi rely on a complex transport mechanism of molecules, organelles and vesicles carried out mainly by nano-motors interacting with the cell cytoskeleton. The cytoskeleton (a highly dynamic three-dimensional network) consists of actin filaments, intermediate filaments (not present in filamentous fungi) and microtubules (MTs), as well as accessory associated proteins. Actin filaments and MTs are tracks by which nano-molecular motors transport organelles and molecular cargoes to specific cellular areas (Fletcher and Mullins 2010; Mostowy and Cossart 2012). MTs are formed by two types of 50 kDa homologous subunits, α and β-tubulin, which are assembled in a helical structure, where both types of tubulins alternate to form the wall of a hollow cylinder (Desai and Mitchison 1997), as shown in Fig 1. A typical MT consists of thirteen protofilaments that are parallel to the longitudinal axis. The diameter of a MT is ~ 25 nm.

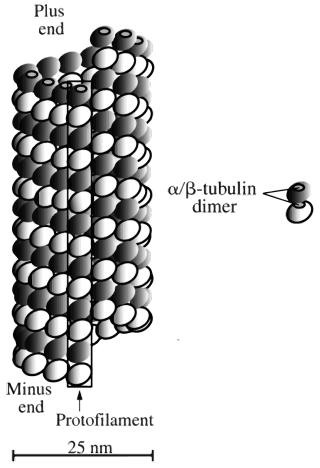

Figure 1. Schematic representation of the helical structure of a MT. α and β-tubulin are assembled in a helical structure, where both types alternate to form the wall of the MT.

There are three types of nano-motors that carry out directed transport of cargoes: Kinesin, dynein and myosin. Both Kinesin and dynein move on MTs, while myosin depends on actin filaments. Within the Kinesin family, Kinesin-1 is the most widely studied. Kinesin-1 participates in intracellular transport, moving on MTs in unidirectional and anterograde (ie towards the plus end of the MTs), so Kinesin-1 usually carries cargoes from the central region towards the periphery of the cell (Ronald D. Vale 2003).

To understand fungal growth, quantitative evaluation of growth dynamics becomes an important aspect of fungal characterization (Samapundo et al. 2007). It is very important to understand how nano-motors perform cargo transport towards understanding fungal growth.

Herein I present the two main results product of my research conducted under the Nanoscience and Materials Doctoral program at IPICyT. First, to asses fungal development, a novel tool for automated tracking of growth in hyphae of the filamentous fungus *Trichoderma atroviride* to perform quantitative analysis of growth rate and morphology was introduced, the latter is presented on Chapter 2. Second, in Chapter 3, the development of a ΔKinesin-1 mutant strain of *T. atroviride* and the study on how the absence of one of the main nano-motors transporter of vesicles (M. Schuster et al. 2012), Kinesin-1, affects hyphal elongation, branching and morphology is presented. several experiments following *T. atroviride* growth stages (germination, vegetative growth and conidiation) were carried out. In each chapter a proper introduction and a summary of results are presented.

Chapter 2. Automated, continuous video microscopy tracking of hyphal growth

2.1 Growth Characteristics of Filamentous Fungi

Filamentous fungi grow as branched filaments termed *hyphae* (sing., hypha), which are collectively called *mycelia* (sing., mycelium). It includes almost the entire fungal kingdom and is used in contradistinction to 'yeasts', which are essentially unicellular fungi with vegetative cells capable of repeated budding. Filamentous fungi are composed mainly of a haploid vegetative part that usually has no coloration and is composed of hyphae.

2.1.1 The fungus *Trichoderma atroviride*

Trichoderma spp. are mainly asexual fungi that are present in all types of agricultural soils and also in decaying wood. The antagonistic activity of *Trichoderma* species showed that it is mycoparasitic on many soil-borne and foliage pathogens. The fungus is also a decomposer of cellulosic waste materials. Recent discoveries show that the fungus not only acts as a biocontrol agent, but also stimulates plant resistance, plant growth and development resulting in an increase in crop production. The biocontrol activity involving mycoparasitism, antibiotics and competition for nutrients, also induces defense responses or systemic resistance responses in plants (CHET and I 1987).

Trichoderma atroviride is used as a photomorphogenetic model due to its ability to conidiate upon exposure to light. In total darkness, *T. atroviride* grows indefinitely as a mycelium provided that nutrients are not limiting. However,

nutrient deprivation and light trigger the development of specialized asexual reproductive structures (conidia). A brief pulse of blue light (400–480 nm) given to a radially growing colony in a Petri dish induces synchronous sporulation. A ring of conidiophores bearing green conidia is produced at what had been the colony perimeter at the time of the light pulse (Casas-Flores et al. 2004).

2.2 Bright Field Microscopy

A Bright field microscope (BFM) is an optical instrument that uses visible light to produce a magnified image of an object (or specimen) that is projected onto the retina of the eye or onto an imaging device. Also called a *compound light microscope*, the word *compound* refers to the fact that two lenses, the objective lens and the eyepiece (or ocular), work together to produce the final magnification of the image.

Figure 2 shows how an image becomes magnified and is perceived by the eye. The figure also points out the locations of important focal planes in relation to the objective lens, the ocular, and the eye. The specimen on the microscope stage is examined by the objective lens, which produces a magnified real image of the object in the image plane of the ocular. When looking in the microscope, the ocular acting together with the eye's cornea and lens projects a second real image onto the retina, where it is perceived and interpreted by the brain as a magnified virtual image about 25 cm in front of the eye.

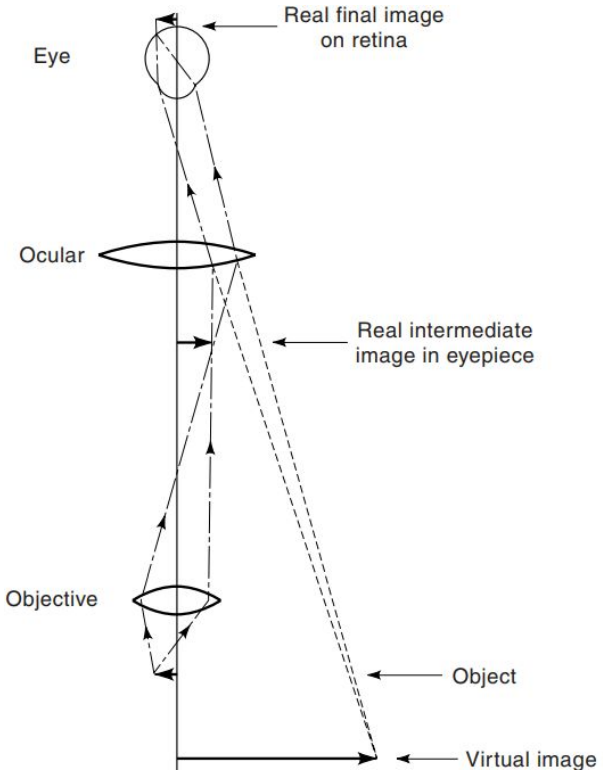

Figure 2. Perception of a magnified virtual image of a specimen in the microscope. The objective lens forms a magnified image of the object (called the real intermediate image) in or near the eyepiece; the intermediate image is examined by the eyepiece and eye, which together form a real image on the retina. Because of the perspective, the retina and brain interpret the scene as a magnified virtual image about 25 cm in front of the eye.

Two microscope components are of critical importance in forming the image: (1) the objective lens, which collects light diffracted by the specimen and forms a magnified real image at the real intermediate image plane near the eyepieces or oculars, and (2) the condenser lens, which focuses light from the illuminator onto a small area of the specimen. The arrangement of these and other components is shown in Figure 3. Other components include the tube and eyepieces, the lamp collector and lamp socket and its cord, filters, polarizers, retarders, and the microscope stage and stand with coarse and fine focus dials. It is of our interest to study specific growth characteristics of the filamentous fungi *T. atroviride*.

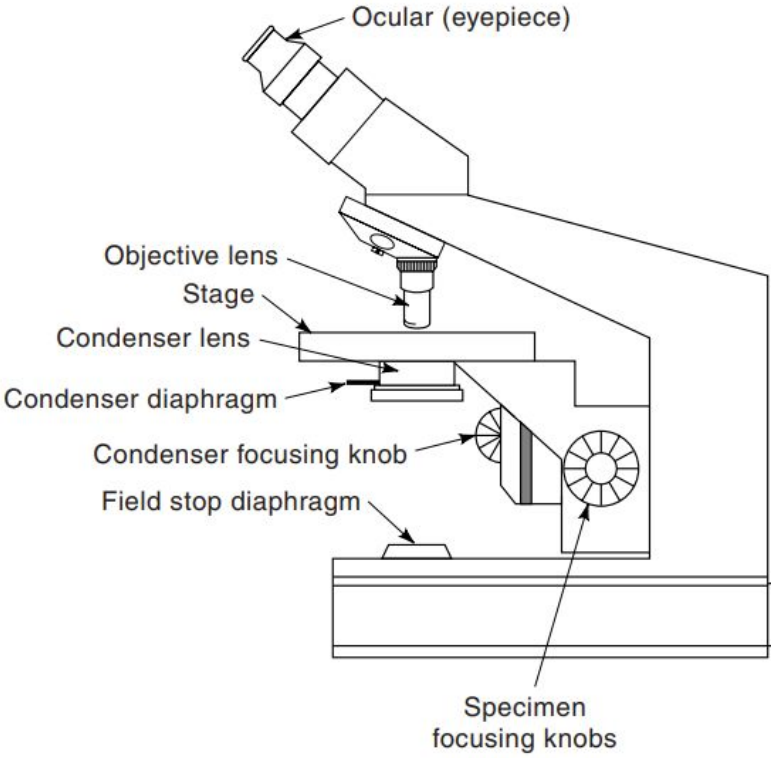

Figure 3. A Bright field microscope. Note the locations of the specimen focus dials, the condenser focus dial, and the focus dial of the collector lens on the lamp housing. Also note the positions of two variable iris diaphragms: the field stop diaphragm near the illuminator, and the condenser diaphragm at the front aperture of the condenser.

2.2.1 Previous studies on filamentous fungi growth

Morphology at the hypha level can be studied using light microscopy, often yielding only qualitative information. To obtain quantitative information in these experiments, labor intensive and sometimes subjective analysis is required by the observer (Paul and Thomas 1998). The introduction of digital image analysis 30 years ago allowed automated studies of fungal morphology (Packer and Thomas 1990), with focus on specific morphological parameters like the number of hyphal tips and branching points in hyphae (Paul and Thomas 1998). Using digital methods, first attempts for real-time quantification of fungal morphology were made either by circulating culture medium in a flow-through

cell (Spohr et al. 1998) or by growing single hyphae onto coverslips (using poly-D-lysine for attachment) and imaging, with acquisition rates of 1 frame every 10 min (Christiansen, Spohr, and Nielsen 1999). These studies typically involved a limited number of pre-selected microscopic images of hyphae and image acquisition was mainly done by an operator (Diano et al. 2009; Lim et al. 2006; Ahamed and Vermette 2009; El-Sabbagh, Harvey, and McNeil 2008; Lübbehüsen, Nielsen, and Mcintyre 2003).

Although different computational workflows have shown to reduce the requirement for manual intervention of an operator during morphological analysis of sequentially recorded microscopic images (Kossen 2000; Barry 2010; Lecault, Patel, and Thibault 2007; Brunk et al. 2018), there is still a pressing need for an integrated approach covering fully automated image acquisition and analysis. To achieve automated tracking of hyphal growth by video microscopy one technical problem must be solved: to keep the hypha under study in focus and within the microscope field of view—over periods of time that may reach several hours.

Here, it is shown that with the combination of computer-controlled bright field microscopy and digital image processing it is possible to achieve time-resolved quantification of growth of individual fungal hyphae. The developed tool is applied to record growth in the filamentous fungus *T. atroviride*, detecting in real-time a single growing hypha element and following it over several hours without manual intervention. The position coordinates of hyphal tips allow us to quantify growth rate and persistence length. Remarkably, it was found that *T. atroviride* stalls prior to apical (and occasionally subapical) branching.

2.3 Microscopy Setup for our study

A student-grade bright field microscope (Amscope, T370B-3M) was modified to enable computer control (Fig. 4). A microscope stage was automated with the use of stepper motors (See 2.3.2 Stage automation). A CCD USB Camera

(Sentech STC-TB33USB-B 640×480 pixel resolution) is mounted on the trinocular port of the microscope and connected to the computer. Objectives used: 10x and 40x magnifications, with a pixel-to-microns conversion factor of 1 px = 1.49 μm and 1 px = 0.37 μm, respectively. The entire microscope system is placed in temperature-controlled room (28 °C).

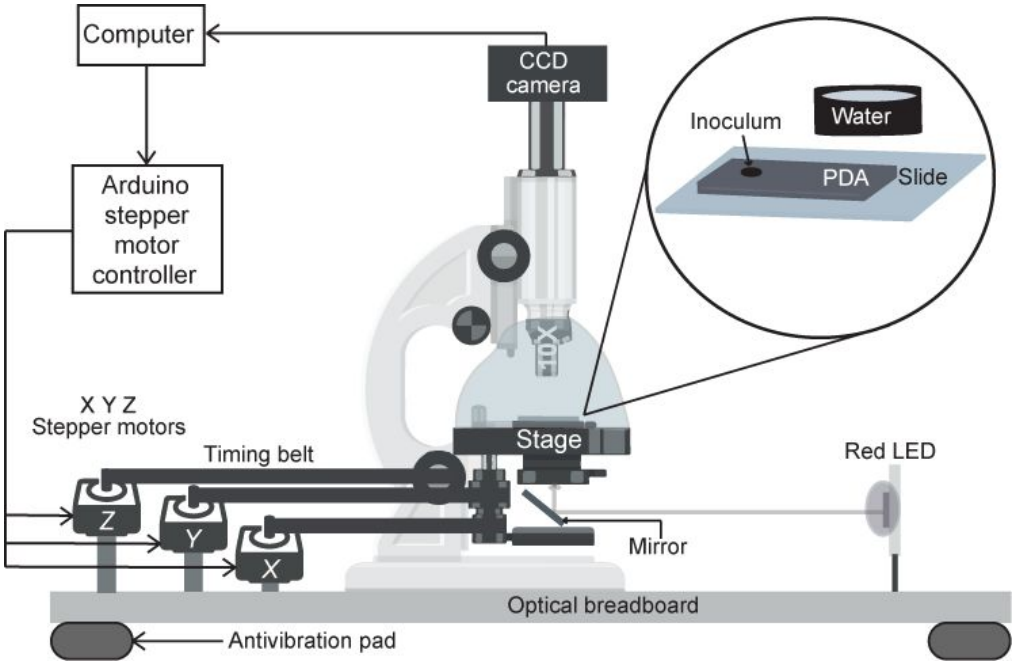

Figure 4. Microscopy setup and sample arrangement. The system is mounted on an optical breadboard with cushion pads to help minimize mechanical noise. To mount the sample (inset) a PDA plug is placed onto a microscope slide and inoculated with the filamentous fungi conidia. Water contained in small caps provides humidity to the sample. The stage and nosepiece of the microscope are covered with packing film plastic to avoid the sample to dry. The stepper motors transmit movement to the X-Y-Z axis knobs of the stage through timing belts. Sample illumination is provided by a red LED. A CCD camera captures images and feeds a computer, which executes the automated tracking routine and controls stepper motor motions (via the Arduino interface).

2.3.1 Illumination Setup

To control lighting sample conditions, the microscope original white light bulb was replaced for a red (peak wavelength, λ = 625 nm) Light Emitting Diode (Luxeon Tristar).

2.3.2 Stage Automation

To allow three-dimensional (3D) X-Y-Z sample manipulation, a NEMA-17 (200 steps per revolution) stepper motor was attached to each axis knob of the microscope stage (Fig. 5). The stepper motors transfer movement to the microscope knobs with the use of timing belts (available at www.adafruit.com, Product ID: 1184). The stepper motors are controlled by two Adafruit's v2 motor shield controllers, each connected to an Arduino UNO SMD board (Product ID: 1438). The X,Y motors are controlled by the same motor shield whereas the Z motor is controlled by the second motor shield. The Arduino boards are connected to a computer by USB ports. The software LabView (National Instruments) is used for stepper motor control.

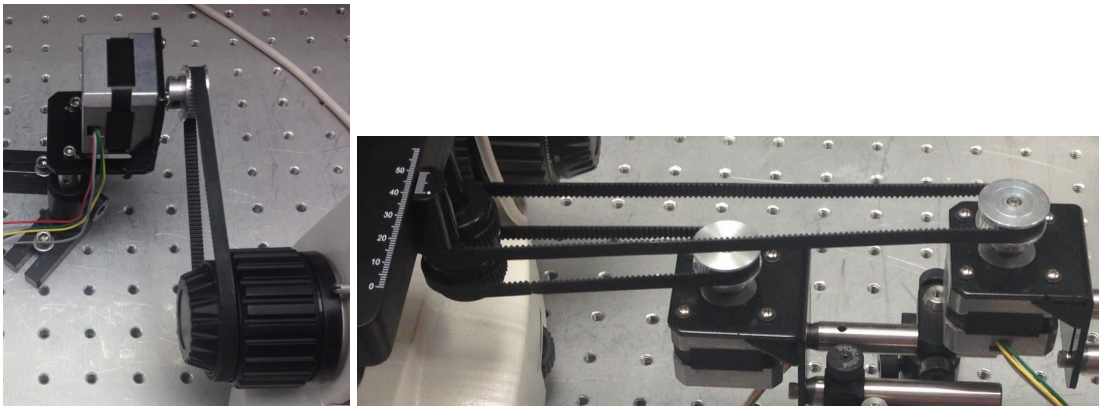

Figure 5. X and Z motors adapted to the stage. The configuration used for the connection between the X and Z motors with their respective axes in the microscope stage is shown. These motors can be moved independently of each other by means of the automatic control of the computer

2.4 Organism and sample preparation

The *Trichoderma atroviride* wild-type strain (IMI 206040) is used for the study. Conidia of *T. atroviride* were collected after 7-10 days of fungal growth on Petri dish with Potato Dextrose Agar (PDA, Difco) medium. Collection was made by adding 1 mL of sterile distilled water to the colony, then a glass handle was used to scrape *T. atroviride* in order to release conidia. Finally, conidia were

collected on a 1.5 mL Eppendorf tube. Dilutions were made to obtain a concentration of ~10 conidia/µL. Then, 1 µL of conidia dilution was inoculated on PDA plugs placed on a microscope slide. After 15 h incubation at 28 °C conidia were taken to the microscope for measurements (Fig. 6).

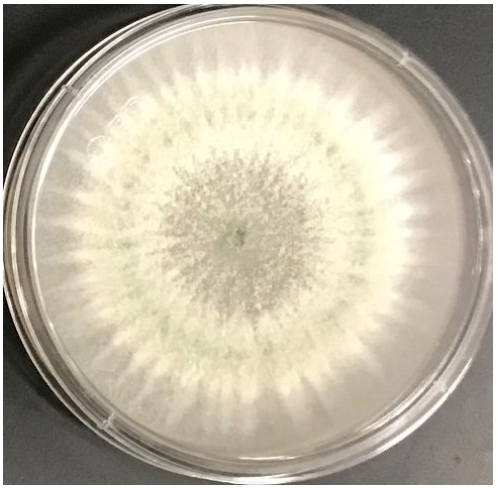

Figure 6. Petri dish with Wild Type strain of *T. atroviride* growing on darkness for 72 h. PDA growth medium.

2.5 Image processing and tracking algorithm development

Figure 7 shows the followed workflow diagram to perform tracking of a single hypha, details on each process are explained and shown with detail in the following paragraphs.

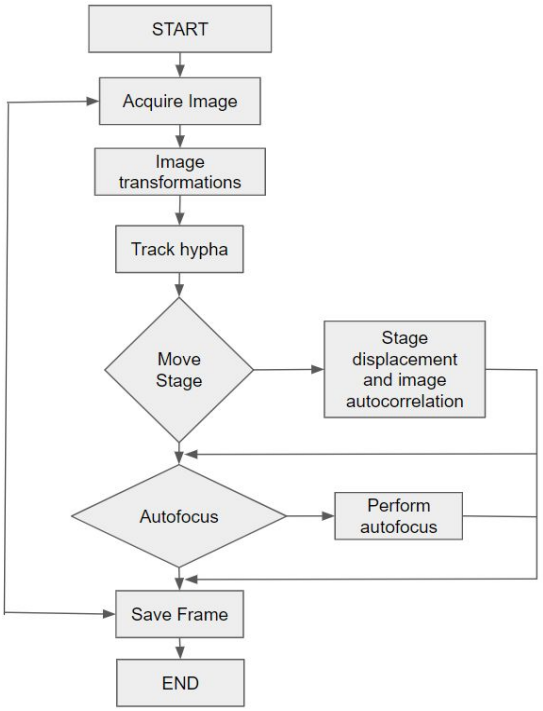

Figure 7. General workflow followed by the developed system to perform track of a single hypha. The system starts with the acquisition of an image, followed by image transformations to clean noise on the image and to segment the hypha from the background. The system determines if the hypha is near to be out-of-bounds and the stage must be displaced and performs an autofocus routine to keep the sample in focus.

Once the sample is placed on the microscope stage, image acquisition is started and a Region Of Interest (ROI) is manually set around the hyphal tip to be tracked by the system (Fig. 8A). After this point, the system is fully automated and no further user intervention is required. A set of image transformations (described below) are applied to the ROI to determine the (x,y) coordinates of the hyphal tip, allowing tracking of apical growth as the hypha develops.

Starting from a bright field image, the system performs image segmentation (i.e. separation of object and background) by applying the following elemental transformations: (i) Threshold, producing a binary image (Fig. 8B), (ii) Erode, that eliminates isolated background pixels (Fig. 8C), (iii) Skeletonize, where pixels are removed from the edges of the binary structure until an object skeleton is left at one pixel wide (Fig. 8D). Once the skeletonized image of the

hyphal tip has been obtained, a search is performed (left-to-right and top-to-bottom) until the first non-zero pixel value is found (Fig. 8E). This routine therefore follows a hypha growing from right to left in the field of view. In every frame recorded, the system stores the found (x,y) coordinates of the detected hyphal tip and builds a new ROI around these coordinates to be passed to the next image. In this manner the ROI will always be centered at the last stored coordinate. These series of steps are iterated every 1.3 s, which is the sampling time interval of the developed system. In addition, video frames are stored every 10th data point, providing a record in video of the tracked hyphal growth (Fig. 8F). The above image processing procedure was followed for 10x and 40x magnification (with the exception of the Skeletonize operation at 40x).

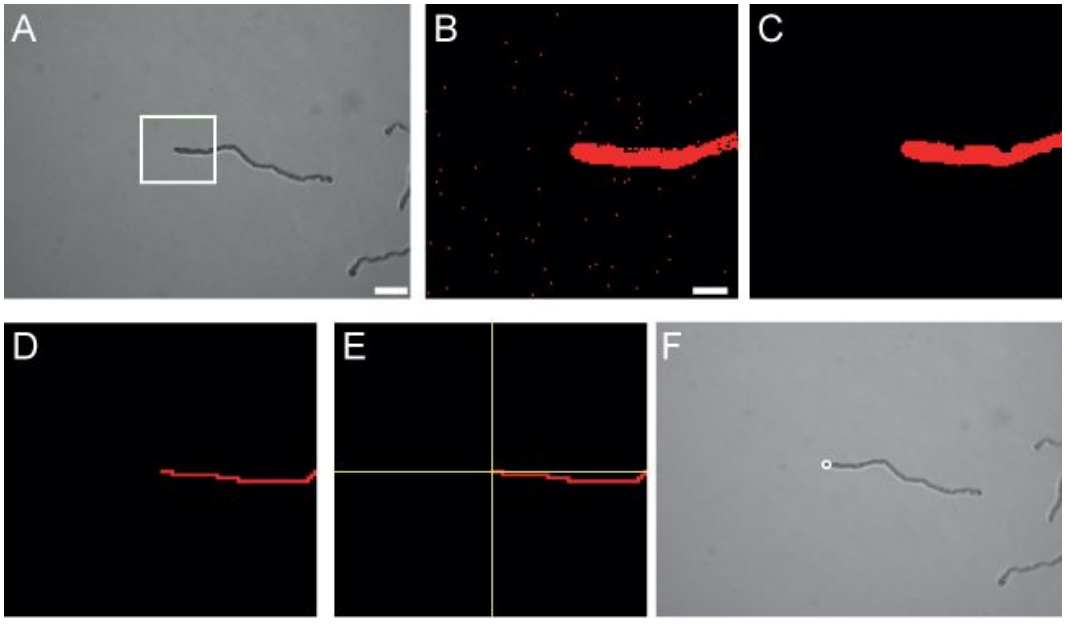

Figure 8. Finding the hyphal tip using digital image processing. (A) A region of interest (ROI, white rectangle) is selected. Scale bar, 20 μm. (B) The resulting image of the ROI after a threshold operation; most of the background is removed. Scale bar, 10 μm. (C) Isolated noise pixels in the background and hyphal surroundings are removed using an erode operation. (D) After a skeleton operation is applied, leaving a structure only one pixel wide. (E) The system searches from left-to-right and top-to-bottom for the first non-zero pixel value and marks that pixel as the position of the hyphal tip (yellow cross). (F) The system stores (x,y) position coordinates of the hyphal tip (white circle) and an image every 10th data point.

As the hypha grows it reaches the boundaries of the microscope visual field. These events are detected by comparing the x or y coordinate with predetermined lower (or higher) limit values (typically a 50-pixel boundaries form the upper, bottom and left frame edges are established). Once an off-limits event is detected the microscope stage is displaced using the X or Y stepper motors by a predetermined number of steps so that the tip of the hypha of interest is brought back well within the boundaries of the field of view. To maintain tracking of the same hypha, a cross-correlation operation is performed between the last image recorded prior to stage motion (template image) and the first image after the stage has been moved (actual image). In image correlation, the template image is overlaid to the actual image and displaced in two dimensions (2D), one pixel at a time. At every pixel step the displaced template and the actual image are multiplied, and the sum of all pixel counts of the product image is computed. This operation defines a new pixel map where the maximum count corresponds to the position where the displaced template most resembles the actual image. Accordingly, the maximum of the resulting correlation image is identified and the corresponding (x,y) coordinates are set as the current position of the hyphal tip (Fig. 9B). This procedure enables continuity in the tracking of a given hypha (Fig. 9A and 9C). Image processing is performed using the LabView IMAQ Vision module. Image correlation is performed using the Vision function IMAQ-Correlate.

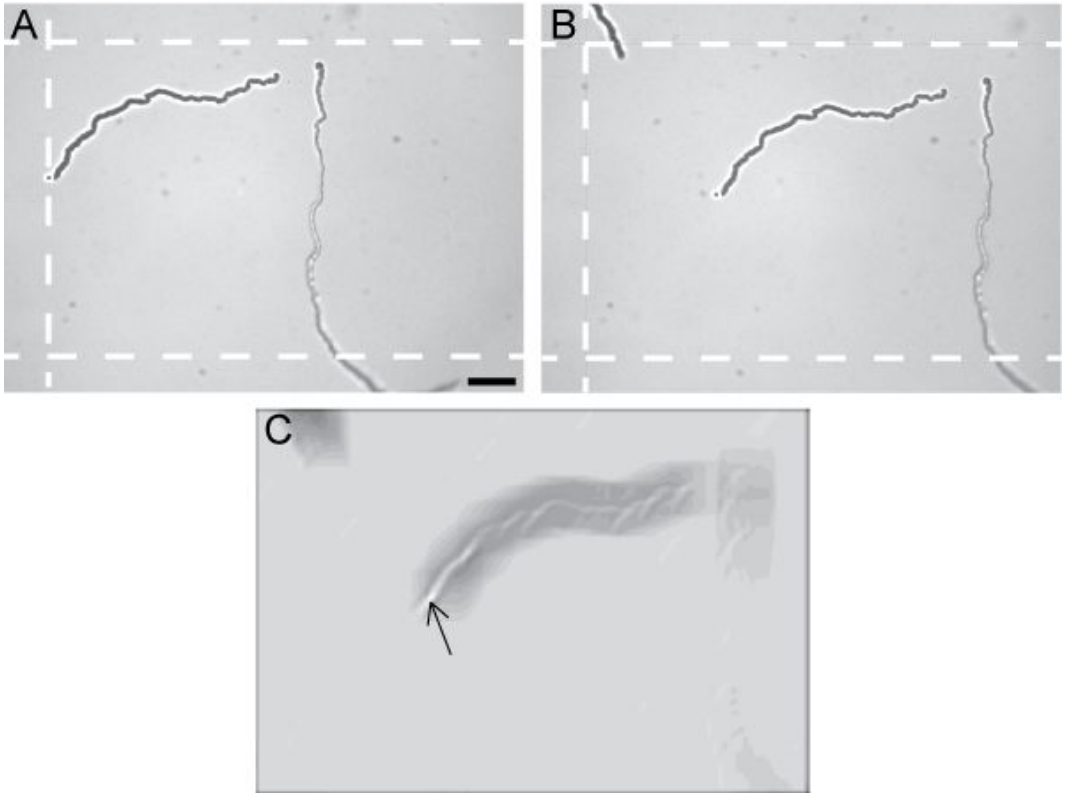

Figure 9. Stage motion and image correlation maintain continuity of hyphal tracking.(A) The tracked hyphal tip (with a white circle drawn over) reaches visual limits (dashed white lines). Scale bar, 20 μm. When the system detects such an event it displaces the stage. (B) The tracked hypha is brought back to the field of view. (C) Result of the image correlation process of images shown in (A) and (B). The pixel with the highest intensity value (black arrow) signals the position of maximum correlation and enables to determine the new hyphal tip (x,y) coordinates.

2.6 Microscope focus drift correction

Although the microscope system is in a temperature-regulated room, residual drift in the microscope focus was present (Fig. 10A). The sample is kept focused in an automated manner, using the known property of bright-field microscopy that the image of an unstained object changes from bright to dark as it is defocused. First, the Z-axis stepper motor displaces the microscope stage several steps from its actual position. Next, the stage is moved stepwise back to its original position while images of the defocused hypha are taken

every motor step, producing a z-image stack. Using the previously determined binary image corresponding to the hypha of interest (Fig. 10B) a mask is applied on every image of the stack to obtain the gray-value pixel intensity limited to the area of the hypha (Fig. 10C). Then, the gray-value pixel intensity values are summed over the whole image for every image and displayed as a function of the Z-motor step position. The resulting plot (Fig. 10D) allow to identify a reference point with good image contrast (darkened hyphae images over a bright background). Finally, the stage is moved to the reference position, bringing the hypha back to the amount of defocus that optimizes tracking (Fig. 10E). For 40x magnification this procedure was omitted, and drift correction was achieved by displacing the Z-motor at a constant rate of one step every 50 sampling cycles.

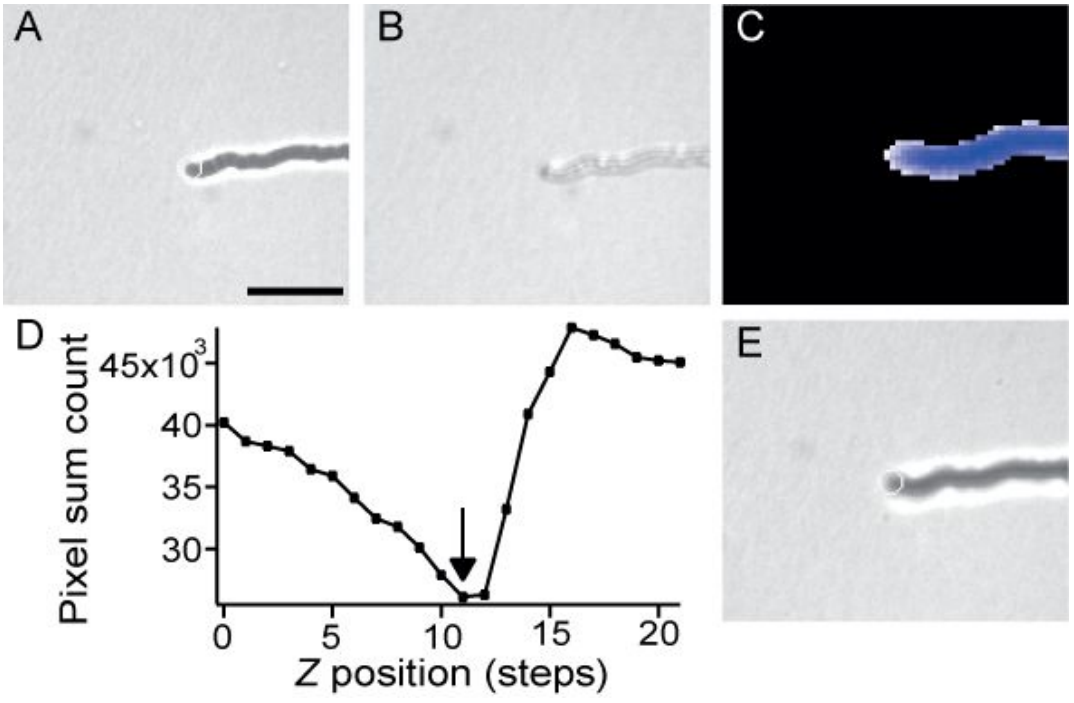

Figure 10. Microscope drift correction. (A) A hypha is observed under an amount of defocus appropriate for tracking. (B) The same hypha after increased defocus with respect to (A), unsuitable for tracking. (C) An image of the hypha after application of a mask that sets background pixels zero. (D) The sum of the pixel intensities of images such as (C) are computed for various Z-stage positions. A Z-position is selected to maximize image contrast (arrow). (E) Image of the hypha after the motor moves to the selected Z-position, restoring image contrast suitable for tracking. Scale bar, 20 μm.

2.7 Speed of apical growth

The set of (x,y) position coordinate data undergoes smoothing (boxcar, 30 time points) and decimating (10-fold) operations that decrease position variations. Next, the derivative of the x and y coordinates respect to time yields growth speeds along X and Y axes. After performing one last smoothing procedure (median, 10 points), the X and Y speeds are added in quadrature to obtain the final hyphal growth speed. For global analysis of apical growth speed, 18 different speed records were concatenated, resulting in a total of 148.1 h of tracking data, and produced a histogram with its corresponding Gaussian fit. For measuring radial colony growth *T. atroviride* mycelia was inoculated at the edge of Petri dishes containing solid PDA medium. Colonies were kept in the dark at 28° C; radial extent was manually recorded every 12 h during 48 h.

2.8 Hyphal persistence length

A set of (x,y) coordinates corresponding to tracking of a hypha is first smoothed (boxcar, 30 time points) and then decimated (100-fold). Next, arc length (s) and angular correlation values are cos ($\theta(s)$ − $\theta(0)$) calculated as follows. The reference value $\theta(0)$ is the angle of the line tangent to the coordinate path at the first coordinate (x = 0, y = 0). For every subsequent (x,y) point the arc length (computed as the piecewise sum of Euclidean distances between (x,y) coordinates up to the current point) and the angle $\theta(s)$ are obtained, and the value cos ($\theta(s)$ − $\theta(0)$) is computed. This procedure is repeated, now taking as a reference value $\theta(0)$ the angle of the line tangent to the coordinate path at the second (x,y) position. The routine is repeated for every (x,y) position as the reference value $\theta(0)$. Data are then organized by binning arc length values and computing averages of angular correlation values for every arc length bin, yielding angular correlation vs. arc length for that particular (x,y) record. Finally, angular correlation records corresponding to different tracked hyphae are averaged.

For microscopic filament polymers, thermal fluctuations cause fluctuations in shape. In this context, the persistence length is a measure that indicates “the length of filament over which thermal bending becomes appreciable” (Jonathon Howard and Others 2001). To compute this metric, the correlation between tangent angles is used. It can be shown that:

$$\langle \cos[\theta(s) - \theta(0)] \rangle = e^{-\left(\frac{s}{2L_p}\right)}, \qquad (1)$$

where θ(*s*) is the tangent angle at arc length *s* and L_p is the persistence length (Jonathon Howard and Others 2001). Therefore, the persistence length is the characteristic distance over which tangent angle correlations are preserved.

The notion of tangent angle correlation to characterize the path followed by fungal hyphae during development was borrowed, with the expectation that this correlation will show patterns informative of hyphal architecture (see below). Taking the hyphae itself (or equivalently the path followed by the hyphal tip) as the filament under study, the angular correlations are computed: $\langle \cos cos \left[\theta(s_2) - \theta(s_1)\right] \rangle$. To perform this operation in practice, the following steps are followed (see more details in the Materials and Methods section of the main text). (i) Given the set of (*x*,*y*) coordinates corresponding to tracking of a hypha, $\cos cos \left[\theta(s_2) - \theta(s_1)\right]$ is computed for all possible arc lengths s_1 and s_2. (ii) All $\cos cos \left[\theta(s_2) - \theta(s_1)\right]$ values having the same interval $s_2 - s_1$ are averaged. (iii) $\cos cos \left[\theta(s_2) - \theta(s_1)\right]$ values are organized in a histogram, yielding the “individual angular correlation” ($\langle \cos cos \left[\theta(s_2) - \theta(s_1)\right] \rangle$) vs. arc length for that particular (*x*,*y*) record. Finally, the “angular correlation” is obtained as the average of individual correlations $\langle \cos cos \left[\theta(s_2) - \theta(s_1)\right] \rangle$, for all tracking records. this “angular correlation” is reported (see Fig. 18).

Figure 11 shows individual angular correlations after application of steps (i)-(iii) of the aforementioned procedure to simple n-segment filaments. These examples make evident that high angular correlation corresponds to trajectories presenting little deviations. Figures 12 and 13 show collections of six-segment

uniform and random trajectories, respectively, together with their corresponding angular correlations. The average angular correlations (see black curves in Figs. 12 and 13) make evident that two parameters can be recovered from the analysis. First, the angular correlation decays with a characteristic (arc length) distance. Second, the angular correlation decays to an asymptotic value that is just the cosine of the angular distance between consecutive segments.

In the performed experiments (see Fig. 18), an exponential decay curve is fitted to the average correlation. Persistence length is defined as one-half the decay parameter in the exponential, in analogy with the mechanical filament under thermal bending (see Eq. 1). This persistence length is interpreted as the characteristic distance of hyphal elongation before changes in direction occur (either by branching or by hyphal elongation). Taking branching as the main contributor to direction changes during hyphal growth, the decay curve follows an asymptote whose value informs us on the average angle between parental and branching hyphae.

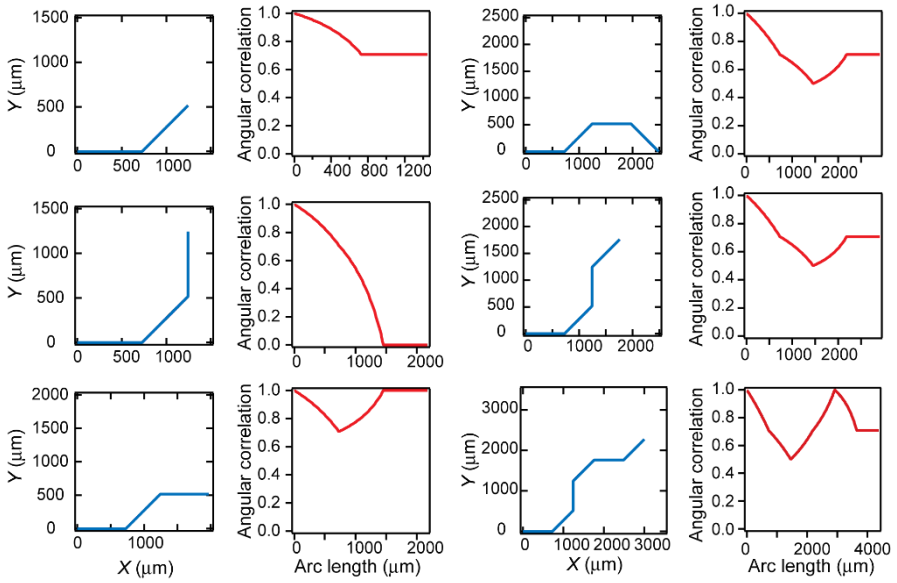

Figure 11. Individual angular correlations for simple mock hyphal trajectories. Hyphal trajectories (blue) were constructed with by joining straight segments of equal length (728 µm) and enforcing angular displacements of ±45 deg between consecutive segments, mimicking hyphal trajectories subject to branching events. Angular correlations (red) quantify changes in direction.

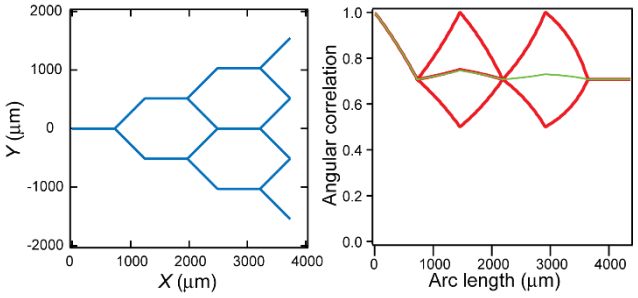

Figure 12. Angular correlation for a collection of segmented trajectories. Each hyphal trajectory (blue) consisted of six straight segments of equal length (728 µm) and angular displacements of ±45 deg between segments. All possible trajectories satisfying the above conditions are shown superposed. The corresponding individual angular correlations (red) are also shown superposed. The average angular correlation (green) shows decay after a distance ~730 µm to the constant value 0.707 (= cos[45 deg]), therefore recovering the main morphological aspects of the trajectories considered.

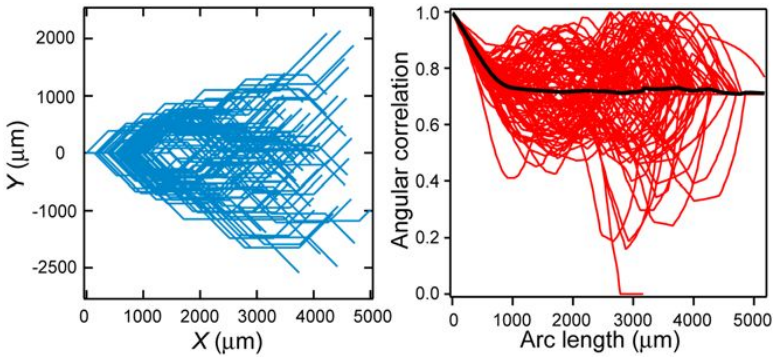

Figure 13. Angular correlation for random segment trajectories. Each hyphal trajectory (blue) consists of six straight segments with ±45 deg angular displacements between adjacent segments. The length of each segment is randomly selected from a Gaussian distribution with mean 728 µm and SD 273 µm. Only forward trajectories were considered. The corresponding individual angular correlations (red) are shown superposed. The average angular correlation (black) shows decay to the constant value 0.7. Number of trajectories, 96.

2.9 Results

This section summarizes the results published in: Gamaliel Sánchez-Orellana, Braulio Gutiérrez-Medina, Sergio Casas-Flores (2018): *Automated, continuous video microscopy tracking of hyphal growth.* Fungal Genetics and Biology Volume 123, February 2019, Pages 25-32.

2.9.1 Automated tracking of hyphal elongation

The developed bright field microscopy system was applied to observe hyphal growth in *T. atroviride* starting from individual conidia. Figure 14 shows a typical succession of observation events, where the system initially detects the tip of a growing germ tube and starts apical tracking (Fig. 14A). When the hyphal tip reaches the boundaries of the visual field (Fig. 14B) the system moves the microscope stage through the stepper motors, bringing back the same hypha within field of view, and identifies the hyphal tip to continue tracking (Fig. 14C). As the hypha continues to grow and a new off-limits event presents (Fig. 14D) the system moves the stage again (Fig. 14E) and resumes tracking (Fig. 14F). Only “forward” growing hyphae are considered; that is, filaments elongating towards the three dotted lines shown in Fig. 9. The system is able to track hyphal growth over several hours (up to 14), limited mainly by the appearance of intruder hyphae that overlap with the hypha of interest (difficulting the correct distinction of tracked objects). This potential problem is minimized by restricting the search area to the ROI established around the tip of the tracked hypha and by using low numbers of conidia (~10 per sample).

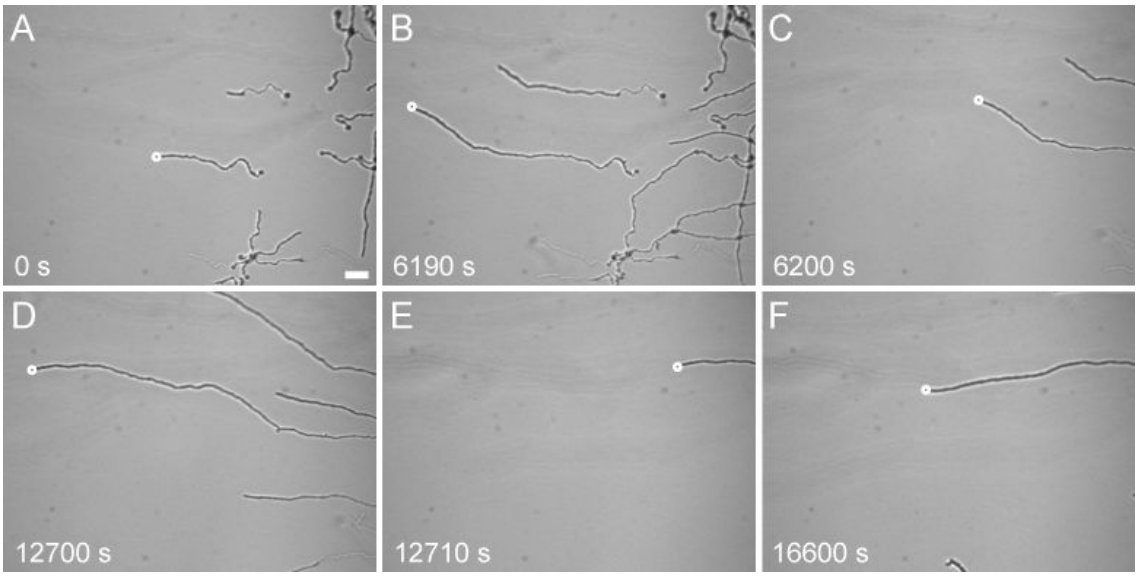

Figure 14. Hyphal tip tracking under execution. (A) The system begins tracking the tip of a selected hypha (white circle). (B) After a period of sustained growth, the tip reaches the boundaries of the microscope field of view. (C) The system returns the hypha under view and finds the new position of the tip. (D) A second off-limits event presents. (E) The hypha after being brought well within view. (F) Tracking continues through several hours. Tracking time is shown. Scale bar, 20 μm.

2.9.2 Hyphal growth speed

The raw tracking data consist of increasing (x,y) position coordinates interrupted by jumps due to the stage motions that keep the same hypha within field of view. After correcting for these jumps, the apical growth speed is computed. The apical elongation rate for *T. atroviride* is approximately constant during the observation period (Fig. 15A,B). Unexpectedly, however, it was frequently found that prior to the emergence of a new hyphal branch the elongation dynamics of the parental hypha stalled completely, resuming growth after the appearance of the new branch (Fig. 15).

The developed system allowed to identify four different types of branching dynamics: (i) Apical branching with preceding growth arrest. Pauses in growth presented typical durations 2-5 min (Fig. 15C-E). (ii) Apical branching with no noticeable growth rate modification. It is possible that here no pauses were present or that pauses lasted less than ~1.3 min, the temporal resolution in

analysis of tracking data. (iii) Subapical branching (> 10 μm from the parental tip) with no noticeable stops in growth. (iv) Subapical branching with parental hypha growth arrest. There were a few instances where the parental hypha stopped growth during several minutes prior to the appearance of a subapical branch. It was also noticeable that the parental hypha often resumed growth after the appearance of a new branch with an elongation rate initially reduced (Fig. 15F-H). Out of 49 branching recorded events, the following for each type were observed: (i) 20, (ii) 18, (iii) 6, and (iv): 5.

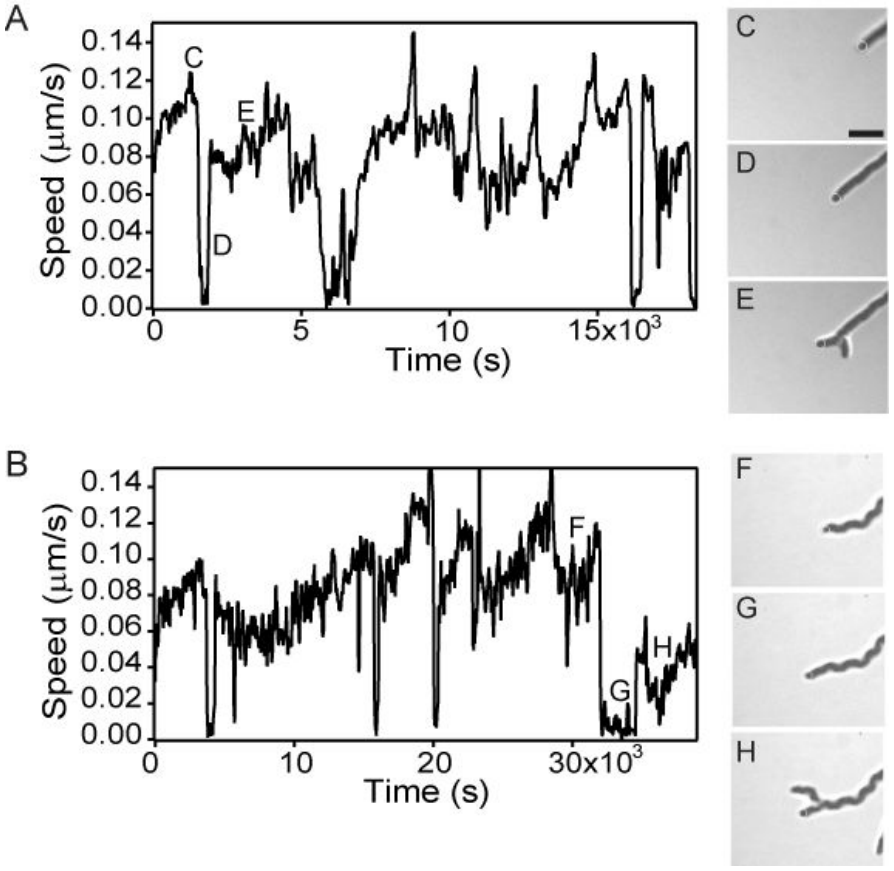

Figure 15. Hyphal elongation rate and branching dynamics. (A)-(B) Two examples of hyphal growth speed. The speed records show noticeable stalls in growth that were noticed to occur prior to the emergence of a branch. Images show apical (C-E) and lateral (F-H) branching events, corresponding to the indicated time points in the speed records. Scale bar, 10 μm.

These results can be contrasted with previous studies of hyphal branching. Two types of branching have been reported for *Neurospora crassa*: apical and

subapical (Meritxell Riquelme and Bartnicki-Garcia 2004). In apical branching the parental hypha was observed to sharply drop its elongation rate, whereas in subapical branching the elongation rate of the parental hypha continued undisturbed. To explain these differences, authors of Ref. (Meritxell Riquelme and Bartnicki-Garcia 2004) suggested that apical branching may involve disruption of cytoplasmic organization, whereas lateral branching probably resulted from subapical accumulation of wall precursors. The observations reported here add two novel elements to the reported branching behavior. First, during apical branching growth is completely arrested (lasting a few minutes). This observation is consistent with disruption of cytoplasmic organization prior to the branching event. Second, subapical branching sometimes also involves parental arrest in elongation. This previously unknown type of branching event may be consistent with accumulation of cytoplasmic cell wall material near the (arrested) hyphal tip. Future studies involving observation of cytoplasmic organization during branching should help to better understand these effects.

Analysis of growth speed data for several samples (Fig. 16) yields an average of 0.072 ± 0.016 μm/s. This microscopic hyphal elongation rate can be compared to macroscopic radial growth (Fig. 16). Colony measurements were carried out using the same lighting, medium and temperature growth conditions as in the microscopic experiments. During the first few hours of observation radial growth is 0.104 μm/s (Fig. 16). The lower apical elongation rate compared to the colony radial extension rate has been observed before for *N. crassa* (0.70 μm/s vs. 0.19 μm/s, respectively) (Lopez-Franco, Bartnicki-Garcia, and Bracker 1994) and *Aspergillus nidulans* (0.04 μm/s vs. 0.02 μm/s) (Trinci, n.d.). This difference in growth rates can reflect the fact that in radial growth hyphae located at the colony edge correspond the fastest growing and/or the ones that changed direction little, whereas at the individual hypha level the mean value of extension rate is reported. In addition, growth delays due to branching and other unknown factors in individual hyphae reduce average elongation rates.

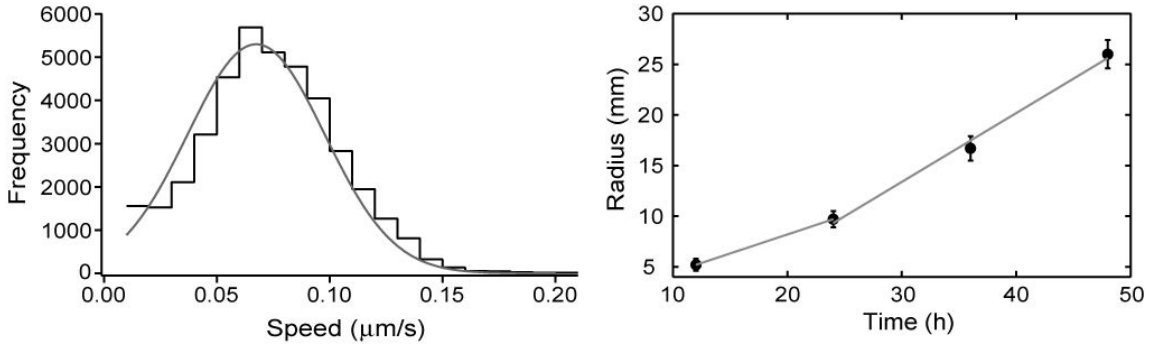

Figure 16. Microscopic and macroscopic growth rate of *T. atroviride*. Left: Histogram of hyphal elongation rate obtained from 18 different tracking runs. A Gaussian fit to data (gray line) yields the average growth speed of hyphae: 0.072 ± 0.016 μm/s (average ± standard deviation). Right: Colony radial growth. The first two datapoints define a line (in gray) with slope: 0.104 μm/s. The last three datapoints are adjusted to a line (in gray) of slope 0.189 ± 15 μm/s (error from the fit). N = 3.

2.9.3 Tracking hyphal growth at increased magnification

To further assess the capabilities of the developed system, tracking of hyphal growth at a higher microscope magnification (40x) was performed. A few technical challenges present in this case. The much-reduced objective working distance (0.6 mm at 40x vs. 5.5 mm at 10x) limited the amount of defocusing of samples, whereas image contrast did not allow efficient auto-focus. It was found that the microscope axial drift increased linearly; therefore, the auto-focus routine was disabled and the Z-motor advanced by one step every 50 sampling cycles, maintaining the sample at optimal focus. With regard to correction of off-limits events, only one or two X,Y motor steps (step distance at the sample plane, ~60 μm) was enough to bring the tracked hypha within field of view. From this observation it was noted that the X,Y motor step size is thus the main limitation that precludes the system to work at higher magnifications. Finally, as the digital image processing routines were tested to function with wider filament objects, it was found that the Skeletonize operation was not a required to perform tracking. It can only be expected that in research-grade microscopes some of these constraints may not be limiting at all.

Figure 17A shows images of hyphal tracking at 40x magnification. In this condition, the frequency of off-limits events increases significantly compared to 10x, and the automated routine performs effective correction many times over a number of hours. Measurements of growth speed derived from (x,y) tracking data (Fig. 17B) agree well with measurements at lower magnification. It is interesting to note that at 40x the shape of single hypha can be distinguished. This characteristic can prove useful for future studies aimed at the study of hyphal tip morphology over prolonged times using the developed automated tracking system.

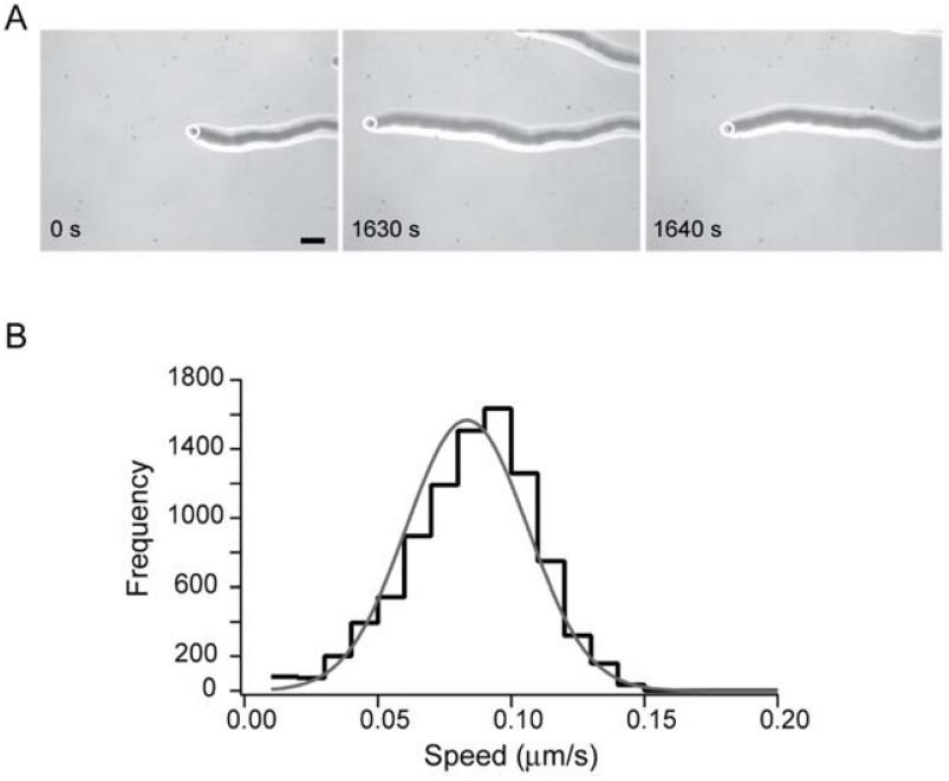

Figure 17. Tracking hyphal growth at 40x microscope magnification. (A) Sequence of bright field images showing a hypha under tracking at an initial position (left), close to the off-limits range (center), and upon return to the field of view (right). Scale bar, 20 µm. (B) Histogram of hyphal elongation rate obtained from eight different tracking runs (total tracking time, 37.8 h). A Gaussian fit to data (gray line) yields average speed: 0.083 ± 0.014 µm/s (mean ± sd).

2.9.4 Hyphal path tangent angle correlation and persistence length

The availability of (x,y) coordinates corresponding to hyphal tip elongation provide the opportunity to compute the persistence length associated to the filamentous hypha. The persistence length is a measure often used in polymer mechanics, that indicates “the length of filament over which (…) bending becomes appreciable” (Jonathon Howard and Others 2001). In the context of filamentous fungal growth, the persistence length can therefore quantify the characteristic distance before hyphae present changes in direction. This microscopic measure could provide useful information in understanding how growth direction is set in fungal hyphae (M. Riquelme et al. 1998) and to build models of macroscopic fungal architecture and organization (Boswell and Hopkins 2008).

To assess persistence length, the set of (*x*,*y*) coordinates associated to the tip of hyphae during growth is recognized as the path that defines the shape of that hypha. The extension of this path is given by the arc length, *s*. As the arc length increases changes in path direction will dictate changes in the angles of lines tangent to the path (Fig. 18A). This is the main idea behind the analysis that follows.

To quantify changes in direction in the hyphal path, the correlation between tangent angles $\theta(s)$ is computed as the average of: $\cos cos\,(\theta(s)-\theta(0))$. Figure 18B shows the average angular correlation as a function of arc length for a set of 16 different tracking records. An exponential fit to these data yields the persistence length: L_p = 725 µm, and the asymptote of the angular correlation for long arc lengths: ζ = 0.73.

Tangent angle correlation provides information on the characteristic distance of hyphal elongation before changes in direction and the average angle followed during these changes. Based on this notion, it is concluded that a growing

hypha elongates by ~700 μm before changing direction (by either elongation or branching). Furthermore, the asymptotic value ζ = 0.73 corresponds to a mean angle of 43 deg. Interestingly, this value is essentially the same as the branching angle experimentally found in *N. crassa* (45 deg) growing on a surface of agar (Held, Edwards, and Nicolau 2011), suggesting that the main mechanism for hyphae to change direction is branching. Further work should test this inference in *T. atroviride* and other fungi.

The angular correlation analysis presented here is amenable to alternative procedures of microscopic hyphal growth characterization. In particular, the analysis could be applied at the whole-colony scale. Using straightforward image processing procedures, the image of an entire colony can provide the set of (*x*,*y*) coordinates that define the path of all hyphae involved. As described here, these coordinates provide the starting point to compute tangent angle correlation. Therefore, the analysis proposed in this work has the potential to provide information on hyphal morphology for a colony without counting or measuring individual elongating, branching or pausing events.

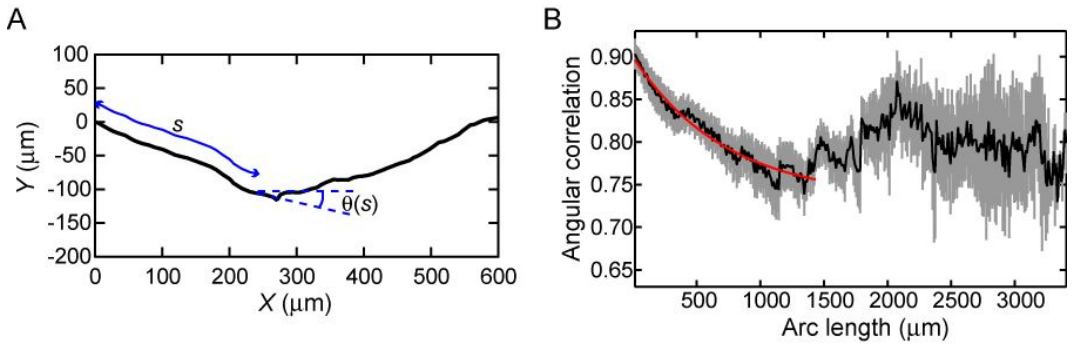

Figure 18. Angular correlation and persistence length of hyphal growth. (A) The path followed by a hypha is shown (black line) along with an arc length (s) and the angle of the tangent to the path at s. (B) The average angular correlation (⟨cos $(\theta(s) - \theta(0))\rangle$) shows initial decay followed by asymptotic behavior (N = 16, records vary in arc length total extent). Averages (black) and S.E. (gray region) are displayed. An exponential fit to data (red line), limited to values where at least 10 angular correlation records were used to compute averages, yields Lp = 725 ± 60 μm, and the asymptote of the angular correlation for long arc lengths: 0.73 ± 0.01 (errors from the fit).

2.9.5 Conclusions

In this chapter the development of an accessible video microscopy method that allows real-time continuous tracking of a single hypha was presented. The system operates in an automated fashion over extended periods of time (up to 14 h) with a sampling time interval of 1.3 s. The quantitative value of this method was tested by obtaining the growth speed and the persistence length associated to hyphae of *T. atroviride*.

In particular, It is shown how tangent angle correlation can provide information on the characteristic distance of hyphal elongation before changes in directions occur and the average angle between parental and branching hyphae. The temporal sampling rate of the developed system allowed detecting branching dynamics not previously reported. This methodology should prove useful for the analysis of fungal hyphae growth dynamics under different treatments, conditions or strains.

2.10 Future work

It is of main interest to further test the growth dynamics of *T. atroviride* by changing the growth conditions to: different lighting (wavelengths), change of nutrients or temperature. The developed system would provide valuable information on how growth conditions may affect the growth speed at the single hypha level.

Chapter 3. Kinesin-1 on *Trichoderma atroviride* growth

3.1 Kinesin-1

Kinesin-1 is a member of a large superfamily of proteins (Alberts 2017), Figure 19. It was identified in 1985 as a motor involved in intracellular transport in axons and it was isolated from neuronal cell extracts (R. D. Vale, Reese, and Sheetz 1985). Next, some of the basic aspects of what is known so far about Kinesin-1 and its mechanisms of performing intracellular transport are reviewed. Kinesin-1 has been found present in all eukaryotic organisms with the exception of the yeast *Saccharomyces cerevisiae*, which uses myosin for most intracellular transport.

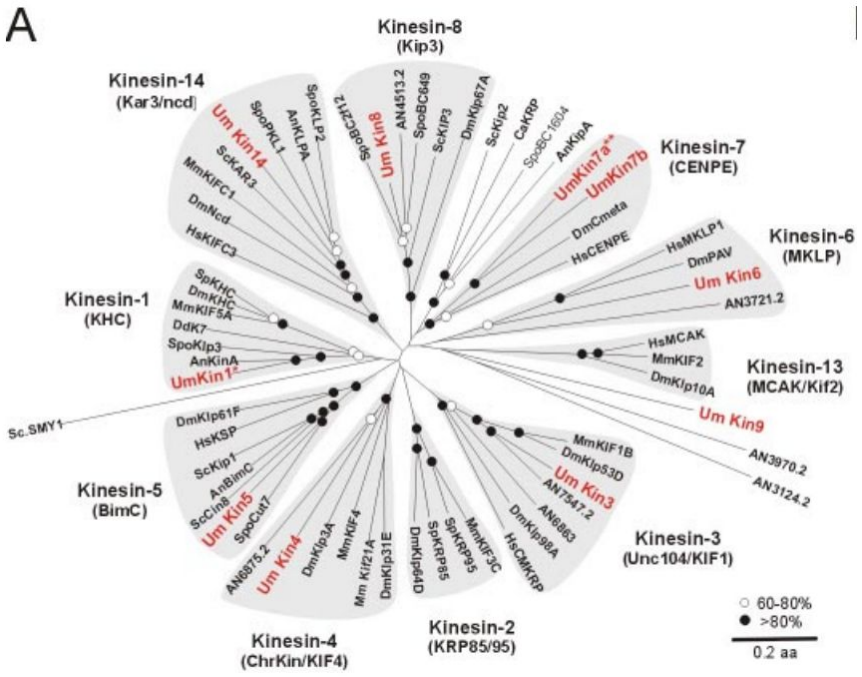

Figure 19. Kinesin superfamily tree. The tree is based on an alignment of the motor domain of fungal and animal kinesins. Cn, *Cryptococcus neoformans*; Um, *U. maydis*; Hs, *Homo sapiens*; Mm, *Mus musculus*; Dm, *Drosophila melanogaster*; Sp, *Strongylocentrotus purpuratus*; Spo, *S. pombe*; Sc, *S. cervisiae*; Ca, *Candida albicans*; Nc, *Neurospora crassa*; An/AN, *A. nidulans*. Note that only selected kinesins from animal and fungal species were included. Image modified from (Schuchardt et al. 2005).

In metazoans it has been found that Kinesin-1 participates in the intracellular transport of organelles, including mitochondria, lysosomes, endoplasmic reticulum and vesicles. Likewise, it also transports other types of cargoes, such as mRNAs and intermediate filaments (Ronald D. Vale 2003). In fungi, it has been found that Kinesin-1 participates in the transport of secretion vesicles directed towards the growing apical region (Egan, McClintock, and Reck-Peterson 2012).

A comparative (protein vs protein) search performed using *T. atroviride* genome database (http://genome.jgipsf.org/Triat2/Triat2.home.html) shows the Kinesin orthologues for: *N. crassa, S. cerevisiae, S. pombo, T. atroviride* and the identity shared between *T. atroviride* and *N. crassa* Kinesins (Table 1).

Kinesin NCU no.	Orthologue(s)				Family/Class	Proposed role(s)	Identity w/ *N. crassa*
	N. crassa	***S. cerevisiae***	***S. Pombo***	***T. atroviride***			
NCU09730.7	nkin1	Smy1p	Klp3 (SPAC1834.07)	Kin1	Conventional Kinesin	Transport of secretory vesicles, nuclear positioning, microtubule dynamics	77%
NCU06733.7	nkin2	NF	NF	Kin2	Unc104	Vesicular transport	71%
NCU03715.7	Kin-3	NF	SPAC144.14	Kin-3	-	-	68%
NCU06832.7	NF	NF	NF	NF	kif21/chromokinesin	Vesicular transport, DNA binding	67%
NCU04581.7	NF	Kar3p	Pkl1/Klp1(SPAC3A11.14C)	NF	C-Terminal	Dynamics of spindle microtubules, counteracts BimC-like motors	56%
NCU06144.7	NF	Kip3p	klp5(SPBC2F12.13)	NF	Kip3	Spindle positioning, spindle elongation during anaphase, microtubule disassembly	55%
NCU00927.7	NF	Kip1p, Cin8p	Cut7(SPAC25G10.07C)	NF	BimC/Eg5	Spindle assembly and centrosome separation during mitosis	58%
NCU05180.7	NF	NF	SPB1504.01C	NF	Fast evolving/pavarotti	Organization of the mitotic spindle,	49%
NCU02626.7	NF	Kip2p	Klp4/Tea2(SPBC1604.20C)	NF	Kip2	Kip2p has mitotic functions, Tea2 seems to alter the dynamics of interphase microtubules	63%
NCU05028.7	NF	NF	NF	NF	KID	Chromosome alignment in metaphase	73%

Table 1. Orthologue Kinesins identified in orthologous organisms to *T. atroviride*. In the table it can be seen the number of protein from which the search was performed, as well as the genetic name of the orthologues, the family to which it corresponds, its function and the percentage of identity that exists between *T. atroviride* and *N. crassa* in each Kinesin.

3.1.1 Kinesin-1 main characteristics

Structure. Kinesin-1 is a homodimeric protein, formed by two identical polypeptide chains called heavy chains, which consist of ~ 1000 amino acids each, which dimerize by means of an elongated and flexible structure of stem type through "coiled-coil" domains (Figure 20) (Ronald D. Vale 2003; Egan, McClintock, and Reck-Peterson 2012).

Each of the two heavy chains that make up the homodimer has a catalytically active domain at its N-terminal end called "head". The head domain is globular and has subdomains with ATPase activity as well as affinity to MTs. At the C-terminal end of each heavy chain globular domains known as "tail" are located, which are involved in the binding of cargo as well as processes of self-inhibition of the ATPase activity of the head domain when the Kinesin-1 is not binding any cargo. In metazoans, the Kinesin-1 also associates two identical polypeptide chains called light chains. The light chains join the tail of the heavy chains and participate in the recognition of cargoes. Studies in filamentous fungi indicate that the conventional Kinesin-1 of these organisms lacks the light chains (Seiler et al. 2000).

Due to its importance, the atomic level structure of the kinesin head domain was already obtained by X-ray crystallography (Kozielski et al. 1997), which has made it possible to characterize ATP and MTs binding sites, as well as the so-called protein "neck-linker": a region of ~ 13 amino acids that connects the head domain with the stem-type dimerization domain. The neck-linker is of great importance for the mechanism that generates motility (displacement) in the protein (Rice et al. 1999).

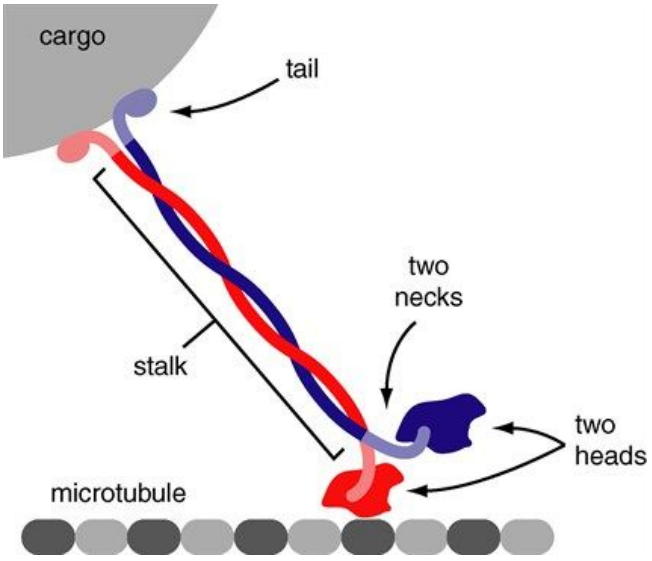

Figure 20. A molecule of Kinesin-1 composed of two heavy chains (blue and red). The two alpha helices of the chains are wrapped around each other to form the stem. The tail has a binding site for cargoes. The head domain has subdomains with ATPase activity as well as affinity to MTs.

Mechanism of movement. The movement of a Kinesin-1 is progressive (Figure 21). It is known that in this movement the two heads of the Kinesin-1 do not act independently and move through biochemical interactions on the MTs. To achieve a progressive movement, Kinesin-1 requires at least two anchoring points so that one of the heads can be bound to the MT, while the other one advances through it (J. Howard, Hudspeth, and Vale 1989; S. M. Block, Goldstein, and Schnapp 1990). The two heads of Kinesin-1 are strictly necessary so that it can move progressively (Berliner et al. 1995; Hancock and Howard 1998).

There is also a crucial feature for the correct functioning of the Kinesin-1 motor mechanism: the addition of ATP strongly increases the affinity of Kinesin-1 for MTs. On the other hand the motor walks unidirectionally on the MTs (Visscher, Schnitzer, and Block 1999; Steven M. Block et al. 2003) and follows a parallel path on it (Gelles, Schnapp, and Sheetz 1988; Ray et al. 1993). To achieve this

movement, the first Kinesin-1 head must not be released from its MTs junction until the second head is attached to another section of the MTs. In a few seconds, a single molecule of Kinesin-1 advances an average of 100 steps before being released from the MTs.

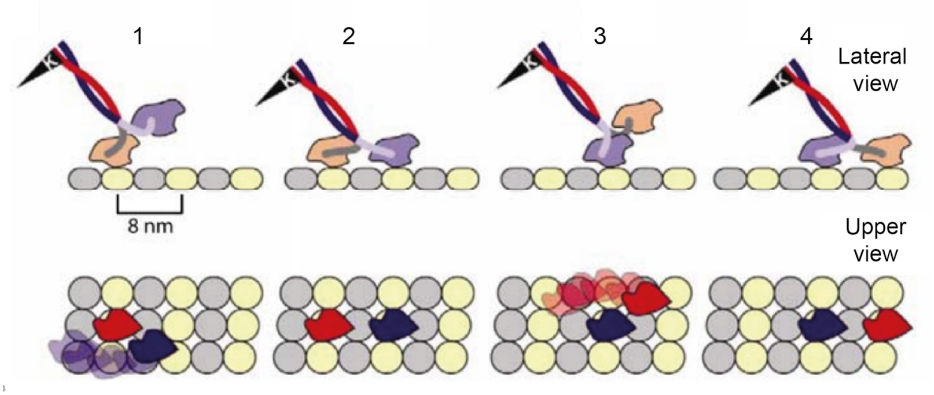

Figure 21. Movement of a Kinesin-1 on a MT. (1) One of the two heads of a Kinesin-1 molecule, initially both in the ADP form, binds to the MT. (2) The release of ADP and the union with ATP produces a conformational change that adheres the head to the MT and pushes the nexus of union (orange) to the head domain, displacing the second domain towards the end (+) of the MT. (3) When the second head interacts with the MT, the hydrolysis of ATP takes place. (4) The exchange of ATP by ADP in the second head displaces the first head of the MT, releasing Pi and displacing the first domain along the MT. The cycle repeats, displacing the Kinesin-1 dimer along the MT. Image taken from the reference.

Transport mechanism in the cellular context. Although studies on the mechanism of transport carried out by Kinesin-1 in the cellular context or in complex environments that resemble it are incipient, progress has been made in this regard. As already mentioned, Kinesin-1 carries out its transport task under the influence of diffusion and a highly populated medium (it is estimated that the content of proteins in the cellular cytoplasm is ~ 20% weight, a percentage that is sufficient even to crystallize some proteins) (Luby-Phelps 2000). As part of that medium, MTs form an interconnected and dynamic network that influences the regulation of Kinesin-1 dynamics. In this regard, it

has been found that Kinesin-1 binds preferentially to MTs that exhibit post-translational modifications. On the contrary, the presence of microtubule-associated proteins (MAPs) decreases the motility of Kinesin-1 (Verhey and Hammond 2009). On the other hand, thanks to studies with cell extracts, it has been established that multiple Kinesins, as well as molecular motors of other types, are linked to the same vesicle typical of the cytoplasm (Holzbaur and Goldman 2010; Tabb et al. 1998). Regarding this, *in vitro* experiments have found that groups of kinesins acting on the same load contribute to increase the distance traveled on a MT compared to a single motor (Holzbaur and Goldman 2010). On the other hand, when motors of different types such as kinesins and dyneins act on the same vesicle, a competition is established between the anterograde (Kinesin-1) and retrograde (Dynein) movements, which results in an alternation in the direction of the displacements of the vesicle on the MT (Holzbaur and Goldman 2010).

In addition to the *in vitro* studies, several optical microscopy observations of transport carried out by Kinesin-1 in living cells have already been carried out (Verhey, Kaul, and Soppina 2011). To achieve this, these experiments have followed two types of strategies: (i) exogenous introduction of recombinant kinesins labeled with quantum dots (fluorescent semiconductor particles) or (ii) endogenous expression of kinesins genetically labeled with fluorescent proteins. The initial conclusions of these studies indicate that Kinesin-1 behaves in a manner very similar to that reported *in vitro*, suggesting that the dense intracellular medium does not significantly affect the motor properties of the protein (Verhey, Kaul, and Soppina 2011). Finally, it should be noted that a recent experiment, performed on neurons in order to know what happens to the Kinesin-1 after reaching the end (+) of the MTs, found that the Kinesin-1 is recycled, returning to the end (-) of MTs essentially by a diffusion process (Blasius et al. 2013).

3.1.2 Kinesin-1 in filamentous fungi

Filamentous fungi are organisms whose cells develop in the form of hyphae. They have a polarized cytoskeleton, so there is active intracellular transport associated with MTs (Egan, McClintock, and Reck-Peterson 2012). It is known that in the genome of filamentous fungi there are approx. 10 kinesins, of which Kinesin-1 and Kinesin-3 participate in transport processes (Steinberg 2011). In contrast, the yeast *Saccharomyces cerevisiae* does not present the genes encoding Kinesin-1 and Kinesin-3, suggesting that these kinesins are necessary for transport involving long distances in hyphae (Lillie and Brown 1998). Indeed, it has been shown that in transport carried out in MTs, Kinesin-1 and Kinesin-3 are actively involved in the anterograde transport of cargoes necessary for the development of the hyphae of the fungus *Ustilago maydis(Schuchardt et al. 2005)*. However, only Kinesin-1 is located at the apex, participating in the formation of *Spitzenkörper*, a specific cellular structure that concentrates secretion vesicles that participate in controlled exocytosis in order to produce cell wall (Meritxell Riquelme 2013; Schuchardt et al. 2005).

Null mutant strains in Kinesin-1 of *N. crassa*, *A. nidulans* and *U. maydis* exhibit a severe alteration in apical growth rate (Seiler et al. 1997; Requena et al. 2001; Schuchardt et al. 2005). A recent study in *U. maydis* suggests that the proteins chitin synthase-5 and chitin synthase-6 (CHS) are taken to the growing apical regions through vesicles transported by Kinesin-1 (together with the motor protein Myosin-V, associated with actin), which are then secreted by exocytosis (M. Schuster et al. 2012).

3.1.3 Study strategy

It is of main interest to study specific aspects of the role of kinesin-1 in the development and growth of the filamentous fungus *Trichoderma atroviride*. This work seeks to study how the absence of Kinesin-1, one of the main

nano-motors transporter of vesicles essential for growth (reported for other filamentous fungi), affects hyphal elongation, branching and morphology of *T. atroviride.* The approach to observe the importance of Kinesin-1 in the growth of *T. atroviride* will be the generation of a mutant strain lacking the gene encoding Kinesin-1. Several phenotype experiments regarding the following *T. atroviride* growth stages (germination, vegetative growth and conidiation) will be carried out.

***T. atroviride* main characteristics.**

T. atroviride is a filamentous ascomycete fungus widely used in the biological control of a variety of phytopathogenic fungi (A. Schuster and Schmoll 2010). *T. atroviride* is also a model organism in photomorphological studies, because it presents a relatively simple phenotype when exposed to light corresponding to the blue region (Herrera-Estrella and Horwitz 2007). In the dark *T. atroviride* grows indefinitely in the form of mycelium, but upon receiving a pulse of light develops specialized structures of asexual reproduction (conidiophores) that contain conidia. The photoreceptor complex in this photocontraction process has already been identified (Casas-Flores et al. 2004), as well as a series of genes regulated by light (Rosales-Saavedra et al. 2006). On the other hand, the complete sequence of the genome of *T. atroviride* is already available (http://genome.jgipsf.org/Triat2/Triat2.home.html). From this sequence, it is known that *T. atroviride* has at least one Kinesin-1 gene (access number GenBank EHK43157.1), whose hypothetical protein shows 77% identity in sequence of amino acids with respect to the Kinesin-1 of the *N. crassa* ascomycete fungus (GenBank AAB52961.1) and 42% identity with respect to the Kinesin-1 sequence of *Drosophila melanogaster* (GenBank AAF58029).

3.2 ΔKinesin-1 strain development

T. atroviride deletion mutant strains will be generated by using the gene replacement technique by double homologous recombination. The next steps will be followed (Casas-Flores et al. 2004):

1) Design and construction of appropriate vectors containing a selection marker (the *hph* gene, which confers resistance to hygromycin), under regulation of the TrpC promoter and flanked by the 5' untranslated region and the 3' untranslated region of the open reading frame of the Kinesin-1 gene.
2) Transformation of *T. atroviride* protoplasts.
3) Selection of colonies resistant to hygromycin.
4) Screening of transformant colonies by PCR analysis using the genomic DNA of the corresponding transformant strains as a template.

3.2.1 Strain development process

1) Design and construction of appropriate constructions:

Specific oligonucleotides were designed to obtain the knockout construct; 25-30 bases of homology to the 2nd fragment of the fusion were added at the 5 ' end of the 1st fragment to carry out the fusion of the fragments (Yu et al. 2004) (Figure 22). Fragments were amplified in separate PCR reactions by using the enzyme Herculase II Fusion DNA High fidelity polymerase (Agilent Technologies) (which shows no activity of terminal transferase). The amplified fragments were: Kin1 5' Promoter, 1st and 2nd half of the hph selection marker, and the Kin1 3' region outside the Open Reading Frame (ORF). The designed oligonucleotides and the full sequences used for the latter are shown in The PCR programs in Appendix Table 1 and 2. The products were purified with the Wizard® SV Gel and PCR Clean-Up kit System (Promega) following the manufacturer's instructions. Subsequently, two fragments of the first fusion were mixed in a single reaction (molar ratio 1:3) to carry out a second round of

PCR without oligonucleotides. The latter was repeated for the second fusion. The PCR programs and electrophoresis gels showing the fuse of the fragments are shown in Table 2 and Figure 23 in the main text. The final amplification was carried out using the enzyme GoTaq DNA Polymerase using the fusion fragments to generate enough concentration needed for transformation (5 ug of purified DNA for each fusion).

Figure 22. Designed construction to transform *T. atroviride* WT. The construction consists of 2 fragments. 1) Kin1 5' promoter fused to the first half of the *hph* gene. 2) 2nd half of the *hph* gene fused to the Kin1 3' Region downstream its ORF.

Gene or amplified sequence	PCR program used
Kin1 5' Promoter	Initial cycle of 94 °C for 3 min, 30 cycles of: 94 °C 30 s, 55 °C 30 s y 72 °C 90 s, a final cycle of 72 °C 3 min.
Hygromycin 1st half	Initial cycle of 94 °C for 3 min, 30 cycles of: 94 °C 30 s, 55 °C 30 s y 72 °C 90 s, a final cycle of 72 °C 3 min.
Hygromycin 2nd half	Initial cycle of 94 °C for 3 min, 30 cycles of: 94 °C 30 s, 55 °C 30 s y 72 °C 90 s, a final cycle of 72 °C 3 min.
Kin1 3' Region	Initial cycle of 94 °C for 3 min, 30 cycles of: 94 °C 30 s, 55 °C 30 s y 72 °C 90 s, a final cycle of 72 °C 3 min.

Table 2. PCR program used for amplification of each fragment used on the construction.

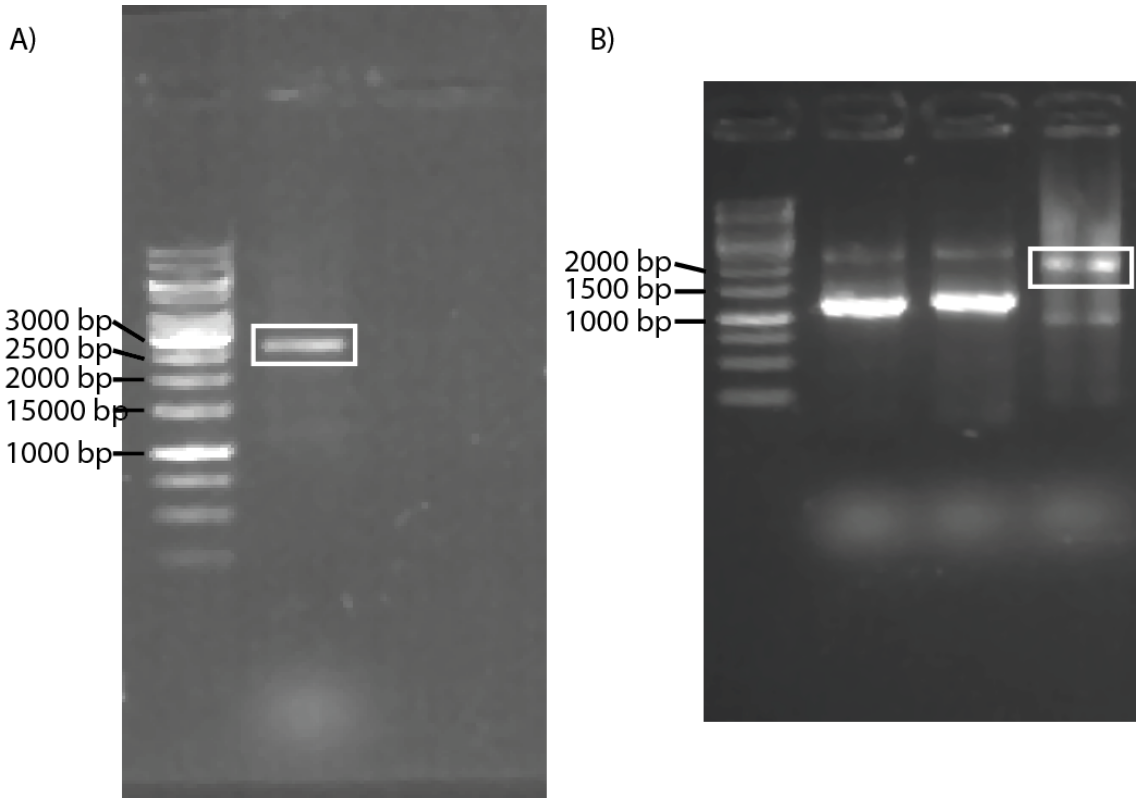

Figure 23. Fused fragments to build the Kinesin-1 knockout cassette. A) Kin1 5' Promoter + Hygromycin 1st half ~ 2843 bp. B) Hygromycin 2nd half + Kin1 3' Region ~ 1905 bp.

2) Transformation of *T. atroviride*

The constructions originated by the Double Joint-PCR were amplified by conventional PCR and were used for the transformation of *T. atroviride*. Figure 24 shows how the recombination occurs during the transformation process.

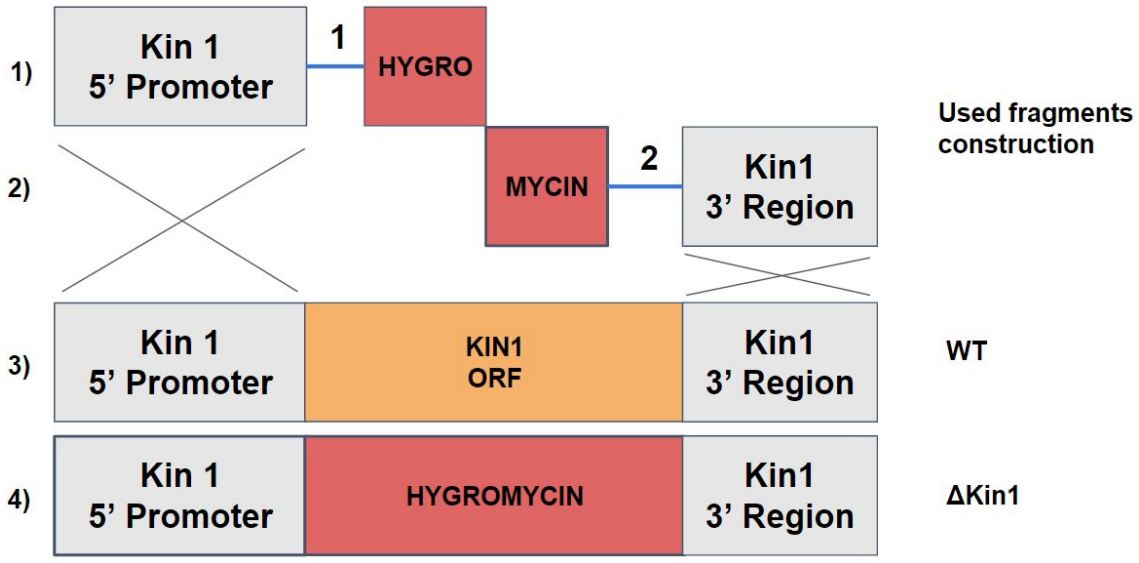

Figure 24. Diagram showing how the recombination occurs during the transformation process. 1) Kin1 5' Promoter region was amplified and fused with the 1st half of the *hph* gene. 2) 2nd half of the *hph* gene with Kin1 3' region. 3) Original genomic sequence of *T. atroviride* WT; this region will be recombined with the introduced fragments due to homologous double recombination. 4) Resulting sequence after the transformation; the Kin1 ORF was replaced for the hph gene; this will provide the mutant resistance to *hph*.

Transformation protocol: Protoplasts were obtained according to the protocol described by (Baek and Kenerley 1998) with the following modifications: 10^8 conidia were inoculated in 100 mL of PDYCB (Dextrose Potato Broth DIFCOTM 24 g / L, Yeast Extract 2 g / L and Casamino acids 1.2 g / L) and incubated for 24 h at 28 °C with shaking 250 rpm. The mycelium was collected by filtration, washed with water and 0.5 grams (weight wet) were resuspended in Osmoticum (50 mM CaCl2, 0.5 M Mannitol and MES 50 mM, pH 5.5) with 15 mg / mL of lytic enzymes of *Trichoderma harzianum* (LET) (Sigma). The mixture was incubated at 28 °C with gentle agitation for 5 h. The protoplasts were collected by filtration through a nylon mesh sterile with pores of 100 µm and subsequently, 5 mL of Osmoticum was added on the nylon meshes to recover the protoplasts that could have been got caught in these. The sample was centrifuged at 1500 rpm for 20 min.

Finally, the sample was resuspended in Osmoticum at a concentration of $1x10^8$ protoplasts / mL. 10 µl of the suspension were taken to observe the integrity of the protoplasts in an optical microscope at a magnification of 40X. Then 10-20 µg of transforming DNA were added to 250 µl of protoplasts. The mixture was then incubated on ice for 20 min and then 250 µl of PEG-4000 was added to the 60%, and incubated at room temperature for 20 min. From the obtained mixture different dilutions were made and mixed with 7 mL of selection medium with soft agar at 0.8% and 50 µg / mL hygromycin and were inoculated into Petri dishes with selective medium. The dishes were incubated at 28 °C for 72 h and to allow regeneration of protoplasts resistant to hygromycin.

3) Selection of colonies with gene replacement

To obtain the transformed strains several monosporic cultures were carried out, in which a certain number of spores were inoculated on the selection medium for later isolation of colonies originated from a conidia. This way, the latter are prone to have a single nucleus. The monosporic colony was then isolated and transferred to a medium without antibiotic selection for its development.

4) Screening of transformant colonies by PCR analysis

Colonies that showed growth given by the resistance cassette were selected and DNA extraction (Table 4) was performed to perform a PCR analysis (Figure 25) using the following Oligonucleotides:

-Flanking the 5 'promoter region of Kinesin with part of the *Hph* gene and
-The rest of the *Hph* gene with the 3 'region of Kinesin-1

Filamentous fungi DNA extraction protocol
1.- Grind mycelium with N_2 2.- Add 500 uL of extraction buffer and vortex

3.- Add 500 uL of phenol chloroform and vortex
4.- Centrifuge at 14,000 rpm for 15 min, transfer supernatant to a new tube
5.- Repeat Steps 3 and 4
6.- Add 2 volumes of isopropanol (cold), mix by inversion and leave 1 hour at -20 C
7.- Centrifuge at 14,000 rpm for 15 min
8.- Discard supernatant and wash with 500 uL 70% ethanol (cold)
9.- Centrifuge at 14,000 rpm for 5 min
10.- Throw supernatant and dry pellet
11.- Resuspend in 200 uL of injectable sterile water and store at -20 C
[RNAse treatment]
12.- Add 2 uL of RNAse (1 mg / uL) and 100 uL of H2O, 30 minutes at 37 C
13.- Add 200 uL of isoamyl chloroform and vortex
14.- Centrifuge 5 min at 14,000 rpm. Take aqueous phase
15.- Repeat steps 13 and 14
16.- Precipitate with 2 volumes of cold ethanol without salts, centrifuge 5 min
17.- Discard supernatant and wash the pellet twice with 70% ethanol (add ethanol, centrifuge, discard supernatant and dry pellet)
18.- Dry the pellet and resuspend in 30 uL of H2O

Table 4. Protocol used for filamentous fungi DNA extraction.

If bands of the expected size are observed in the gel electrophoresis, it means that the gene of *hph* is found in the DNA of the mutant strain, replacing Kinesin-1. In this case, out of the 13 possible mutant strains that were obtained derived from the transformation, in 2 of them the expected bands were observed, which means that these 2 strains have mutated the gene of Kinesin-1.

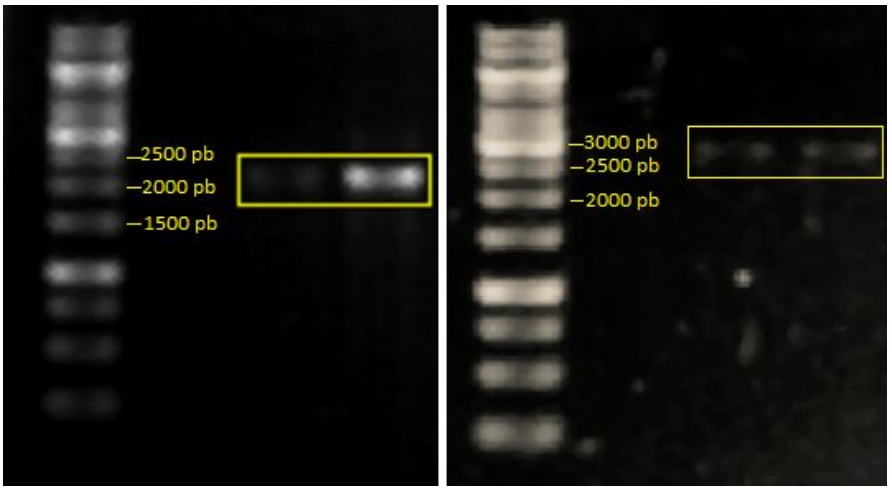

Figure 25. The bands of the 2 strains are shown in which if a band was observed showing the gene replacement of Kinesin-1 by *hph*. Left: region 5 ' promoter outside the Kinesin-1 ORF part of the *hph* gene. Right: the rest of the *hph* gene with the 3 ' outside the ORF of Kinesin-1. Expected size of the bands (~ 2300 and ~ 2700 pb respectively).

3.2.1 Genomic Characterization of ΔKin-1 strain

Real-time PCR measures the amount of amplicon produced during each cycle of amplification using fluorescence-based technology. Real-time PCR can quantify amplicon production at the exponential phase of the PCR reaction in contrast to measuring the amount of product end-point reaction. The amplicon is monitored in “real-time,” or as it is being produced, by labeling and detecting the accumulating product with a fluorescently tagged substrate during the amplification procedure. This method has many advantages over conventional PCR including increased speed due to reduced cycle number, lack of post-PCR gel electrophoresis detection of products, and higher sensitivity of the fluorescent dyes used for the detection of the amplicon (*Real-Time PCR* 2006). Quantitative real-time PCR is the conversion of the fluorescent signal of each reaction into a numerical value for each sample (Tevfik Dorak 2007).

It was necessary to carry out a real-time PCR experiment to determine if the observed phenotype is the result of a single copy of the mutated gene of

Kinesin-1 in the strain, and that no other mutation has occurred which results in having more than one copy in the genome of the strain. The number of copies of the hph gene was verified in the null mutant strains of Kinesin-1. Figure 26 shows the graph corresponding to the real-time PCR experiment.

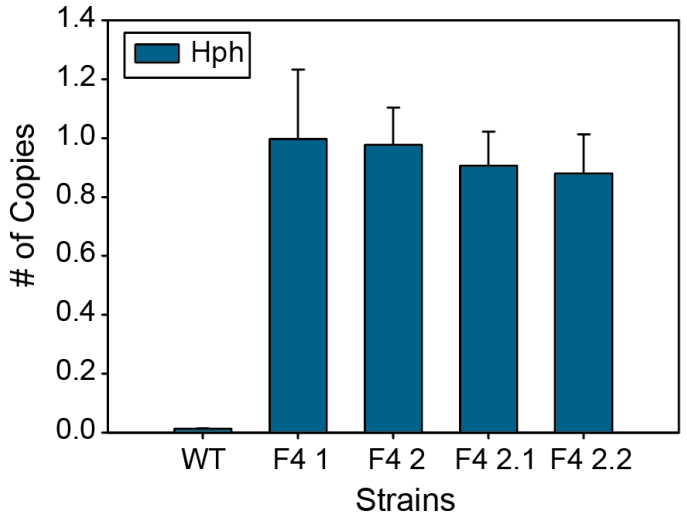

Figure 26. The number of copies obtained in the real-time PCR experiment is observed. In all the strains it was determined that there is only a single copy of the hph gene.

This allows us to determine that only gene replacement was performed in the desired region of the genome, and that the observed mutant strains correspond to the absence of Kinesin-1 in *T. atroviride*. The following oligonucleotides were designed inside the Kinesin-1 ORF to perform a negative control on the mutant strains (Appendix 1) and Figure 27:

-Kin1-Fw: TAAATTGACCCGTATCCTCCAGG

-Kin1-Rv (5-3'): ACAGAGAAAGAATCGCTGGCTGC

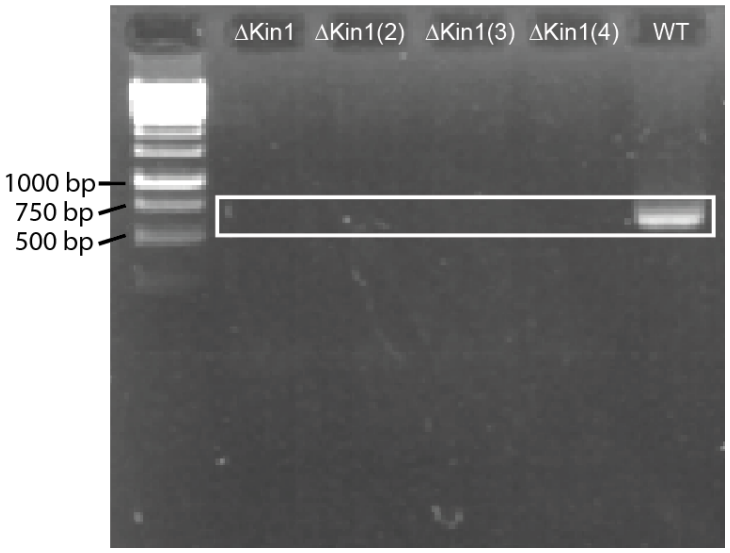

Figure 27. Kinesin-1 ID amplification. As a negative control, a PCR was performed using identificacion oligonucleotides over 4 ΔKin1 strains DNA. Positive Control: *WT* DNA. Expected band size ~519bp.

3.3 Main Results

This section summarizes the results obtained from the morphological characterization of the ΔKin-1 strain. *T. atroviride* main development stages were followed for the study (germination, elongation, conidiation). Also, key morphological characteristics of *T. atroviride* including its mycoparasit activities on phytopathogens were assessed.

3.3.1 Germination characterization

Conidia germination experiments were carried out to assess the characteristic germination time of ΔKin-1 strain. WT strain and ΔKin-1 were inoculated on Petri dishes with PDA under constant 28° C temperature. Hourly observations under the microscope were done starting from 6 h after inoculation through 14 h (Figure 28). There was a delay in the germination time of the conidia of the ΔKin-1 strain. 10 h after inoculation ~ 90% of WT conidia presented a germ tube whilst only ~ 10% of ΔKin-1 conidia had developed a germ tube. Further

experiments should be carried out to assess the role of Kinesin-1 on germination, for there is no evidence that Kinesin-1 participates on germ tube development (Seiler et al. 1997).

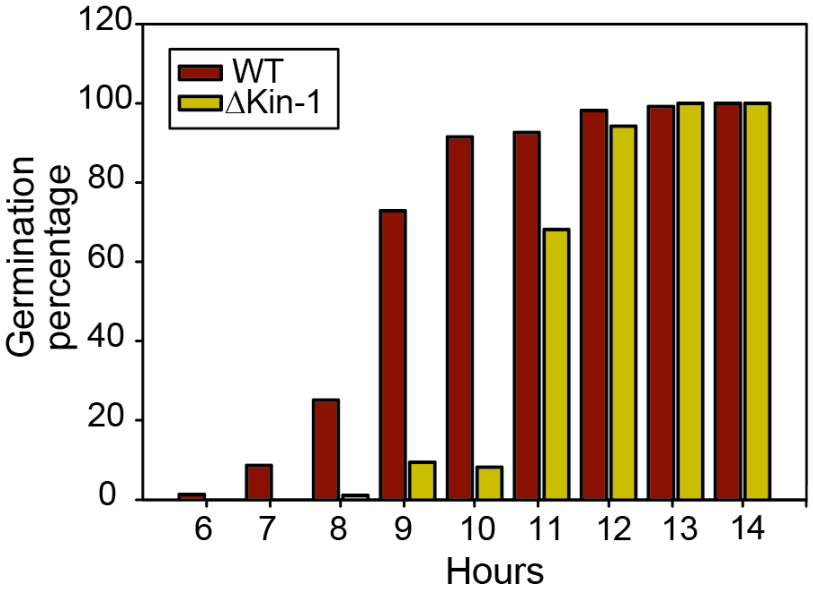

Figure 28. Germination time of WT and ΔKin-1 strains. Hourly observations under bright field microscope were done. A 40x magnification objective was used. n = 50.

3.3.2 Bipolar germination

An effect that was observed in early stages of germination of mutant conidia is that they presented bipolar germination. That is, in ~ 50% of the mutant conidia two germ tubes emerged (Figure 29); this agrees with the reported bipolar extension of germ tubes reported for *N. crassa* Kinesin-1 null strain (Seiler et al. 1997). It is necessary to further assess these preliminary results and determine why this process occurs in early stages where Kinesin-1 does not participate in the establishment of germ tube polarity.

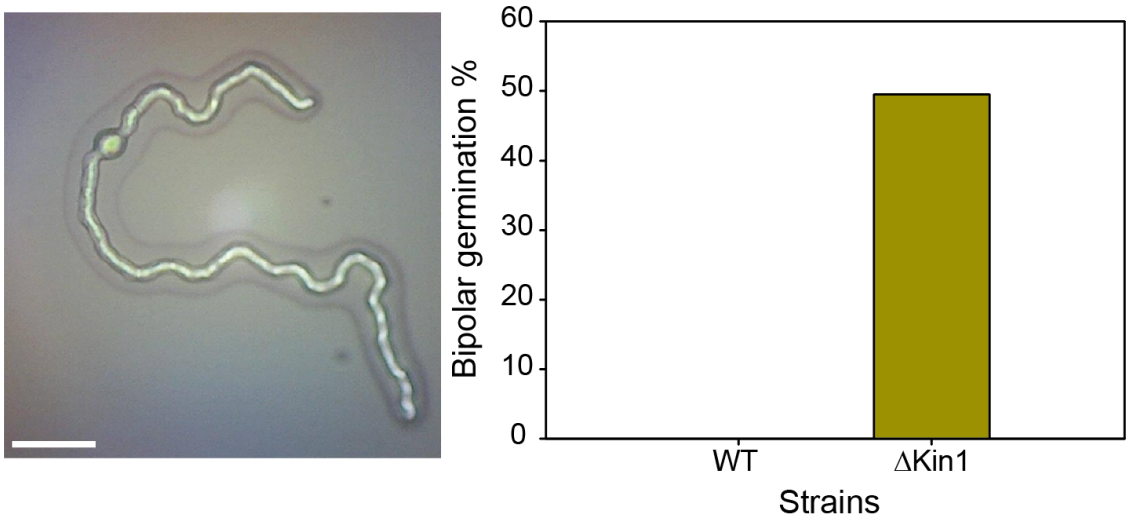

Figure 29. Bipolar germination of ΔKin1 conidia. Left panel, spores of the mutant strain with two germ tubes are observed. Right panel, the graph is observed (normalized with respect to the number of conidia counted) of the percentage of conidia of the mutant strain that present bipolar germination.

3.3.3 Growth morphology

The mutant strains obtained present a similar phenotype, and as can be seen in Figure 30, their growth is notoriously diminished compared to the WT strain; this agrees with that reported in other fungal species with mutations in Kinesin-1 (M. Schuster et al. 2012).

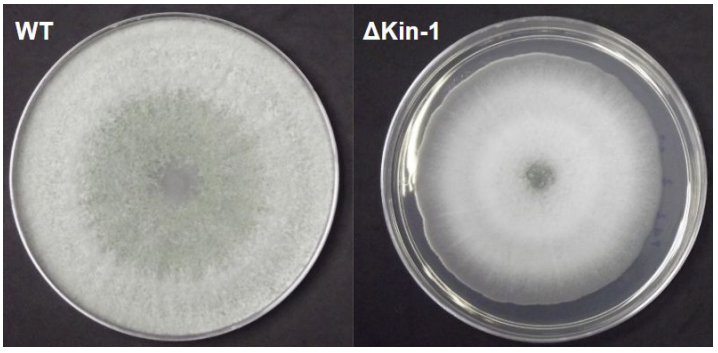

Figure 30. The differences between the WT strain and the ΔKin1 mutant. 72 Hrs after its inoculation with conidia in PDA medium, are observed.

3.3.4 Automated tracking of ΔKin-1

The developed automated tracking method was used to determine the ΔKin-1 growth characteristics. The ΔKin-1 strain presents a characteristic erratic growth

(Figures 31B and 32) that, with the tracking method, (see Chapter 2 section 2.5) allows us to track up to 1 h of growth. Applying the developed method it was determined that ΔKin-1 grows at a characteristic speed of ~ 30 nm/s. This ~ 50% speed reduction agrees with the reported reduction on other Kinesin-1 mutant strains in other filamentous fungi (Seiler et al. 1997; Schuchardt et al. 2005). The most likely explanation for these alterations is a defect in the transport pathway and deployment of secretory vesicles to sites of cell wall formation. Further experiments should be done to test this hypothesis.

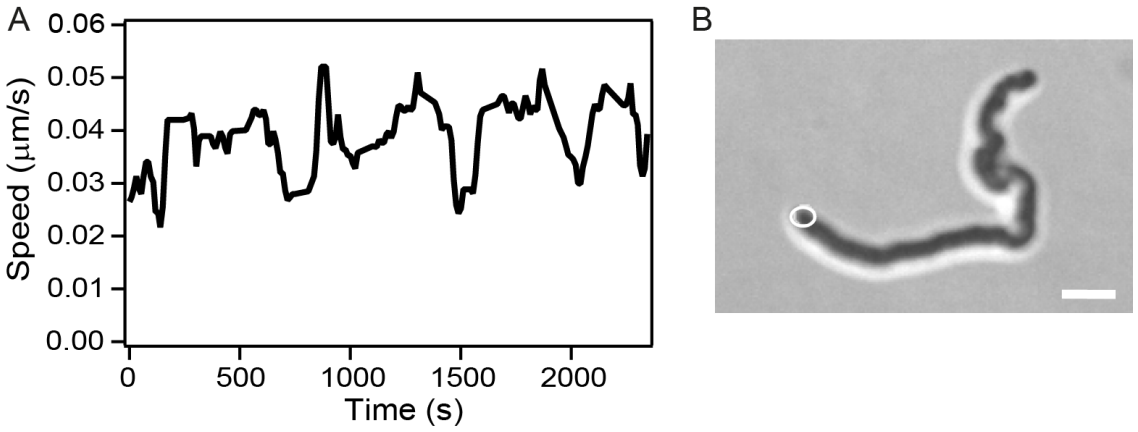

Figure 31. Growth speed and tracking of ΔKin-1 strain of *T. atroviride*. **A)** Graph of hyphal growth speed on ΔKin-1. **B)** Execution of the tracking method on ΔKin-1 using 10x magnification. Scale bar = 20 µm.

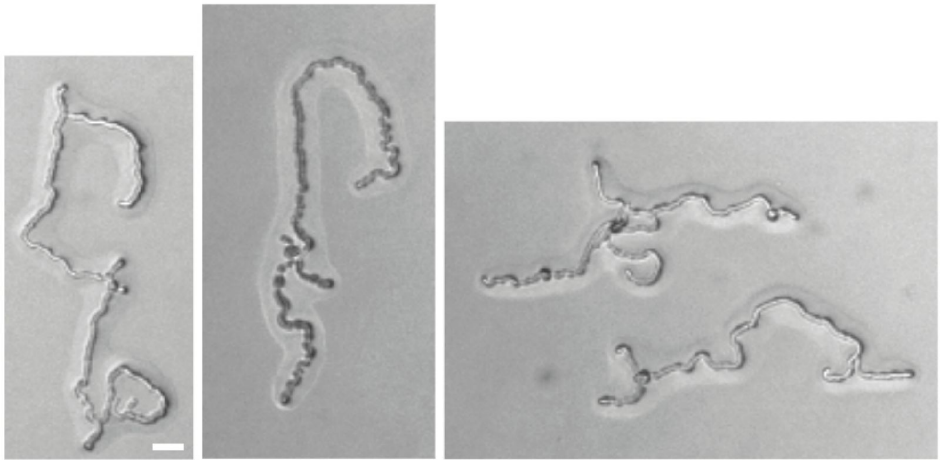

Figure 32. ΔKin-1 characteristic growth. Set of images showing the characteristic growth of ΔKin-1 strain. It presents an erratic growth, which results in hyphae with no defined growth direction. Scale bar = 50 µm.

3.3.5 Lighting experiments

Light / dark experiments were performed to know if the behavior of the mutant strain is modified in dark conditions. The experiment consisted of inoculating WT and ΔKin-1 strains on petri dish with PDA, keeping the strains in the dark for 24 h, then giving a pulse of light corresponding to 1200 µmol, and keeping the strains again in the dark for 48 h. Figure 33 shows the phenotypes presented by the different mutant strains vs WT. As can be seen, the growth of the mutant is similar in the two conditions, however the development of a ring of conidia is very noticeable under light conditions in the mutant strains.

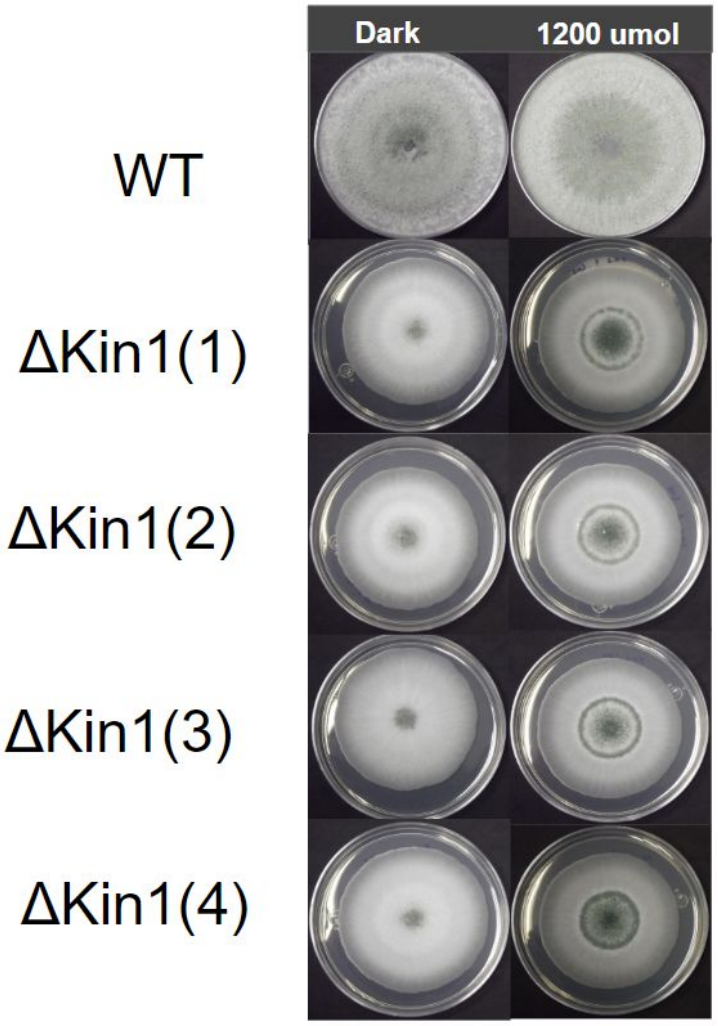

Figure 33. The differences between light and dark conditions of the WT strain vs the ΔKin1 strain are observed. 72 H of growth. PDA medium.

3.3.6 Mass quantification

Mass quantification for the diminished growth of the mutant was performed. One of the first hypotheses was that the observed diminished radial growth phenotype on ΔKin1 was due to the fact that the hyphae remained concentrated in a delimited region but could be growing at a speed similar to the WT strain (similar speed as WT but in a delimited region due to the loss of steady directional growth). The above can be determined, if the total weight of the mutant colonies is quantified. In figure 34, the result of the experiment performed is observed.

It was possible to determine that the weight of the mutant strain is ~ 50% compared to the wild type; probably this means that the observed phenotype is due to the fact that the hyphae can not grow with the same speed as the wild type strain. This data was confirmed with the reported ~ 50% elongation rates from the automated tracking method.

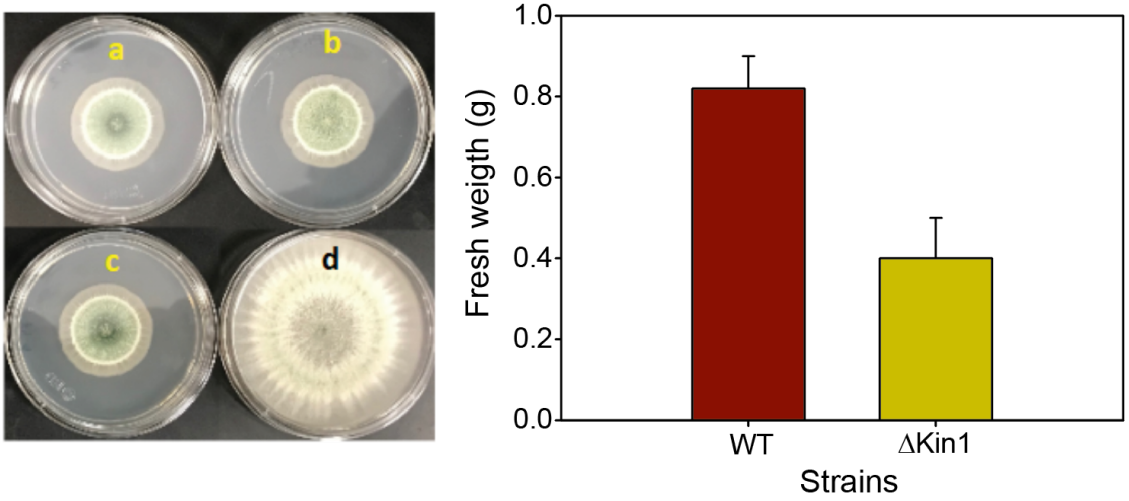

Figure 34. Mass quantification of WT vs ΔKin-1 strains. Left panel, the mutant strains used in the experiment (a, b and c) and the wild strain (d) are observed. Right panel, the fresh weight plot of the mutant strains is observed compared with the wild strain of T. atroviride. 9 replicas were used for each strain.

3.3.7 Conidia counts

To determine if in addition the mutant strain produces a greater quantity of conidia, the concentration of these was quantified (Figure 35). It can be observed that in effect, the observed phenotype of hyper-conidiation is due to the existence of a higher concentration of conidia. This preliminary result suggests that the mutant strain probably branches at a higher rate than the WT, which in turn, promotes the generation of more conidiophores and conidia per area.

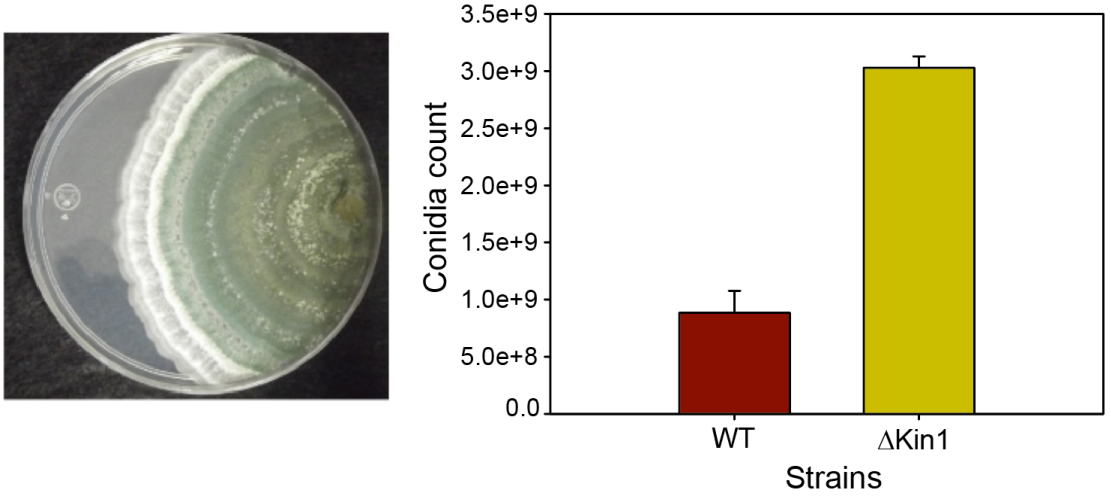

Figure 35. Conidia counts of WT and ΔKin-1 strains. Left panel, the mutant strain and its conidiation phenotype are observed. Right panel, the graph of number of conidia WT vs mutant is observed.

3.3.8 Conidiophore characterization

It is probable that the presented hyper conidiation phenotype is due to the generation of more conidiophore per area. Bright field microscopy was used to analyze this characteristic. On preliminar images (Fig. 36) it was found that ΔKin-1 apparently does present more conidiophore than the WT strain. These

results need to be confirmed by carrying out more bright field microscopy on several hyphae of both strains.

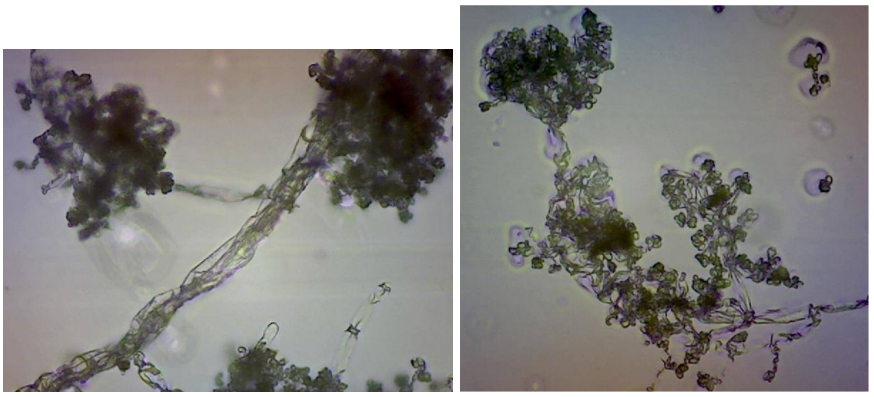

Figure 36. Conidiophore imaging. Left panel, conidiophores corresponding to the WT strain. Right panel, conidiophores corresponding Kin1 mutant strain.

3.3.9 Fluorescence cell wall labeling

To determine if there are differences in the cell wall of the mutant, hyphae were stained with wheat germ agglutinin (WGA, for its acronym in English). In filamentous fungi, it is known that WGA interacts specifically with chitin (Seiler et al. 1997). The majority of the hyphae of the wild type strain (Figure 37, left panel) were preferentially labeled at the apex, while in the mutant (Figure 37, right panel), the fluorescence was observed distributed throughout the hyphae. This agrees with the reported differences between WT and ΔKin-1 strains on *N. crassa (Seiler et al. 1997)*.

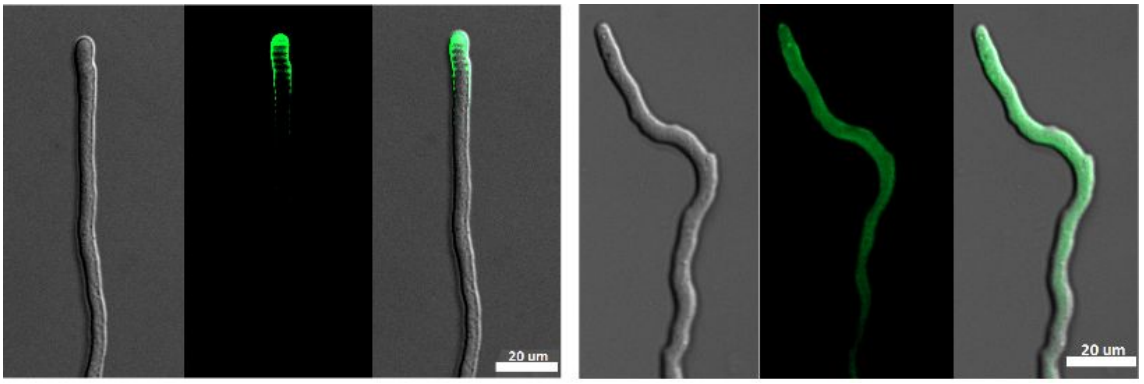

Figure 37. Fluorescence observation of WT and ΔKin-1 strains. Left panel, the wild strain is observed (micrograph by DIC, fluorescence and sum of the two). Right panel, mutant strain is observed (micrograph by DIC, fluorescence and sum of both).

3.3.10 Antibiosis

To assess if the ΔKin-1 strain loses any of its capabilities of secondary metabolite secretion, antibiosis experiments were carried out. A first approach to assess this is to perform an antibiosis experiment, in which 96 h of WT and mutant strain growing mycelium (PDYCB medium) are filtered and keep only the medium with its secreted enzymes and/or metabolites. Next, 60% PDA/ 40% filtrated medium were prepared on petri dishes and inoculate *R. solani*. As seen in figure 38, there is no important difference between *R. solani* growing on WT filtrated medium vs Kin1 mutant strain medium.

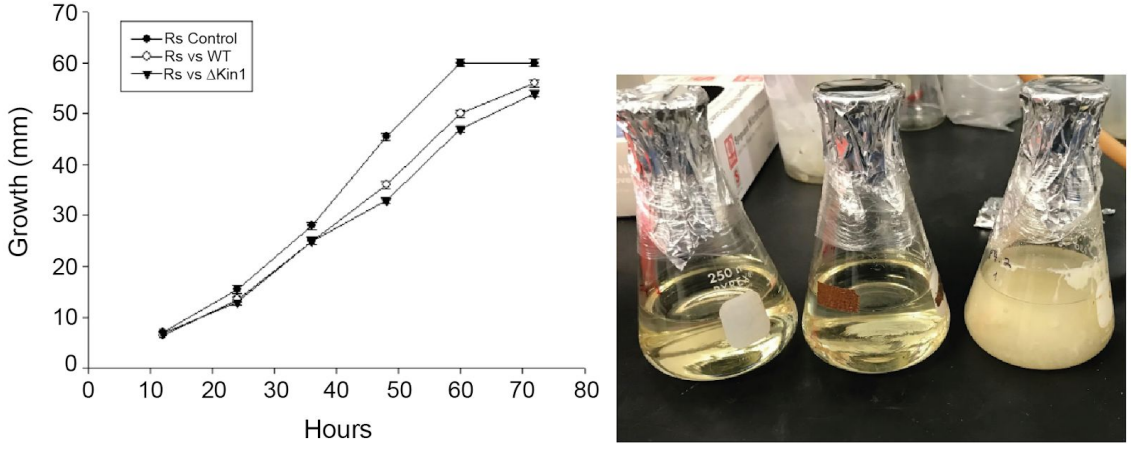

Figure 38. Antibiosis experiment. Left panel, growth in mm as a function of growth in h. No major differences between the growth of *R. solani* in WT filtrates vs ΔKin1 strain filtrates were detected. Right panel, PDYCB medium before (right side flask) filtration and after (left and center flask).

3.3.11 Confrontation capabilities

It is of interest to know if the mycoparasitic capacity of *T. atroviride* is affected in the absence of Kinesin-1. Experiments of mutant confrontation vs *R. solani* (Fig

39) were carried out. These experiments help us determine if Kinesin-1 can indirectly participate in the mycoparasitic capacity of *T. atroviride.* It is hypothesized that the diminished growth presented by ΔKin1 strain over *R. solani* is due to its low growth kinetics.

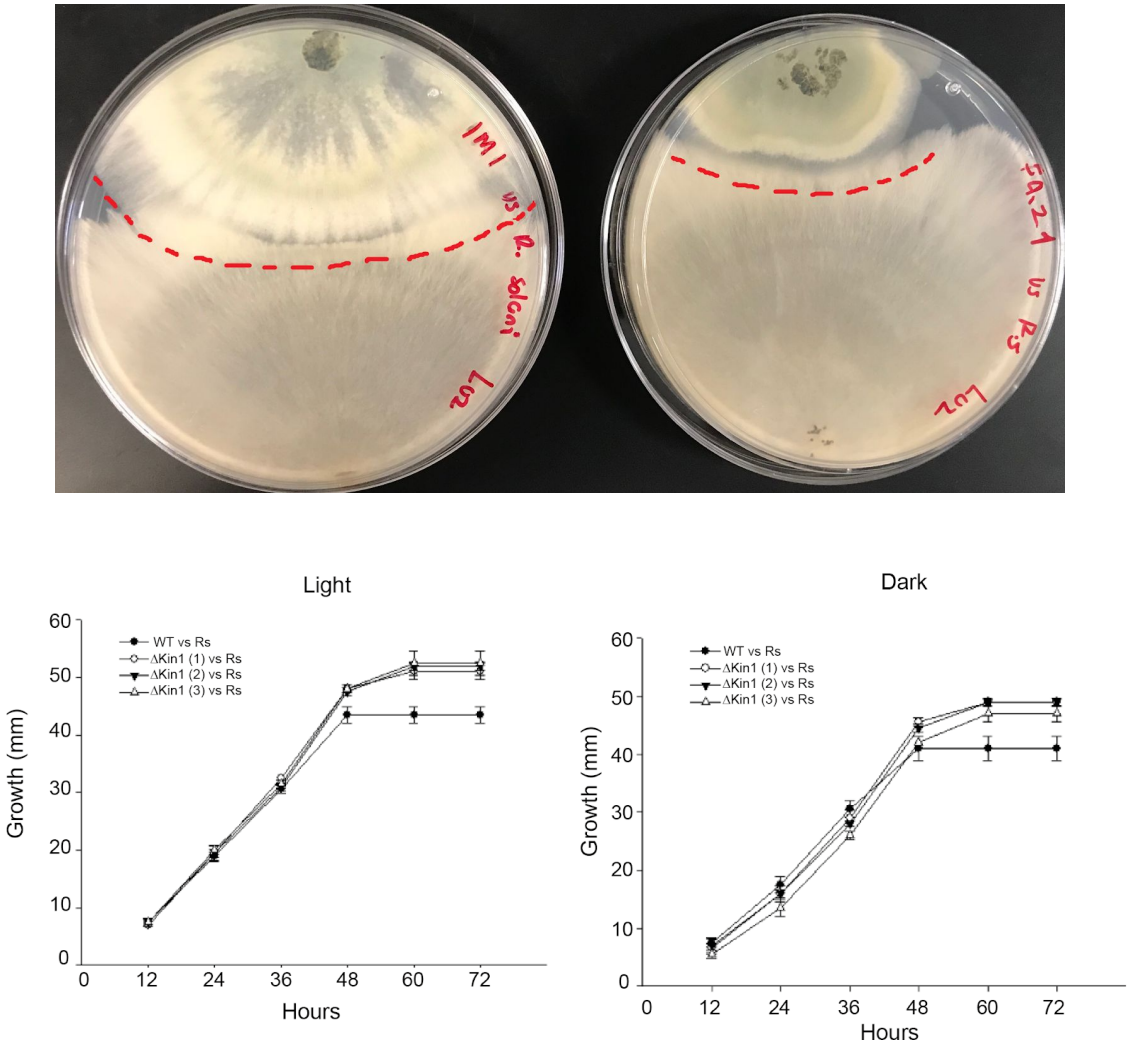

Figure 39. Confrontation capabilities. Upper panel, WT strain vs *R. solani* on the left side (*T. atroviride* on the upper side of the Petri Dish), ΔKin1 mutant strain vs *R. solani* on the right side (ΔKin1 on the upper side of the Petri Dish). A decrease in the ability to grow over *R. solani* hyphae accomplished by the mutant strain compared to WT strain is seen. Dashed red lines, growth reach of WT or mutant strain. Lower panel, comparison of *R. solani* growth vs WT and the different ΔKin1 strains under light (left side) and dark (right) conditions.

3.3.12 Conclusions

By developing a ΔKinesin-1 strain, it was studied how the absence of Kinesin-1, one of the main nano-motors transporter of essential growth vesicles affects hyphal elongation, branching and morphology of *T. atroviride*. Several morphological experiments were carried out following *T. atroviride* growth stages (germination, vegetative growth and conidiation) and determined that: The absence of Kinesin-1 modifies *T. atroviride* germination resulting in ~50% of conidia presenting bipolar germination. Vegetative growth is highly decreased with respect to the WT strain with characteristic elongation rates of ~ 30 nm/s vs ~70 nm/s WT. Conidiation is also modified with ΔKinesin-1 producing ~30x10^8 conidia vs ~8x10^8 WT.

In conclusion, these preliminary results show how the absence of the nano-motor Kinesin-1 results in high modifications of hyphal growth in *T. atroviride*. The results observed in *T. atroviride* morphological stages suggests a defect in the long-range transport and correct delivery of secretory vesicles required for normal hyphal growth during the absence of Kinesin-1, as reported for other filamentous fungi. The most likely explanation for these alterations is a defect in the transport pathway and deployment of secretory vesicles to sites of cell wall formation. This defects needs to be assessed more clearly in future studies.

3.4 Future Work

It is of great importance to further assess how the absence of Kinesin-1 affects the growth of *T. atroviride*. The latter, by generating a fluorescence labeled strain of *T. atroviride* that would allow to gain insight on how the dynamics of Kinesin-1 change on the different growth stages of *T. atroviride*. On the germination process, this approach is expected to help to understand why is the germination delayed on ΔKin-1 by screening if Kinesin-1 is playing a role on germination. On elongation and branching it would be possible to visualize the spatial localization of Kinesins prior, during and after a branching has occurred.

Insights into which transport activities fail when Kinesin-1 is lost can be gained from a closer examination of the null phenotype. Overall, this would help us to further gain insight on the importance of Kinesin-1 in fungal growth.

Chapter 4. Final Comments

In this work, the development of an accessible video microscopy method that allows real-time continuous tracking of a single hypha was presented. The system operates in an automated fashion over extended periods of time (up to 14 h) with a sampling time interval of 1.3 s. The quantitative value of this method was tested by obtaining the growth speed and the persistence length associated to hyphae of *T. atroviride*.

In particular, It is shown how tangent angle correlation can provide information on the characteristic distance of hyphal elongation before changes in directions occur and the average angle between parental and branching hyphae. The temporal sampling rate of the developed system allowed detecting branching dynamics not previously reported. This methodology should prove useful for the analysis of fungal hyphae growth dynamics under different treatments, conditions or strains.

Regarding the role of the nano-motor Kinesin-1 in the growth of *T. atroviride*, by developing a ΔKinesin-1 strain, it was studied how the absence of Kinesin-1, affects hyphal elongation, branching and morphology of *T. atroviride*. Several morphological experiments were carried out following *T. atroviride* growth stages (germination, vegetative growth and conidiation) and determined that: The absence of Kinesin-1 modifies *T. atroviride* germination resulting in ~50% of conidia presenting bipolar germination. Vegetative growth is highly decreased with respect to the WT strain with characteristic elongation rates of ~ 30 nm/s vs ~70 nm/s WT. Conidiation is also modified with ΔKinesin-1 producing ~$30x10^8$ conidia vs ~$8x10^8$ WT.

In conclusion, these preliminary results show how the absence of the nano-motor Kinesin-1 results in high modifications of hyphal growth in *T. atroviride*. The results observed in *T. atroviride* morphological stages suggests

a defect in the long-range transport and correct delivery of secretory vesicles required for normal hyphal growth during the absence of Kinesin-1, as reported for other filamentous fungi. The most likely explanation for these alterations is a defect in the transport pathway and deployment of secretory vesicles to sites of cell wall formation. This defects needs to be assessed more clearly in future studies.

REFERENCES

Ahamed, Aftab, and Patrick Vermette. 2009. “Effect of Culture Medium Composition on Trichoderma Reesei’s Morphology and Cellulase Production.” *Bioresource Technology* 100 (23): 5979–87.

Alberts, Bruce. 2017. *Molecular Biology of the Cell*. Garland Science.

Baek, J. M., and C. M. Kenerley. 1998. “The arg2 Gene of Trichoderma Virens: Cloning and Development of a Homologous Transformation System.” *Fungal Genetics and Biology: FG & B* 23 (1): 34–44.

Barry, David. 2010. “Development of Novel Image Analysis Methods for the Morphological Quantification of Filamentous Fungi,” Doctoral, . https://doi.org/10.21427/D7730D.

Berliner, E., E. C. Young, K. Anderson, H. K. Mahtani, and J. Gelles. 1995. “Failure of a Single-Headed Kinesin to Track Parallel to Microtubule Protofilaments.” *Nature* 373 (6516): 718–21.

Blasius, T. Lynne, Nathan Reed, Boris M. Slepchenko, and Kristen J. Verhey. 2013. “Recycling of Kinesin-1 Motors by Diffusion after Transport.” *PloS One* 8 (9): e76081.

Block, S. M., L. S. Goldstein, and B. J. Schnapp. 1990. “Bead Movement by Single Kinesin Molecules Studied with Optical Tweezers.” *Nature* 348 (6299): 348–52.

Block, Steven M., Charles L. Asbury, Joshua W. Shaevitz, and Matthew J. Lang. 2003. “Probing the Kinesin Reaction Cycle with a 2D Optical Force Clamp.” *Proceedings of the National Academy of Sciences of the United States of America* 100 (5): 2351–56.

Boswell, Graeme P., and Steven Hopkins. 2008. “Linking Hyphal Growth to Colony Dynamics: Spatially Explicit Models of Mycelia.” *Fungal Ecology* 1 (4): 143–54.

Brunk, Michael, Sebastian Sputh, Sören Doose, Sebastian van de Linde, and Ulrich Terpitz. 2018. “HyphaTracker: An ImageJ Toolbox for Time-Resolved Analysis of Spore Germination in Filamentous Fungi.” *Scientific Reports* 8 (1): 605.

Casas-Flores, Sergio, Mauricio Rios-Momberg, Martha Bibbins, Patricia Ponce-Noyola, and Alfredo Herrera-Estrella. 2004. “BLR-1 and BLR-2, Key Regulatory Elements of Photoconidiation and Mycelial Growth in Trichoderma Atroviride.” *Microbiology* 150 (Pt 11): 3561–69.

CHET, and I. 1987. “Trichoderma: Application, Mode of Action, and Potential as Biocontrol Agent of Soilborne Plant Pathogenic Fungi.” *Innovative Approaches to Plant Disease Control*, 137–60.

Christiansen, Torben, Anders B. Spohr, and Jens Nielsen. 1999. “On-Line Study of Growth Kinetics of Single Hyphae of Aspergillus Oryzae in a Flow-through Cell.” *Biotechnology and Bioengineering* 63 (2): 147–53.

Desai, A., and T. J. Mitchison. 1997. “Microtubule Polymerization Dynamics.” *Annual Review of Cell and Developmental Biology* 13: 83–117.

Diano, A., J. Peeters, J. Dynesen, and J. Nielsen. 2009. “Physiology of Aspergillus Niger in Oxygen-Limited Continuous Cultures: Influence of Aeration, Carbon Source Concentration and Dilution Rate.” *Biotechnology and Bioengineering* 103 (5): 956–65.

Egan, Martin J., Mark A. McClintock, and Samara L. Reck-Peterson. 2012. “Microtubule-Based Transport in Filamentous Fungi.” *Current Opinion in Microbiology* 15 (6): 637–45.

El-Sabbagh, Nasser, Linda M. Harvey, and Brian McNeil. 2008. “Effects of Dissolved

Carbon Dioxide on Growth, Nutrient Consumption, Cephalosporin C Synthesis and Morphology of Acremonium Chrysogenum in Batch Cultures." *Enzyme and Microbial Technology* 42 (4): 315–24.
Enfert, Christophe d'. 1997. "Fungal Spore Germination: Insights from the Molecular Genetics ofAspergillus nidulansandNeurospora Crassa." *Fungal Genetics and Biology: FG & B* 21 (2): 163–72.
Fletcher, Daniel A., and R. Dyche Mullins. 2010. "Cell Mechanics and the Cytoskeleton." *Nature* 463 (7280): 485–92.
Gelles, J., B. J. Schnapp, and M. P. Sheetz. 1988. "Tracking Kinesin-Driven Movements with Nanometre-Scale Precision." *Nature* 331 (6155): 450–53.
Hancock, W. O., and J. Howard. 1998. "Processivity of the Motor Protein Kinesin Requires Two Heads." *The Journal of Cell Biology* 140 (6): 1395–1405.
Held, Marie, Clive Edwards, and Dan V. Nicolau. 2011. "Probing the Growth Dynamics of Neurospora Crassa with Microfluidic Structures." *Fungal Biology* 115 (6): 493–505.
Herrera-Estrella, Alfredo, and Benjamin A. Horwitz. 2007. "Looking through the Eyes of Fungi: Molecular Genetics of Photoreception." *Molecular Microbiology* 64 (1): 5–15.
Holzbaur, Erika L. F., and Yale E. Goldman. 2010. "Coordination of Molecular Motors: From in Vitro Assays to Intracellular Dynamics." *Current Opinion in Cell Biology* 22 (1): 4–13.
Howard, J., A. J. Hudspeth, and R. D. Vale. 1989. "Movement of Microtubules by Single Kinesin Molecules." *Nature* 342 (6246): 154–58.
Howard, Jonathon, and Others. 2001. "Mechanics of Motor Proteins and the Cytoskeleton." https://publications.mpi-cbg.de/213.pdf.
Kossen, N. W. F. 2000. "The Morphology of Filamentous Fungi." In *History of Modern Biotechnology II*, edited by A. Fiechter, 1–33. Berlin, Heidelberg: Springer Berlin Heidelberg.
Kozielski, F., S. Sack, A. Marx, M. Thormählen, E. Schönbrunn, V. Biou, A. Thompson, E. M. Mandelkow, and E. Mandelkow. 1997. "The Crystal Structure of Dimeric Kinesin and Implications for Microtubule-Dependent Motility." *Cell* 91 (7): 985–94.
Lecault, Véronique, Nilesh Patel, and Jules Thibault. 2007. "Morphological Characterization and Viability Assessment of Trichoderma Reesei by Image Analysis." *Biotechnology Progress* 23 (3): 734–40.
Lillie, S. H., and S. S. Brown. 1998. "Smy1p, a Kinesin-Related Protein That Does Not Require Microtubules." *The Journal of Cell Biology* 140 (4): 873–83.
Lim, Jung Soo, Jong Ho Lee, Jung Mo Kim, Seung Won Park, and Seung Wook Kim. 2006. "Effects of Morphology and Rheology on Neofructosyltransferase Production byPenicillium Citrinum." *Biotechnology and Bioprocess Engineering: BBE* 11 (2): 100.
Lopez-Franco, Rosamaria, Salomon Bartnicki-Garcia, and Charles E. Bracker. 1994. "Pulsed Growth of Fungal Hyphal Tips." *Proceedings of the National Academy of Sciences* 91 (25): 12228–32.
Lübbehüsen, Tina Louise, Jens Nielsen, and Mhairi Mcintyre. 2003. "Characterization of the Mucor Circinelloides Life Cycle by on-Line Image Analysis." *Journal of Applied Microbiology* 95 (5): 1152–60.
Luby-Phelps, K. 2000. "Cytoarchitecture and Physical Properties of Cytoplasm: Volume, Viscosity, Diffusion, Intracellular Surface Area." *International Review of Cytology* 192: 189–221.
Mostowy, Serge, and Pascale Cossart. 2012. "Septins: The Fourth Component of the Cytoskeleton." *Nature Reviews. Molecular Cell Biology* 13 (3): 183–94.

Oliver, S. G., and A. P. J. Trinci. 1985. “Modes of Growth of Bacteria and Fungi.” *Comprehensive Biotechnology : The Principles, Applications, and Regulations of Biotechnology in Industry, Agriculture, and Medicine / Editor-in-Chief, Murray Moo-Young*. http://agris.fao.org/agris-search/search.do?recordID=US201301446197.

Packer, H. L., and C. R. Thomas. 1990. “Morphological Measurements on Filamentous Microorganisms by Fully Automatic Image Analysis.” *Biotechnology and Bioengineering* 35 (9): 870–81.

Park, Hee-Soo, and Jae-Hyuk Yu. 2012. “Genetic Control of Asexual Sporulation in Filamentous Fungi.” *Current Opinion in Microbiology* 15 (6): 669–77.

Paul, G. C., and C. R. Thomas. 1998. “Characterisation of Mycelial Morphology Using Image Analysis.” *Advances in Biochemical Engineering/biotechnology* 60: 1–59.

Peberdy, John F. 1980. “Vegetative Growth of Filamentous Fungi.” In *Developmental Microbiology*, edited by John F. Peberdy, 44–68. Boston, MA: Springer US.

Ray, S., E. Meyhöfer, R. A. Milligan, and J. Howard. 1993. “Kinesin Follows the Microtubule’s Protofilament Axis.” *The Journal of Cell Biology* 121 (5): 1083–93.

Real-Time PCR. 2006. Taylor & Francis.

Requena, N., C. Alberti-Segui, E. Winzenburg, C. Horn, M. Schliwa, P. Philippsen, R. Liese, and R. Fischer. 2001. “Genetic Evidence for a Microtubule-Destabilizing Effect of Conventional Kinesin and Analysis of Its Consequences for the Control of Nuclear Distribution in Aspergillus Nidulans.” *Molecular Microbiology* 42 (1): 121–32.

Rice, S., A. W. Lin, D. Safer, C. L. Hart, N. Naber, B. O. Carragher, S. M. Cain, et al. 1999. “A Structural Change in the Kinesin Motor Protein That Drives Motility.” *Nature* 402 (6763): 778–84.

Riquelme, Meritxell. 2013. “Tip Growth in Filamentous Fungi: A Road Trip to the Apex.” *Annual Review of Microbiology* 67 (June): 587–609.

Riquelme, Meritxell, and Salomon Bartnicki-Garcia. 2004. “Key Differences between Lateral and Apical Branching in Hyphae of Neurospora Crassa.” *Fungal Genetics and Biology: FG & B* 41 (9): 842–51.

Riquelme, M., C. G. Reynaga-Peña, G. Gierz, and S. Bartnicki-García. 1998. “What Determines Growth Direction in Fungal Hyphae?” *Fungal Genetics and Biology: FG & B* 24 (1-2): 101–9.

Rosales-Saavedra, T., E. U. Esquivel-Naranjo, S. Casas-Flores, P. Martínez-Hernández, E. Ibarra-Laclette, C. Cortes-Penagos, and A. Herrera-Estrella. 2006. “Novel Light-Regulated Genes in Trichoderma Atroviride: A Dissection by cDNA Microarrays.” *Microbiology* 152 (Pt 11): 3305–17.

Samapundo, Simbarashe, Frank Devlieghere, Bruno De Meulenaer, and Johan Debevere. 2007. “Growth Kinetics of Cultures from Single Spores of Aspergillus Flavus and Fusarium Verticillioides on Yellow Dent Corn Meal.” *Food Microbiology* 24 (4): 336–45.

Schuchardt, Isabel, Daniela Assmann, Eckhard Thines, Christian Schuberth, and Gero Steinberg. 2005. “Myosin-V, Kinesin-1, and Kinesin-3 Cooperate in Hyphal Growth of the Fungus Ustilago Maydis.” *Molecular Biology of the Cell* 16 (11): 5191–5201.

Schuster, André, and Monika Schmoll. 2010. “Biology and Biotechnology of Trichoderma.” *Applied Microbiology and Biotechnology* 87 (3): 787–99.

Schuster, Martin, Steffi Treitschke, Sreedhar Kilaru, Justin Molloy, Nicholas J. Harmer, and Gero Steinberg. 2012. “Myosin-5, Kinesin-1 and Myosin-17 Cooperate in Secretion of Fungal Chitin Synthase.” *The EMBO Journal* 31 (1): 214–27.

Seiler, S., J. Kirchner, C. Horn, A. Kallipolitou, G. Woehlke, and M. Schliwa. 2000. “Cargo Binding and Regulatory Sites in the Tail of Fungal Conventional Kinesin.”

Nature Cell Biology 2 (6): 333–38.
Seiler, S., F. E. Nargang, G. Steinberg, and M. Schliwa. 1997. “Kinesin Is Essential for Cell Morphogenesis and Polarized Secretion in Neurospora Crassa.” *The EMBO Journal* 16 (11): 3025–34.
Spohr, Anders, Carsten Dam-Mikkelsen, Morten Carlsen, Jens Nielsen, and John Villadsen. 1998. “On-Line Study of Fungal Morphology during Submerged Growth in a Small Flow-through Cell.” *Biotechnology and Bioengineering* 58 (5): 541–53.
Steinberg, Gero. 2011. “Motors in Fungal Morphogenesis: Cooperation versus Competition.” *Current Opinion in Microbiology* 14 (6): 660–67.
Tabb, J. S., B. J. Molyneaux, D. L. Cohen, S. A. Kuznetsov, and G. M. Langford. 1998. “Transport of ER Vesicles on Actin Filaments in Neurons by Myosin V.” *Journal of Cell Science* 111 (Pt 21) (November): 3221–34.
Tevfik Dorak, M. 2007. *Real-Time PCR*. Taylor & Francis.
Trinci, A. n.d. “P. J.(1974). A Study of the Kinetics of Hyphal Extension and Branch Initiation of Fungal Mycelia.” *Journal of General Microbiology* 81: 225–36.
Vale, R. D., T. S. Reese, and M. P. Sheetz. 1985. “Identification of a Novel Force-Generating Protein, Kinesin, Involved in Microtubule-Based Motility.” *Cell* 42 (1): 39–50.
Vale, Ronald D. 2003. “The Molecular Motor Toolbox for Intracellular Transport.” *Cell* 112 (4): 467–80.
Verhey, Kristen J., and Jennetta W. Hammond. 2009. “Traffic Control: Regulation of Kinesin Motors.” *Nature Reviews. Molecular Cell Biology* 10 (11): 765–77.
Verhey, Kristen J., Neha Kaul, and Virupakshi Soppina. 2011. “Kinesin Assembly and Movement in Cells.” *Annual Review of Biophysics* 40: 267–88.
Visscher, K., M. J. Schnitzer, and S. M. Block. 1999. “Single Kinesin Molecules Studied with a Molecular Force Clamp.” *Nature* 400 (6740): 184–89.
Yu, Jae-Hyuk, Zsuzsanna Hamari, Kap-Hoon Han, Jeong-Ah Seo, Yazmid Reyes-Domínguez, and Claudio Scazzocchio. 2004. “Double-Joint PCR: A PCR-Based Molecular Tool for Gene Manipulations in Filamentous Fungi.” *Fungal Genetics and Biology: FG & B* 41 (11): 973–81.

Appendix A. Designed oligonucleotides and full sequence used for the amplification of Kin-1

ID 5KIN-FW GCGCAGTTTACTTAACGATCCC

TaKin1-FW GAAAGTAGCTGGGACGACTAAA

KIN1-Fw TAAATTGACCCGTATCCTCCAGG

Kin1-Rv (5-3') ACAGAGAAAGAATCGCTGGCTGC

ID 3Kin-Rv (5-3') ATTTCCGTTGCTAGGAAGGGG

CTTTCGAAGATGGCACATTCCGACTCGTCATGCAGTTTGAAGAACAATACCCAAATAAGCCTCCCCAGGTCAAATTCATCAGCCAAATGTTCCACCCCAACG
TATACGCCACCGGCGAGCTGTGCTTGGACATTCTGCAAAACCGATGGAGTCCGACGTACGACGTTGCTGCTGTATTGACTAGCATCCAGAGGTATGGACACG
GACATGTGTGATGGAGTGCTTTATACATCGTCTACTGCCTCGATGCATTTTTGGCTAACTTGAAGCGAATCACTGCGCAGTTTACTTAACGATCCCAACACT
GGTTCACCAGCAAACGTCGAGGCCTCGAATCTTTACAAAGATAACAGAAAGGAGTATACCAAGCGTGTCCGAGCAACTGTTGAAAGTAGCTGGGACGACTAA
AAAGGATTACATCAAGATGGAAGTACTGAGGAATTATGTGTACCCAAGGCTTCACATGAATCCCAGGTCTACTACACCATCTGAATTCGGATTGTGGACTCA
GTCTGTCAGATCTTTTTGATATGACATGCTGTCCACGAGAGCTTGGAGCTTGATAGAAGGATGGAGAAGATTCATTGCAGGCGTTCTGGTGCACGAGATTGA
ACTGGTTATACCAAGGGAAGGAGGATGAATGCTCGCTTTTGCTCGATATTTTTTTTTTTTTGGTCTTATTTTCTCCTACAGTAATCTAGCGTTTGTTTTTGG
TATCCTCGTCATAGTGGCGTGGATGGCTGGCGAACGAGACATAGGTAGTAGTTATTCAGCGGCGATGGATTGTCAAAACCTTCTTTTTTTTCCAAACTGTTT
TTCTTTCTCATTTTCTTATGGCATACAAAAAGGAAGTGTCAAGTAATCCAACGTGATGATGAAGGTATATGTGACTTGCAAACAGCCACATCTCTCCATTTT
CAACAGAGCCTATACGTTGAACATGGCAAACCAACTTTCTTATTGGGGTAGTCTCTGGCCAGGTATATGAGTAGAATAGAATAGAATAGGATGGGCAGCGGG
CATCGGGCATCGGATTTCAGGTCTGCCTGTCAACACGATTCAGCCACTCACATGTGTCTGCACCAAGTTGGGTCAAAGCCAATCCCAACCCATTGCCTGTAT
CAGCCACCGGCCACTAGCCACTCAGACACCTTTGAGAGCTTCTTCATGATGACACGCTAAGACAAAAGAGAACACGGTTGGCTGCAATCCAGCCCCTGACAG
ACTCGACGATTTTGTGGTTTTCCACTGACGCCATGGCAACATAGAATGGCCAACGCAGATAGCCAGCAGATAGTACTGCCTCGATGACGATGGCCATCTATT
AACGAGGTAGTAAATTTACATATTTGTTTCTCGACCTTGTTTTTAAAACTCTCTGCCATGTTGAAGCTCCTCTAGGTCCAGGAACAAGTTGGCATCTAGTAT
TTAGTCTCCAGCTACCGGCGGCACCTCTTCAGGCGGCTGACCTCCAGCAAAACAGCCCCTCACCCTCCTCATCTTCAGGGCTTCTGGCGGCACCCTCAACCA
CCACGCGGCGACTGCTTTTAGCGCGCTTGTCACCACCGAAACAACCACATTGGCCCTGAACTTTTGGGTCCCCTCCCCGCCAGCCCTTCCCAGACCGCCGTT
CCTATTGCATCCCTAGAACCTCTATTTGTCTTGTGTCTTTTGGATTTTTTTTTCTTCTAACCTCTTCTCTTTTTTCCTCATACTTGTTGTTCTCTTCCCCCC
CTTTTCTCCCCTTAACCACTGATCCTGCGGCGGGGGTTTTTCTTGTTTCTCGTCGTCGCTCGCAGCTTCGATTAGCGATTGCCCGCCTTTGTTTTGTTTCTTC
TTTTTGGCCCCTCTCTCCGTCGGTGGAGCAGCTATCGGAGCCCGCCATTTGGGATCAAGAGAGGACAAGAGAGAGTCTCTGCCAGGAGATAGCGACTTCTCC
TCCTCCCAAGATCGACGGCCTTGCTTGATATCGATCCAACTGCCCAACGCCAACCGCCCACCATGTCAAACAACACCATCAAGGTCGTCGCCCGGTTCAGGC
CCCAGAACCGGATCGAAATCGAATCGGGCGGCAAGCCAATCGTCGCCTTCAGCTCCGAGGACACTTGCACACTTGACGTATGGCTCTCCTCCACCTGAAAGA
CCACATCAAAGCTCACTGCAGAGCTGCGATGATGGCAATACAAGGCTCTCCGCTAACCGTGGCCATGCTCGCTGTAGTCCAAAGAGGCGCAGGGTTCCTTCA
CCTTCGACCGAATCTTTGACATGTCAAGTAGACAACAAGACATCTTCGACTACTCCATTCGCCCAACCGTCGACGATATTCTCAATGGCTACAACGGTACCG
TCTTTGCCTACGGCCAGACTGGTGCTGGTAAATCATACACCATGATGGGCAACATGGACGATCCCGAGCAGAGGGGTGTTATTCCGCGCATCGTCGAGCAAA
TCTTTGCCAGCATCATGTCCAGCCCCAGCACCATCGAGTACACTGTCCGCGTCAGCTACATGGAAATTTACATGGAGAAGATTCGTGATCTGCTCGCCCCTC
AAAACGACAATCTCCCCATCCACGAGGAGAAGAACCGCGGAATTTACGTCAAAGGCCTCCTAGAAATCTATGTCTCCAGCGTCCAAGAAGTGTACGAAGTGA
TGAGGAGGGGAGGTAATGCCCGAGTGGTCTCTTCCACCAACATGAACGCAGAGTCATCACGATCCCACTCCATCTTCGTCGTTACCATTACCCAGAAGAATG
TCGAGACTGGTTCGGCCAAGAGCGGTCAGCTGTTCTTGGTTGATTTGGCTGGTAGTGAAAAGGTCGGCAAGACGGGTGCCAGCGGCCAGACGCTTGAGGAAG
CCAAGAAGATCAACAAAAGTTTGAGTGCCTTGGGTATGGTCATCAACGCCCTGACCGACGGCAAATCTCACTTTGTCCCCTACCGAGACTCTAAATTGACCC
GTATCCTCCAGGAATCTCTGGGTGGTAACAGTCGAACTACTCTCATCATCAACTGCTCTCCCAGCAGTTACAACGACTCTGAAACTCTGGGAACGCTGAGAT
TCGGTACCAGAGCAAAGTCTATTAAGAACAAAGCCAAGGTCAATGCCGAGCTCAGCCCAGCAGAGCTCAAGGCTCTGCTCAAGAAAGCCCAAGGCCAAGTTA
CCAATTTCGAATCTTACATTTCCAATCTCGAAGGCGAAATCCAAATGTGGCGAGCTGGAGAGGCTGTGCCCAAAGACAAGTGGGTTCAGCCCACTGCTGATG
GTGTTGTTGCAGCCAAGGCCGAAGCGAGAGCACCGCGGCCATCAACTCCTTCACGGCTTACAGAAAGCCGCTCAGAGACTCCCATCGCTTCTGATCGTGCTG
GCACCCCCAGCATAACGCTGGAAAAGGATGAGCGGGAAGAGTTCCTGCGCCGCGAAAATGAGCTGCAAGACCAACTTACAGAGAAAGAATCGCTGGCTGCGA
CGGCTGAGAAGCAACTTCGCGAAACCAAAGATGAACTTTCTTTCTTGAAGGAGCACGATAGCAAGATAGGCAAGGAGAATGAGAAGCTGACCACTGAGGTGA
ATGAATTCAAGATGCAGCTGGAGCGGCTGAATTTCGAGGGTAAAGAGGCTCAAATCACCATGGATGCCCTCAAAGAAGCCAACTCGGAACTCACAACTGAGC
TGGACGATATGAAACAGCAATTGTTGGACGCCAAGATGAGCGCTAAAGAGACGGGTGCTGCCCTTGATGAGAAGGAAAAGAAGAAGGCCGAGAAGATGGCCA
AGATGATGGCTGGCTTCGAACTCGGAACCGATGTTTTCAGCGAAAATGAGCGATCTATTGCTGAAACTATCAAGCACATTGATGCCCTGCTCGAACAGAGCT
CAATCGGCGATCACATTGCACCAGACGAGTTCAAGGTACTCCGAGCAAAGATGGTCGAGACTCAGGGCATCGTGAGACAAGCAGAGCTGTCCATGTACAGCG
GATCATCTAACGATCTGGATGCCCGACGGAGGCAGGAGCTTGAGGCTAAGATGGAGGCCTTGCAACAAGAATACGAGGAAGTATTGACACGCAATCTCAGCG
AGGCCGATGTGGAAGAGGTCAAGGCACGACTAGAAGCCGTCTACGCTAAACGCGAGAAGTCTGAGACTCAGCTTGTCGAAGAGCTCAAGGCTGATCTGAACC
AAAAGGCTTCTGAGAACGCAAGGATGAAGACTCTCATCGAGGAGCTTCAGCAGCGCGTCAAGGCTGGCGGCGCCGGTGCCATGGCCAATGGCAAGACTGTCC
AACAGCAGATTGCCGAGTTTGACGTGATGAAGAAGAGTCTCATGCGAGATTTGCAGAACCGCTGCGAGCGTGTCGTCGAGCTGGAGATTTCACTCGACGAGA
CCCGCGAGCAGTACAACAACGTGCTGCGGACATCCAACAACCGTGCTCAGCAGAAGAAGATGGCCTTCCTGGAGAGGAATCTGGAGCAGCTTACCCAGGTTC
AACGCCAGCTGGTTGAGCAGAACTCTTCCCTGAAGAAGGAAGTTGCCATTGCCGAGCGTAAACTCATTGCGAGAAACGAGCGCATCCAGAGTCTGGAGAGCC
TGCTGCAAGACAGCCAGGAGAAGATGGCAACTGCCAATCACAAGTACGTATCACCCGTCATCTTCCCCCTTTTTTTTTTCATTCTCTGTGACGGCAGCACAT
CATCAATGGATTGCCAGTAAAAGAAACATGATAAAACGCTTGGTGCTGACCTAGACTCCCCCCCTATCTAGGTTCGAGGTCCAACTTGCTTCCGTCAAGGAG
CGCCTCGAGGCTGCCAAAGCTGGCAGCACCCGTGGCCTTGGTGGTGCCGGCGGCTTCAGCTTCTCTGGCGCTGGTAGCCGCATCGCCAAGCCTCTGCGTGGC
GGCGGCGGCGATGCCCCCTCGACCCCCACGATCCAAGGCGGCGACGGAACCAGCAGCAAGCGCGGTAGTTGGTTCTTCAACAAGTCGTAGATTTCTTTTTTT
ACAAAAGAAAACCTGCGTTCTTCCGGAACGGCGTTATGACATACACTAGATGCGAGGTTTTTTTTTTTCACGAAACTACACACGTTTTAGAAACCACCATA
CCAACAAAACTCTGAAGAACCCCTTAAACCTCAATCCTCCTCTCACTCACTCTCTTCTTTGTCCACTCTTACTTCTTTTCTCTTCACTCTCGCTCTTCCT
TCGCTTTCACGCACATGCCCTGCTGACTTTGCTGGTTAAGGCTTTATCCGTTTTTGATTTCTTCTTTTGCCTTGTATCTTTTGATATGTCTTGCTCTTACTT
CTGCTCCCCCTGCTCTCTTATCTGCATTTTGAAAGGTCGGAATGAGGGGATTGACGAAAGAGAAGCATATGCGTGCCCCTTTGTCACGATTCTATATGCATT
ATTGGGTGTATATGCATGTGAGCGTCAGGAGAGTGATTGATGAATGACGATTGTTGGATTCTGGGTCCTTTTTTTTCTTTACGAACTTTTTTTTTTATCTGA
TGGCTACACGTTTGAATGAATTAAGAGAGCTTGGCACGGACGAATGAATGAGCAAAGAAGGACAGAGATAGCGATGAACCAAAGAGAAAGAAGAAAAAAAGA
GAAAAGAGAAGAGCTGGCAGTAGGTGGCTTAGAGAGATTTCTATTGTTGGAGTTACGCGGTTGGGGGGTAGGAGGGGGGGGGGGGGGAGGGATATATTTTTA
TATATATGATAAAGATGTCACGCATGAAAGAATAAAGAGTTAAAGAACAAATGAGATATTAAAACAGATTTTATTTTATTTTATGAACAAGTATCAATATCG
TGTGCATAAATCATGAAAAGTTTATCAAGTTGGTGGTGATGCGTGACGCGATTTGTCTCATGGGAATCGCAGTATGAATTGTCAGTGGATAATTTTCTTGCT
GGCAAGCAATTAGGTGCTCTTTGAGCCAAACTTCATCAGGAGCAGGCCAGTGGGAATGAGAATGGCCCAAGAAAAGACCATGGTGGCCACAACGACGCCGAA
AATCTTGGCGTACAGGATGACCACGCGTCTCCAAGCAGCCTTGGAAAAGGTAGACCAGGCGTTGGCAACGGTGGCGTAGCCCAGGCCACCTACTACTGCAGG
CTCAACCTTGCCATCGAAAGATCGGTCGAAGGGGATGATGGCGTCCTCGTCCTCGGGTAGAAGCGAAGCCTGGACACGGACGAGAACGACGCGGGCGGGGAT
GATGACAACGACCCACAACATTGTGCTGAGGAGGAAATACACTCCCGCCTTGATCATATAAGCGATCTTGTGTTCGCTGAAGTCGTCAGGAATGCCAGAGCC

CCAGCGGAAGGATGGTGCGTCAAAGCCAATCAGGCCGGACAGCAAGATGGGAACCCATTGGTGGACTTGGGTAGCAACCCAGTAAATCACAACGGGCTTCCA
AGTAGCATTGAAGGCGCGCTTGAAGGTAGGCAGGCGGCGCCAAAACTTTCGGGGGGAAGGGTGCGAGATGACAATGTGAACCCAAGCAGTGGCGTATTGAAC
CATGATCAAGGATGCCAGCAGCTCGGCAAAGGGCCTAGCAGGGAACCAAGAGAAGAACGAGGCGACAACACCGCTGAGGACATTCTGTGCTAGAAGACACAT
GAATCCACGGAAGTTGGCTCGGAAGCCACCATACGAGGTGAGGAGGCGGTTGATGGAGCGAAGAGAAGAGGTCACAGTTCGAGGGGCGCCGTCGGTAGGCTT
GGGGCCGCCAGCGGTGGCCTCTTCATCATCATTTCCGTTGCTAGGAAGGGGCTCATAGGCAGGAGGGTTCTCGTCTTCAATGATGGTGAAGACGGGGTAGAT
GTAGAGCAGGGTATATTGGACCTATATGCTGATGTTAGTGGAAACAAGAAGAGCTGCAGAAAGCAATGATAATACTCACCAGAAGCGAAATGGGAATCAGAA
TAATGGCGTCGACGAGAATCAGAGGCCAGCCCCAAGCCGGCATATGAAAC

Table 1. Designed oligonucleotides and full sequence used for the amplification of Kin-1 5' Promoter, 1st and 2nd half of the hph selection marker, and the Kin1 3' region outside the ORF. The table contains the Kin1 ORF.

TA5kin1-fushph-Rv + Fw:
CTCCTTCAATATCAGTTAACGTCGATCTGTCCTCTCTTGATCCCAAATG

HY-Rv TACTTCGAGCGGAGGCATCC

DJ-KCT hph-Fw GATCGACGTTAACTGATATTGAAGGAG

Hy-Fw CGTTGCAAGACCTGCCTGAA

DJ-KCT hph-Rv CAGCACTCGTCCGAGGGCAAAGGAATAG

Ta3Kin-Rv TAAATCACAACGGGCTTCCA

Hph-2doR+TaKinLeft-Fw CAGCACTCGTCCGAGGGCAAAGGAATAGTCAATCCTCCTCTCACTCACT

CTTTCGAAGATGGCACATTCCGACTCGTCATGCAGTTTGAAGAACAATACCCAAATAAGCCTCCCCAGGTCAAATTCATCAGCCAAATGTTCCACCCCAACG
TATACGCCACCGGCGAGCTGTGCTTGGACATTCTGCAAAACCGATGGAGTCCGACGTACGACGTTGCTGCTGTATTGACTAGCATCCAGAGGTATGGACACG
GACATGTGTGATGGAGTGCTTTATACATCGTCTACTGCCTCGATGCATTTTTGGCTAACTTGAAGCGAATCACTGCGCAGTTTACTTAACGATCCCAACACT
GGTTCACCAGCAAACGTCGAGGCCTCGAATCTTTACAAAGATAACAGAAAGGAGTATACCAAGCGTGTCCGAGCAACTGTTGAAAGTAGCTGGGACGACTAA
AAAGGATTACATCAAGATGGAAGTACTGAGGAATTATGTGTACCCAAGGCTTCACATGAATCCCAGGTCTACTACACCATCTGAATTCGGATTGTGGACTCA
GTCTGTCAGATCTTTTTGATATGACATGCTGTCCACGAGAGCTTGGAGCTTGATAGAAGGATGGAGAAGATTCATTGCAGGCGTTCTGGTGCACGAGATTGA
ACTGGTTATACCAAGGGAAGGAGGATGAATGCTCGCTTTTGCTCGATATTTTTTTTTTTTTGGTCTTATTTTCTCCTACAGTAATCTAGCGTTTGTTTTTGG
TATCCTCGTCATAGTGGCGTGGATGGCTGGCGAACGAGACATAGGTAGTAGTTATTCAGCGGCGATGGATTGTCAAAACCTTCTTTTTTTTCCAAACTGTTT
TTCTTTCTCATTTTCTTATGGCATACAAAAAGGAAGTGTCAAGTAATCCAACGTGATGATGAAGGTATATGTGACTTGCAAACAGCCACATCTCTCCATTTT
CAACAGAGCCTATACGTTGAACATGGCAAACCAACTTTCTTATTGGGGTAGTCTCTGGCCAGGTATATGAGTAGAATAGAATAGAATAGGATGGGCAGCGGG
CATCGGGCATCGGATTTCAGGTCTGCCTGTCAACACGATTCAGCCACTCACATGTGTCTGCACCAAGTTGGGTCAAAGCCAATCCCAACCCATTGCCTGTAT
CAGCCACCGGCCACTAGCCACTCAGACACCTTTGAGAGCTTCTTCATGATGACACGCTAAGACAAAAGAGAACACGGTTGGCTGCAATCCAGCCCCTGACAG
ACTCGACGATTTTGTGGTTTTCCACTGACGCCATGGCAACATAGAATGGCCAACGCAGATAGCCAGCAGATAGTACTGCCTCGATGACGATGGCCATCTATT
AACGAGGTAGTAAATTTACATATTTGTTTCTCGACCTTGTTTTTAAAACTCTCTGCCATGTTGAAGCTCCTCTAGGTCCAGGAACAAGTTGGCATCTAGTAT
TTAGTCTCCAGCTACCGGCGGCACCTCTTCAGGCGGCTGACCTCCAGCAAAACAGCCCCTCACCCTCCTCATCTTCAGGGCTTCTGGCGGCACCCTCAACCA
CCACGCGGCGACTGCTTTTAGCGCGCTTGTCACCACCGAAACAACCACATTGGCCCTGAACTTTTGGGTCCCCTCCCCGCCAGCCCTTCCCAGACCGCCGTT
CCTATTGCATCCCTAGAACCTCTATTTGTCTTGTGTCTTTTGGATTTTTTTTTCTTCTAACCTCTTCTCTTTTTTCCTCATACTTGTTGTTCTCTTCCCCCC
CTTTTCTCCCCTTAACCACTGATCCTGCGGCGGGGTTTTTCTTGTTTCTCGTCGTCGCTCGCAGCTTCGATTAGCGATTGCCCGCCTTTGTTTTGTTTCTTC
TTTTTGGCCCCTCTCTCCGTCGGTGGAGCAGCTATCGGAGCCCGCCATTTGGCATCAAGACAGGACAAGAGAGAGTCTCTGCCAGGAGATAGCGACTTCTCC
TCCTCCCAAGATCGACGGCCTTGCTTGATATCGATCCAACTGCCCAACGCCAACCGCCCACCGATCGACGTTAACTGATATTGAAGGAGCATTTTTTGGGCT
TGGCTGGAGCTAGTGGAGGTCAACAATGAATGCCTATTTTGGTTTAGTCGTCCAGGCGGTGAGCACAAAATTTGTGTCGTTTGACAAGATGGTTCATTTAGG
CAACTGGTCAGATCAGCCCCACTTGTAGCAGTAGCGGCGGCGCTCGAAGTGTGACTCTTATTAGCAGACAGGAACGAGGACATTATTATCATCTGCTGCTTG
GTGCACGATAACTTGGTGCGTTTGTCAAGCAAGGTAAGTGGACGACCCGGTCATACCTTCTTAAGTTCGCCCTTCCTCCCTTTATTTCAGATTCAATCTGAC
TTACCTATTCTACCCAAGCATCCAAATGAAAAAGCCTGAACTCACCGCGACGTCTGTCGAGAAGTTTCTGATCGAAAAGTTCGACAGCGTCTCCGACCTGAT
GCAGCTCTCGGAGGGCGAAGAATCTCGTGCTTTCAGCTTCGATGTAGGAGGGCGTGGATATGTCCTGCGGGTAAATAGCTGCGCCGATGGTTTCTACAAAGA
TCGTTATGTTTATCGGCACTTTGCATCGGCCGCGCTCCCGATTCCGGAAGTGCTTGACATTGGGGAGTTCAGCGAGAGCCTGACCTATTGCATCTCCCGCCG
TGCACAGGGTGTCACGTTGCAAGACCTGCCTGAAACCGAACTGCCCGCTGTTCTCCAGCCGGTCGCGGAGGCCATGGATGCGATCGCTGCGGCCGATCTTAG
CCAGACGAGCGGGTTCGGCCCATTCGGACCGCAAGGAATCGGTCAATACACTACATGGCGTGATTTCATATGCGCGATTGCTGATCCCCATGTGTATCACTG
GCAAACTGTGATGGACGACACCGTCAGTGCGTCCGTCGCGCAGGCTCTCGATGAGCTGATGCTTTGGGCCGAGGACTGCCCCGAAGTCCGGCACCTCGTGCA
TGCGGATTTCGGCTCCAACAATGTCCTGACGGACAATGGCCGCATAACAGCGGTCATTGACTGGAGCGAGGCGATGTTCGGGGATTCCCAATACGAGGTCGC
CAACATCCTCTTCTGGAGGCCGTGGTTGGCTTGTATGGAGCAGCAGACGCGCTACTTCGAGCGGAGGCATCCGGAGCTTGCAGGATCGCCGCGCCTCCGGGC
GTATATGCTCCGCATTGGTCTTGACCAACTCTATCAGAGCTTGGTTGACGGCAATTTCGATGATGCAGCTTGGGCGCAGGGTCGATGCGACGCAATCGTCCG
ATCCGGAGCCGGGACTGTCGGGCGTACACAAATCGCCCGCAGAAGCGCGGCCGTCTGGACCGATGGCTGTGTAGAAGTACTCGCCGATAGTGGAAACCGACG
CCCCAGCACTCGTCCGAGGGCAAAGGAATAGAGTAGATGCCGACCGGGAACCAGTTAACGTCGATCAGAAAAAATTTCTTTTTTTACAAAAGAAAACCTGCG
TTCTTCCGGAACGGCGTTATGACATACACTAGATGCGAGGTTTTTTTTTTTTCACGAAACTACACACGTTTTAGAAACCACCATACCAACAAAACTCTGAAG
AACCCCTTAAACCTCAATCCTCCTCTCACTCACTGTCTTCTCTTTGTCCACTCTTACTTCTTTTCTCTTCACTCTCGCTCTTCCTTCGCTTTCACGCACATG
CCCTGCTGACTTTGCTGGTTAAGGCTTTATCCGTTTTTGATTTCTTCTTTTGCCTTGTATCTTTTGATATGTCTTGCTCTTACTTCTGCTCCCCCTGCTCTC
TTATCTGCATTTTGAAAGGTCGGAATGAGGGGATTGACGAAAGAGAAGCATATGCGTGCCCCTTTGTCACGATTCTATATGCATTATTGGGTGTATATGCAT
GTGAGCGTCAGGAGAGTGATTGATGAATGACGATTGTTGGATTCTGGGTCCTTTTTTTTTCTTTACGAACTTTTTTTTTTATCTGATGGCTACACGTTTGAAT
GAATTAAGAGAGCTTGGCACGGACGAATGAATGAGCAAAGAAGGACAGAGATAGCGATGAACCAAAGAGAAAGAAGAAAAAAAGAGAAAAGAGAAGAGCTGG
CAGTAGGTGGCTTAGAGAGATTTCTATTGTTGGAGTTACGCGGTTGGGGGGTAGGAGGGGGGGGGGGGGGAGGGATATATTTTTATATATATGATAAAGATG
TCACGCATGAAAGAATAAAGAGTTAAAGAACAAATGAGATATTAAAACAGATTTTATTTTATTTTATGAACAAGTATCAATATCGTGTGCATAAATCATGAA
AAGTTTATCAAGTTGGTGGTGATGCGTGACGCGATTTGTCTCATGGGAATCGCAGTATGAATTGTCAGTGGATAATTTTCTTGCTGGCAAGCAATTAGGTGC

TCTTTGAGCCAAACTTCATCAGGAGCAGGCCAGTGGGAATGAGAATGGCCCAAGAAAAGACCATGGTGGCCACAACGACGCCGAAAATCTTGGCGTACAGGA
TGACCACGCGTCTCCAAGCAGCCTTGGAAAAGGTAGACCAGGCGTTGGCAACGGTGGCGTAGCCCAGGCCACCTACTACTGCAGGCTCAACCTTGCCATCGA
AAGATCGGTCGAAGGGGATGATGGCGTCCTCGTCCTCGGGTAGAAGCGAAGCCTGGACACGGACGAGAACGACGCGGGCGGGGATGATGACAACGACCCACA
ACATTGTGCTGAGGAGGAAATACACTCCCGCCTTGATCATATAAGCGATCTTGTGTTCGCTGAAGTCGTCAGGAATGCCAGAGCCCCAGCGGAAGGATGGTG
CGTCAAAGCCAATCAGGCCGGACAGCAAGATGGGAACCCATTGGTGGACTTGGGTAGCAACCCAGTAAATCACAACGGGCTTCCAAGTAGCATTGAAGGCGC
GCTTGAAGGTAGGCAGGCGGCGCCAAAACTTTCGGGGGGAAGGGTGCGAGATGACAATGTGAACCCAAGCAGTGGCGTATTGAACCATGATCAAGGATGCCA
GCAGCTCGGCAAAGGGCCTAGCAGGGAACCAAGAGAAGAACGAGGCGACAACACCGCTGAGGACATTCTGTGCTAGAAGACACATGAATCCACGGAAGTTGG
CTCGGAAGCCACCATACGAGGTGAGGAGGCGGTTGATGGAGCGAAGAGAAGAGGTCACAGTTCGAGGGGCGCCGTCGGTAGGCTTGGGGCCGCCAGCGGTGG
CCTCTTCATCATCATTTCCGTTGCTAGGAAGGGGCTCATAGGCAGGAGGGTTCTCGTCTTCAATGATGGTGAAGACGGGGTAGATGTAGAGCAGGGTATATT
GGACCTATATGCTGATGTTAGTGGAAACAAGAAGAGCTGCAGAAAGCAATGATAATACTCACCAGAAGCGAAATGGGAATCAGAATAATGGCGTCGACGAGA
ATCAGAGGCCAGCCCCAAGCCGGCATATGAAAC

Table 1-2. Designed oligonucleotides and full sequence used for the amplification of Kin1 5' Promoter, 1st and 2nd half of the *hph* selection marker, and the Kin1 3' region outside the ORF. The table contains the hph ORF.

Appendix B. Kinesin-1 fluorescent mutant

To observe the dynamics of Knesins *in vivo*, ΔKin1 will be transformed with a version of the endogenous gene of Kinesin-1 and □-Tubulin phused with fluorescent protein genes. This transformation will be carried out using the same methodology of gene replacement by double homologous recombination used to generate the ΔKin1 strain.

In the PCR fusion technique, the following fragments will be amplified by separate PCR reactions:

-The hygromycin resistance cassette (*Hph*).
-The cassette of resistance to Nourseotricina (*Nat*).
-The Terminator of the *Trpc* gene.
-The markers YFP and mCherry.
-The ORF of Kinesin-1 and □-Tubulin with their promoter regions.

2 different versions of each of the vectors Kinesin-1 and □-Tub were designed with each of the markers (4 different vectors in total), this is observed in Figure 40. By having these 4 versions of the genes with different markers and selection cassettes ΔKin1 strain can transformed and both Kinesin-1 and MTs can be observed *in vivo* by assesing the co-localization of Kinesin-1 (YFP or mCherry) with the MTs (using a different marker than that used for Kinesin-1), and thus be able to differentiate them and observe their dynamics (temporal and spatial localization) in the different stages of *T. atroviride* development: germination, vegetative growth (apical and subapical branching) and conidiation.

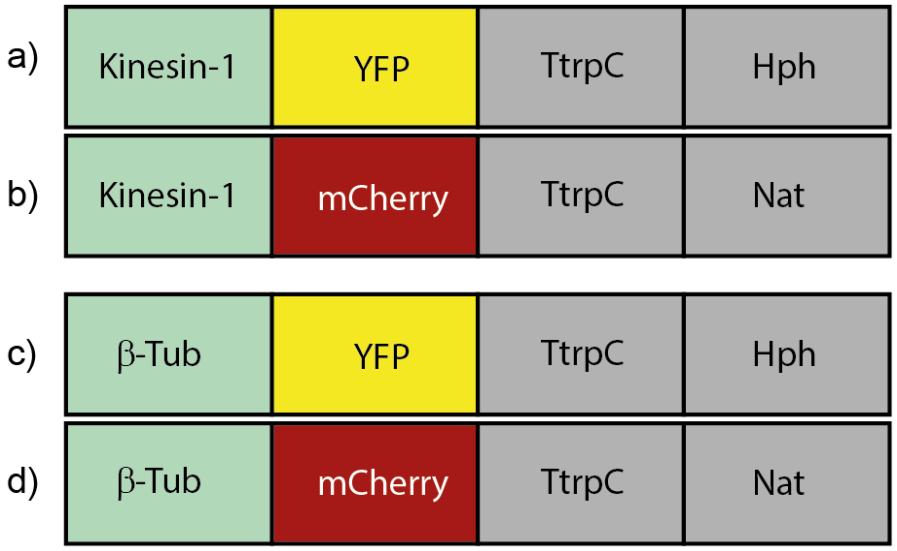

Figure 40. Construction of the different vectors for labeling of Kinesin-1 and MTs. a) and b): There will be two different versions for the same gene (Kinesin-1), one with YFP and the cassette *Hph* and another with mCherry but with a different cassette (*Nat*), the same will happen for c) and d) that correspond to the gene of the MTs. The result of this is that combinations of a) + d) or b) + c) can be used, which will have two different markers and two different selection cassettes.

It was decided to directly clone the fragments of YFP and mCherry (Figure 41) in a plasmid that contained the *Hph* cassette. Thus, the plasmid pBHD was used (Figure 42), which is a variant of pBSK + containing the *Hph* gene.

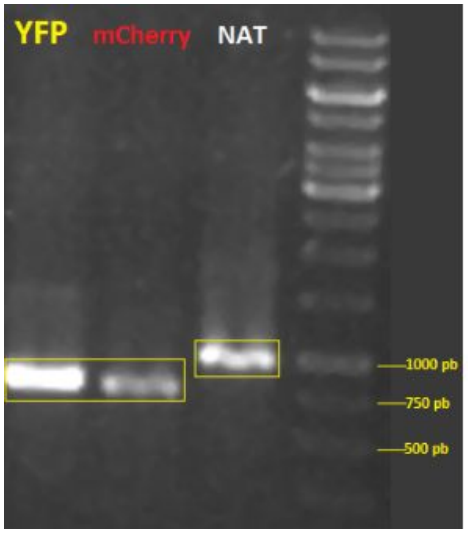

Figure 41. Amplification of YFP (712 pb), mCherry(722 pb), NAT (949 pb) genes.

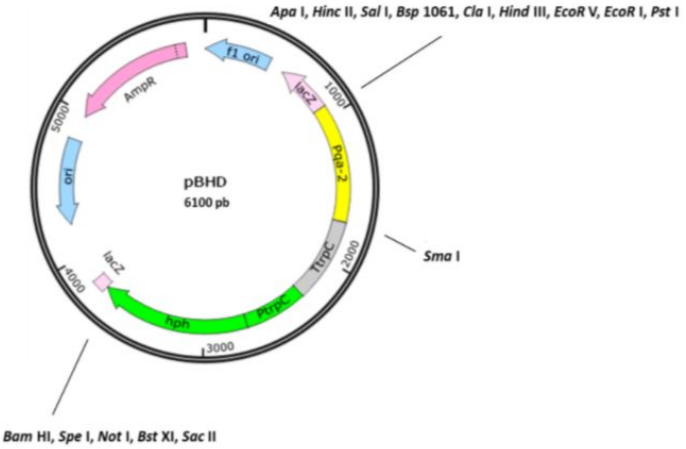

Figure 42. The map of the pBHD plasmid used for the cloning of YFP and mCherry is shown. It was cloned in the *Sma I* site.

After performing the cloning in the pBHD plasmid, a PCR verification was carried out to find out if the plasmids had an insert. 5 positive colonies with the insert were obtained (Figure 43). Once the insertion was verified and its correct orientation (since *Sma I* is blunt), DNA was extracted and sequenced to verify that there were no mutations in the inserts.

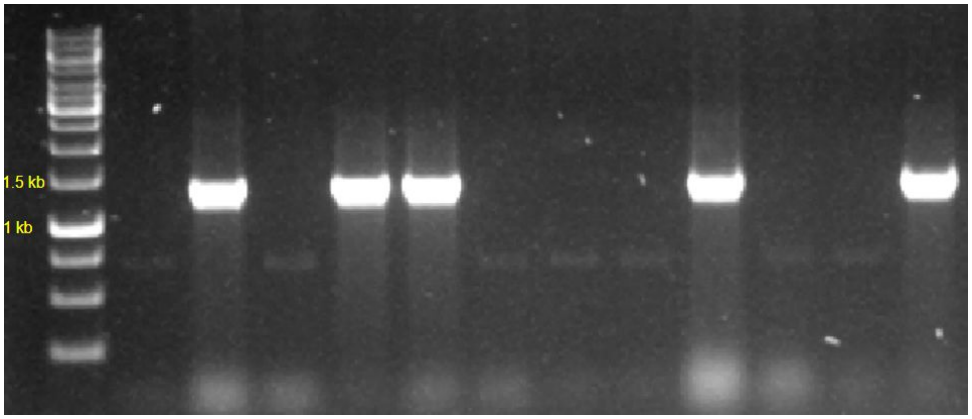

Figure 43. Verification PCR using insert oligos. There are 5 different bands, corresponding to the 5 positive colonies that were obtained, from which DNA was subsequently extracted and sequenced. Expected band 1300 pb.

Currently, work is being done on the cloning of the gene for Kinesin-1 in the plasmid with mCherry (Figure 44).

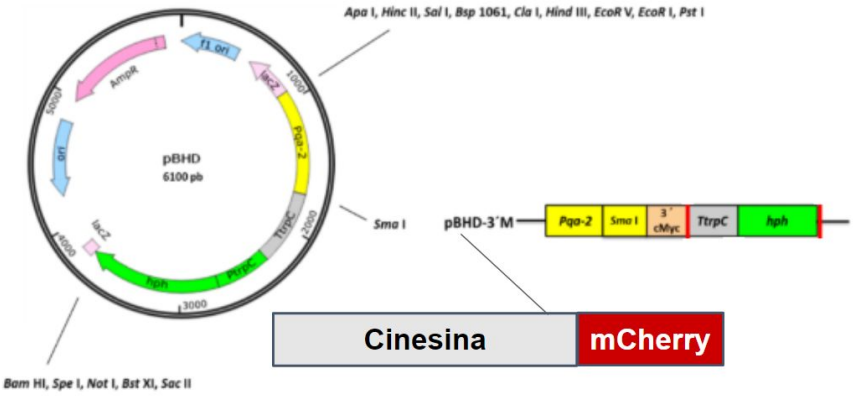

Figure 44. Plasmid pBHD. The region where the gene of mCherry is already cloned is amplified, and where the gene of Kinesin-1 was inserted.

Figure 45 shows the electrophoresis gel of the different candidates who presented the insert of the Kinesin-1 gene.

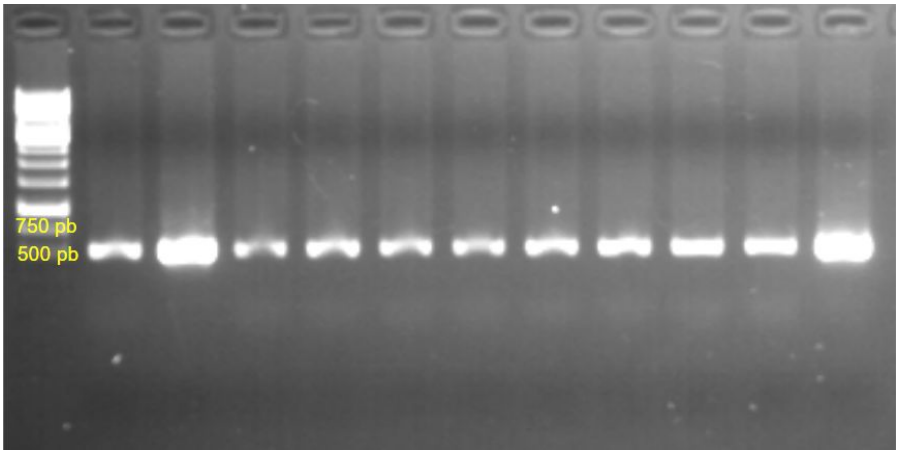

Figure 45. The gel of electrophoresis of the candidates that presented insertion of the gene of the Kinesin-1 by the process of ligation in plasmid and transformation in bacteria is observed. Expected band = 520pb.

It is necessary to identify if the insertion of the Kinesin-1 was performed in the correct orientation in at least one of these candidates. Subsequently, the region of the plasmid where the Kinesin-1 is located will be sequenced, to know if no mutation occurred in the gene that was inserted. Once this is done, a first version of the desired plasmids will be available, in which a plasmid with fluorescent Kinesin-1 will be used to transform the ΔKin1 strain, and thus have a

complementary strain with a fluorescent Kinesin-1. Observations required by fluorescence microscopy can then be performed.

Appendix C.

Fungal Genetics and Biology 123 (2019) 25–32

Contents lists available at ScienceDirect

Fungal Genetics and Biology

journal homepage: www.elsevier.com/locate/yfgbi

Automated, continuous video microscopy tracking of hyphal growth

Gamaliel Sánchez-Orellana[a], Sergio Casas-Flores[b], Braulio Gutiérrez–Medina[a,b,*]

[a] Division of Advanced Materials, Instituto Potosino de Investigación Científica y Tecnológica, Camino a la Presa San José 2055, 78216 San Luis Potosí, Mexico
[b] Division of Molecular Biology, Instituto Potosino de Investigación Científica y Tecnológica, Camino a la Presa San José 2055, 78216 San Luis Potosí, Mexico

ARTICLE INFO

Keywords:
Hyphal growth
Branching
Automated tracking
Video microscopy
Persistence length

ABSTRACT

The growth of filamentous fungi is a complex process that involves hyphal elongation and branching. Microscopic observations provide a wealth of information on fungal growth, although often requiring laborious manual intervention to record and analyze images. Here, we introduce a novel tool for automated tracking of growth in fungal hyphae that affords quantitative analysis of growth rate and morphology. We supplied a student-grade bright field microscope with stepper motors to enable computer-control of the microscope stage. In addition, we developed an image-processing routine that detects in real-time the tip of a hypha and tracks it as the hypha elongates. To achieve continuous observation of hyphal growth, our system automatically maintains the observed sample within field-of-view and performs periodic autofocus correction in the microscope. We demonstrate automated, continuous tracking of hyphal growth in *Trichoderma atroviride* with sampling rates of seconds and observation times of up to 14 h. Tracking records allowed us to determine that *T. atroviride* hyphae grow with characteristic elongation rates of ~70 nm/s. Surprisingly, we found that prior to the occurrence of an apical branching event the parental hypha stopped growing during a few minutes. These arrest events presented occasionally for subapical branching as well. Finally, from tracking data we found that the persistence length (a measure of filament extension before presenting a change in direction) associated to *T. atroviride* hyphae is 362 µm. Altogether, these results show how integration of image analysis and computer control enable quantitative microscopic observations of fungal hyphae dynamics.

1. Introduction

The growth of filamentous fungi is a complex process that starts with the emergence of a germ tube through conidium germination, which is then progressively transformed into mycelia by hyphal elongation and branch formation. A fungal hypha, typically 3–10 µm in diameter, can reach up to several hundred micrometers in length (Oliver and Trinci, 1985). This type of growth enables the organism to increase size maintaining a constant surface to volume ratio, making fungi well adapted to colonization of solid substrates. To understand fungal development and assess effects of environmental factors on growth, quantitative evaluation of morphology dynamics becomes an important aspect of fungal characterization (Samapundo et al., 2007).

Morphology at the hypha level can be studied using light microscopy, often yielding only qualitative information. To obtain quantitative information in these experiments, labor intensive and sometimes subjective analysis is required by the observer (Paul and Thomas, 1998). The introduction of digital image analysis 30 years ago allowed automated studies of fungal morphology (Packer and Thomas, 1990), with focus on specific morphological parameters like the number of hyphal tips and branching points in hyphae (Paul and Thomas, 1998). Using digital methods, first attempts for real-time quantification of fungal morphology were made either by circulating the culture in a flowthrough cell (Spohr et al., 1998) or by fixing single hyphae onto coverslips (using poly-D-lysine) and imaging, with acquisition rates of 1 frame every 10 min (Christiansen et al., 1999). These studies typically involved a limited number of pre-selected microscopic images of hyphae and image acquisition was mainly done by an operator (Diano et al., 2009; Lim et al., 2006; Ahamed and Vermette, 2009; El-Sabbagh et al., 2008; Lübbehüsen et al., 2003).

Although different computational workflows have shown to reduce the requirement for manual intervention of an operator during morphological analysis of sequentially recorded microscopic images (Kossen, 2000; Barry, 2010; Lecault et al., 2007; Brunk et al., 2018), there is still a pressing need for an integrated approach covering fully automated image acquisition and analysis. To achieve automated tracking of hyphal growth by video microscopy one technical problem must be solved: to keep the hypha under study in focus and within the microscope field of view—over periods of time that may reach several hours.

* Corresponding author at: Divisions of Advanced Materials and Molecular Biology, IPICYT, Camino a la Presa San José 2055, 78216 San Luis Potosí, Mexico.
E-mail address: bgutierrez@ipicyt.edu.mx (B. Gutiérrez–Medina).

https://doi.org/10.1016/j.fgb.2018.11.006
Received 9 November 2018; Received in revised form 27 November 2018; Accepted 27 November 2018
Available online 30 November 2018
1087-1845/

Here, we combine computer-controlled bright field microscopy with digital image processing to achieve time-resolved quantification of growth of individual fungal hyphae. We apply the developed tool to record growth in the filamentous fungus *Trichoderma atroviride*, detecting in real-time a single growing hypha element and following it over several hours without manual intervention. The position coordinates of hyphal tips allow us to quantify growth rate, persistence length and mean branching angle. Surprisingly, we find that *T. atroviride* stalls prior to apical (and occasionally subapical) branching.

2. Materials and methods

2.1. Organism and sample preparation

We study *Trichoderma atroviride* wild-type strain (IMI 206040). Conidia of *T. atroviride* were collected after 7–10 days of fungal growth on Petri dish with Potato Dextrose Agar (PDA, Difco) medium. Collection was made by adding 1 mL of sterile distilled water to the colony, then we used a glass handle to scrape *T. atroviride* in order to release conidia. Finally, we collected conidia on a 1.5 mL Eppendorf tube. Dilutions were made to obtain a concentration of ~10 conidia/μL. We inoculated 1 μL of conidia dilution on PDA plugs placed on a microscope slide. After 15 h incubation at 28 °C conidia were taken to the microscope for measurements.

2.2. Microscopy system

A student-grade bright field microscope (Amscope, T370B-3M) was modified to enable computer control (Fig. 1). To allow three-dimensional (3D) *X-Y-Z* sample manipulation, we attached a NEMA-17 (200 steps per revolution) stepper motor to each axis knob of the microscope stage. The stepper motors transfer movement to the microscope knobs with the use of timing belts (available at www.adafruit.com, Product ID: 1184). The stepper motors are controlled by two Adafruit's v2 motor shield controllers, each connected to an Arduino UNO SMD board (Product ID: 1438). The *X,Y* motors are controlled by the same motor shield whereas the *Z* motor is controlled by the second motor shield. The Arduino boards are connected to a computer by USB ports. The estimated motor step sizes at the sample plane were 80 μm (*X*, *Y*) and 5 μm (*Z*). To control lighting sample conditions, we replaced the microscope original white light bulb for a red (peak wavelength, λ = 625 nm) Light Emitting Diode (LED, Luxeon Tristar). A CCD USB Camera (Sentech STC-TB33USB-B 640 × 480 pixel resolution) is mounted on the trinocular port of the microscope and connected to the computer. Objectives used: 10x and 40x magnifications, with a pixel-to-microns conversion factor of 1 px = 1.49 μm and 1 px = 0.37 μm, respectively. The entire microscope system is placed in temperature-controlled room (28 °C). The software LabView (National Instruments) is used for stepper motor control. Unless otherwise noted, all data presented correspond to 10x magnification.

2.3. Image processing and continuous tracking of hyphal elongation

Once the sample is placed on the microscope stage, we start image acquisition and manually set a Region Of Interest (ROI) around the hyphal tip we want the system to track (Fig. 2A). After this point, the system is fully automated and no further user intervention is required. A set of image transformations (described below) are applied to the ROI to determine the (*x*,*y*) coordinates of the hyphal tip, allowing tracking of apical growth as the hypha develops.

Starting from a bright field image, we perform image segmentation (i.e. separation of object and background) by applying the following elemental transformations: (i) Threshold, producing a binary image (Fig. 2B), (ii) Erode, that eliminates isolated background pixels (Fig. 2C), (iii) Skeletonize, where pixels are removed from the edges of the binary structure until an object skeleton is left at one pixel wide (Fig. 2D). Once we have a skeletonized image of the hyphal tip, a search is performed (left-to-right and top-to-bottom) until the first non-zero pixel value is found (Fig. 2E). This routine therefore follows a hypha growing from right to left in our field of view. In every frame recorded, the system stores the found (*x*,*y*) coordinates of the detected hyphal tip and builds a new ROI around these coordinates to be passed to the next image. In this manner the ROI will always be centered at the last stored coordinate. These series of steps are iterated every 1.3 s, which is the sampling time interval of our system. In addition, we store video frames every 10th data point, providing a record in video of the tracked hyphal growth (Fig. 2F). The above image processing procedure was followed for 10x and 40x magnification (with the exception of the Skeletonize operation at 40x).

As the hypha grows it reaches the boundaries of the microscope visual field. These events are detected by comparing the *x* or *y* coordinate with predetermined lower (or higher) limit values (we

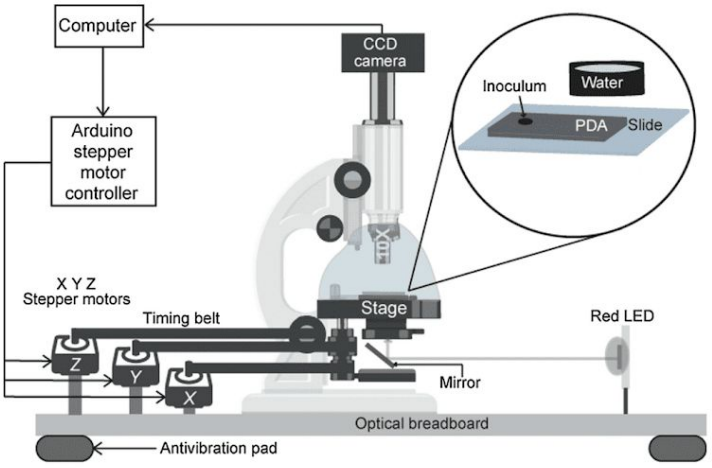

Fig. 1. Microscopy setup and sample arrangement. The system is mounted on an optical breadboard with cushion pads to help minimize mechanical noise. To mount the sample (inset) a PDA plug is placed onto a microscope slide and inoculated with the filamentous fungi conidia. Water contained in small caps provides humidity to the sample. The stage and nosepiece of the microscope are covered with packing film plastic to avoid the sample to dry. The stepper motors transmit movement to the *X-Y-Z* axis knobs of the stage through timing belts. Sample illumination is provided by a red LED. A CCD camera captures images and feeds a computer, which executes the automated tracking routine and controls stepper motor motions (via the Arduino interface). (For interpretation of the references to colour in this figure legend, the reader is referred to the web version of this article.)

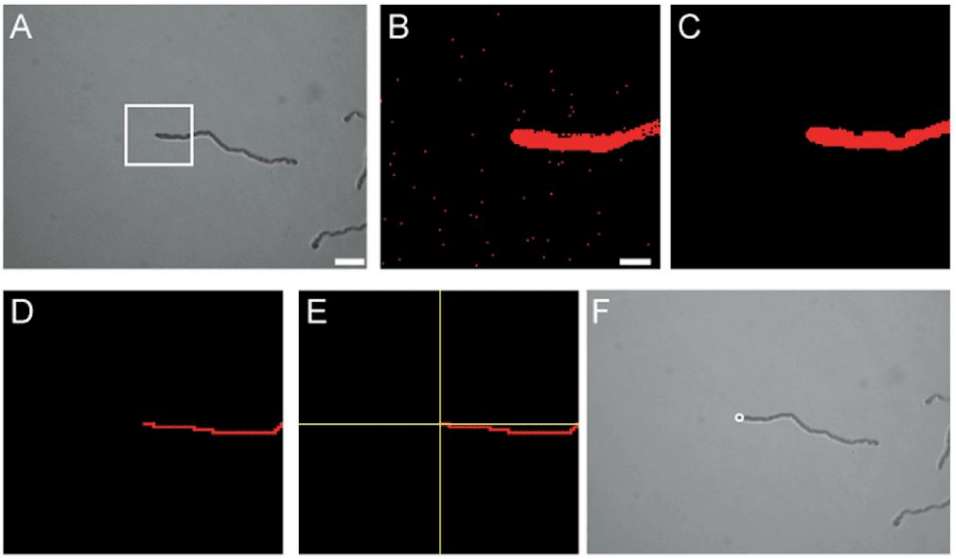

Fig. 2. Finding the hypal tip using digital image processing. (A) A region of interest (ROI, white rectangle) is selected. Scale bar, 20 μm. (B) The resulting image of the ROI after a threshold operation; most of the background is removed. Scale bar, 10 μm. (C) Isolated noise pixels in the background and hyphal surroundings are removed using an erode operation. (D) After a skeleton operation is applied, leaving a structure only one pixel wide. (E) The system searches from left-to-right and top-to-bottom for the first non-zero pixel value and marks that pixel as the position of the hyphal tip (yellow cross). (F) The system stores (*x*,*y*) position coordinates of the hyphal tip (white circle) and an image every 10th data point. (For interpretation of the references to colour in this figure legend, the reader is referred to the web version of this article.)

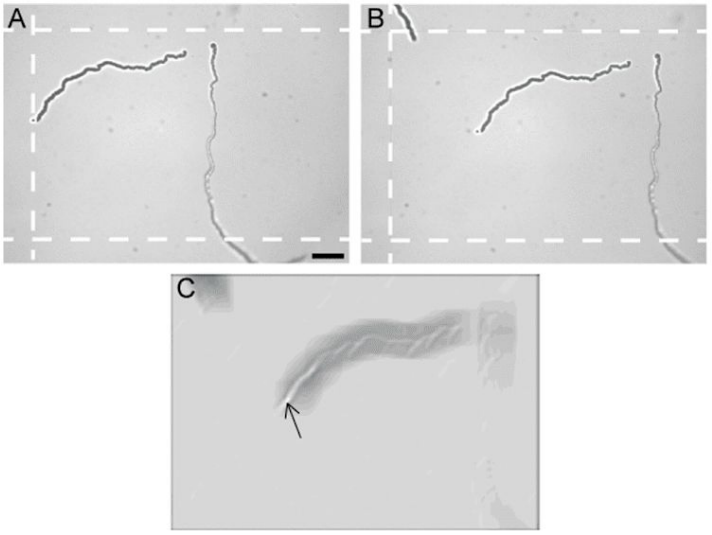

Fig. 3. Stage motion and image correlation maintain continuity of hyphal tracking. (A) The tracked hyphal tip (with a white circle drawn over) reaches visual limits (dashed white lines). Scale bar, 20 μm. When the system detects such an event it displaces the stage. (B) The tracked hypha is brought back to the field of view. (C) Result of the image correlation process of images shown in (A) and (B). The pixel with the highest intensity value (black arrow) signals the position of maximum correlation and enables to determine the new hyphal tip (*x*,*y*) coordinates.

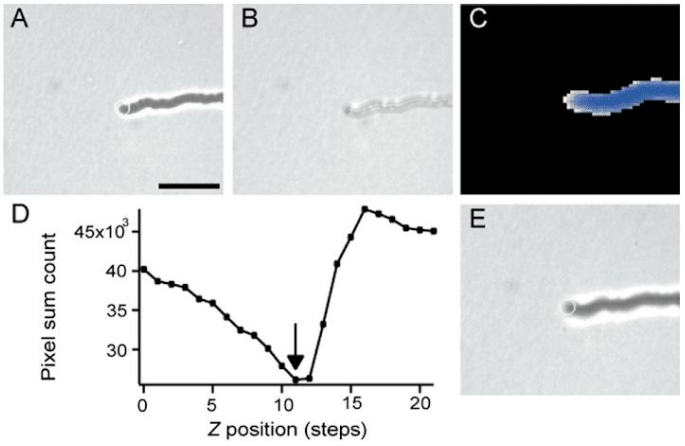

Fig. 4. Microscope drift correction. (A) A hypha is observed under an amount of defocus appropriate for tracking. (B) The same hypha after increased defocus with respect to (A), unsuitable for tracking. (C) An image of the hypha after application of a mask that sets background pixels zero. (D) The sum of the pixel intensities of images such as (C) are computed for various *Z*-stage positions. A *Z*-position is selected to maximize image contrast (arrow). (E) Image of the hypha after the motor moves to the selected *Z*-position, restoring image contrast suitable for tracking. Scale bar, 20 µm.

typically establish 50-pixel boundaries form the upper, bottom and left frame edges). Once an off-limits event is detected the microscope stage is displaced using the *X* or *Y* stepper motors by a predetermined number of steps so that the tip of the hypha of interest is brought back well within the boundaries of the field of view. To maintain tracking of the same hypha, a cross-correlation operation is performed between the last image recorded prior to stage motion (template image) and the first image after the stage has been moved (actual image). In image correlation, the template image is overlaid to the actual image and displaced in two dimensions (2D), one pixel at a time. At every pixel step the displaced template and the actual image are multiplied, and the sum of all pixel counts of the product image is computed. This operation defines a new pixel map where the maximum count corresponds to the position where the displaced template most resembles the actual image. Accordingly, we identify the maximum of the resulting correlation image and set the corresponding (*x*,*y*) coordinates as the current position of the hyphal tip (Fig. 3B). This procedure enables continuity in the tracking of a given hypha (Fig. 3A and C). Image processing is performed using the LabView IMAQ Vision module. Image correlation is performed using the Vision function IMAQ-Correlate.

2.4. Microscope focus drift correction

Although our microscope system is in a temperature-regulated room, residual drift in the microscope focus was present (Fig. 4B). We keep the sample focused in an automated manner, using the known property of bright-field microscopy that the image of an unstained object changes from bright to dark as it is defocused. First, the *Z*-axis stepper motor displaces the microscope stage several steps from its actual position. Next, the stage is moved stepwise back to its original position while images of the defocused hypha are taken every motor step, producing a *z*-image stack. Using the previously determined binary image corresponding to the hypha of interest (Fig. 2B) a mask is applied on every image of the stack to obtain the gray-value pixel intensity limited to the area of the hypha (Fig. 4C). Then, the gray-value pixel intensity values are summed over the whole image for every image and displayed as a function of the *Z*-motor step position. The resulting plot (Fig. 4D) allows us to identify a reference point with good image contrast (we chose to work with darkened hyphae images over a bright background). Finally, the stage is moved to the reference position, bringing the hypha back to the amount of defocus that optimizes tracking (Fig. 4E). For 40x magnification this procedure was omitted, and drift correction was achieved by displacing the *Z*-motor at a constant rate of one step every 50 sampling cycles.

2.5. Speed of apical growth

The set of (*x*,*y*) position coordinate data undergoes smoothing (boxcar, 30 time points) and decimating (10-fold) operations that decrease position variations. Next, the derivative of the x and y coordinates respect to time yields growth speeds along *X* and *Y* axes. After performing one last smoothing procedure (median, 10 points), the *X* and *Y* speeds are added in quadrature to obtain the final hyphal growth speed. These operations establish the temporal resolution of our system to detect changes in speed. Based on analysis of a test pulse signal, we estimate that this temporal resolution is 1.3 min. For global analysis of apical growth speed, we concatenated 18 different speed records, resulting in a total of 148.1 h of tracking data, and produced a histogram with its corresponding Gaussian fit. For measuring radial colony growth we inoculated *T. atroviride* mycelia at the edge of Petri dishes containing solid PDA medium. Colonies were kept in the dark at 28° C; radial extent was manually recorded every 12 h during 48 h.

2.6. Angular correlation and persistence length

A set of (*x*,*y*) coordinates corresponding to tracking of a hypha is first smoothed (boxcar, 30 time points) and then decimated (100-fold). Next, arc length (s) and angular correlation values $\cos(\theta(s) - \theta(0))$ are calculated as follows. The reference value $\theta(0)$ is the angle of the line tangent to the coordinate path at the first coordinate ($x = 0, y = 0$). For every subsequent (*x*,*y*) point the arc length (computed as the piecewise sum of Euclidean distances between (*x*,*y*) coordinates up to the current point) and the angle $\theta(s)$ are obtained, and the value $\cos(\theta(s) - \theta(0))$ is computed. This procedure is repeated, now taking as a reference value $\theta(0)$ the angle of the line tangent to the coordinate path at the second (*x*,*y*) position. The routine is repeated for every (*x*,*y*) position as the reference value $\theta(0)$. Data are then organized by binning arc length values and computing averages of angular correlation values for every arc length bin, yielding angular correlation vs. arc length for that particular (*x*,*y*) record. Finally, angular correlation records corresponding to different tracked hyphae are averaged. See additional information in the Supplementary Information.

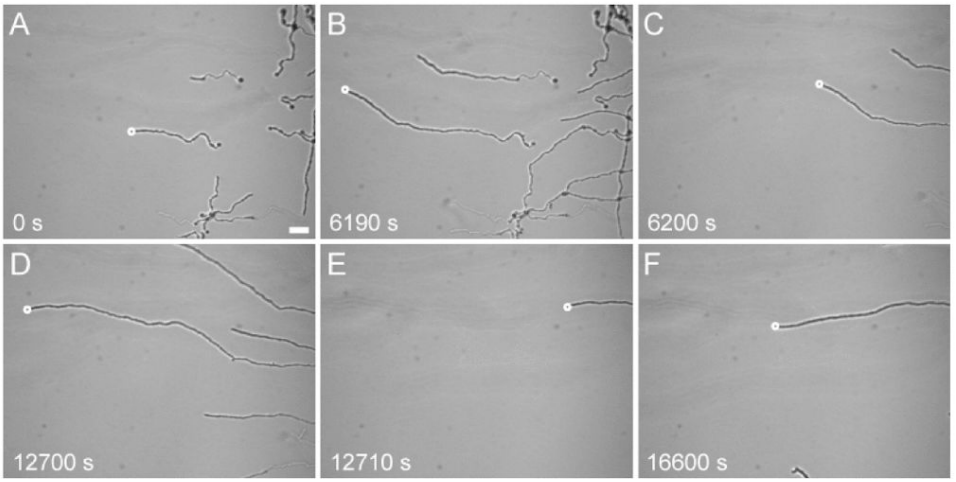

Fig. 5. Hyphal tip tracking under execution. (A) The system begins tracking the tip of a selected hypha (white circle). (B) After a period of sustained growth, the tip reaches the boundaries of the microscope field of view. (C) The system returns the hypha under view and finds the new position of the tip. (D) A second off-limits event presents. (E) The hypha after being brought well within view. (F) Tracking continues through several hours. Tracking time is shown. Scale bar, 20 μm.

3. Results and discussion

3.1. Automated tracking of hyphal elongation

We apply the developed bright field microscopy system to observe hyphal growth in *T. atroviride* starting from individual conidia. Fig. 5 and Supplementary Video 1 show a typical succession of observation events, where the system initially detects the tip of a growing germ tube and starts apical tracking (Fig. 5A). When the hyphal tip reaches the boundaries of the visual field (Fig. 5B) the system moves the microscope stage through the stepper motors, bringing back the same hypha within field of view, and identifies the hyphal tip to continue tracking (Fig. 5C). As the hypha continues to grow and a new off-limits event presents (Fig. 5D) the system moves the stage again (Fig. 5E) and resumes tracking (Fig. 5F). We consider only "forward" growing hyphae; that is, filaments elongating towards the three dotted lines shown in Fig. 3.

Our system is able to track hyphal growth over several hours (up to 14), limited mainly by the appearance of intruder hyphae that overlap with the hypha of interest (difficulting the correct distinction of tracked objects). We minimize this potential problem by restricting our search area to the ROI established around the tip of the tracked hypha and by using low numbers of conidia (~10 per sample).

3.2. Speed of hyphal growth

The raw tracking data consist of increasing (x,y) position coordinates interrupted by jumps due to the stage motions that keep the same hypha within field of view. After correcting for these jumps, the apical growth speed is computed (see Materials and Methods). The apical elongation rate for *T. atroviride* is approximately constant during the observation period (Fig. 6A and B). Unexpectedly, however, we frequently found that prior to the emergence of a new hyphal branch the elongation dynamics of the parental hypha stalled completely, resuming growth after the appearance of the new branch (Fig. 6).

Our system allowed us to identify four different types of branching dynamics: (i) Apical branching with preceding growth arrest. Pauses in

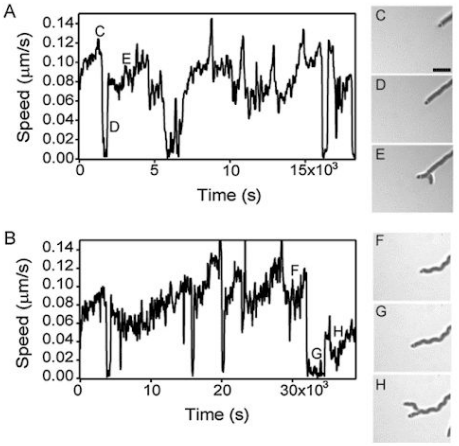

Fig. 6. Hyphal elongation rate and branching dynamics. (A)–(B) Two examples of hyphal growth speed. The speed records show noticeable stalls in growth that we noticed occur prior to the emergence of a branch. Images show apical (C–E) and lateral (F–H) branching events, corresponding to the indicated time points in the speed records. Scale bar, 10 μm.

growth presented typical durations 2–5 min (Fig. 6C–E). (ii) Apical branching with no noticeable growth rate modification. It is possible that here no pauses were present or that pauses lasted less than ~1.3 min, the temporal resolution in analysis of tracking data. (iii) Subapical branching (> 10 μm from the parental tip) with no noticeable stops in growth. (iv) Subapical branching with parental hypha growth arrest. There were a few instances where the parental hypha stopped growth during several minutes prior to the appearance of a subapical branch. We also noticed that the parental hypha often

resumed growth after the appearance of a new branch with an elongation rate initially reduced (Fig. 6F–H). Out of 49 branching recorded events, we observed the following for each type: (i) 20, (ii) 18, (iii) 6, and (iv): 5.

These results can be contrasted with previous studies of hyphal branching. Two types of branching have been reported for *Neurospora crassa*: apical and subapical (Riquelme and Bartnicki-Garcia, 2004). In apical branching the parental hypha was observed to sharply drop its elongation rate, whereas in subapical branching the elongation rate of the parental hypha continued undisturbed. To explain these differences, authors of Ref. Riquelme and Bartnicki-Garcia (2004) suggested that apical branching may involve disruption of cytoplasmic organization, whereas lateral branching probably resulted from subapical accumulation of wall precursors. Our observations add two novel elements to the reported branching behavior. First, during apical branching growth is completely arrested (lasting a few minutes). This observation is consistent with disruption of cytoplasmic organization prior to the branching event. Second, subapical branching sometimes also involves parental arrest in elongation. In this case, a relationship between apical growth arrest and subapical branching needs to be confirmed. Future studies involving observation of cytoplasmic organization during branching should help to better understand these effects.

Analysis of growth speed data for several samples (Fig. 7) yields an average of 0.072 ± 0.016 μm/s. This microscopic hyphal elongation rate can be compared to macroscopic radial growth (Fig. 7). We carried out colony measurements using the same lighting, medium and temperature growth conditions as in the microscopic experiments. During the first few hours of observation radial growth is 0.104 μm/s (Fig. 7). The observed lower apical elongation rate compared to the colony radial extension rate is consistent with previous reports for *N. crassa* (0.19 μm/s vs. 0.70 μm/s, respectively) (López-Franco et al., 1994) and *Aspergillus nidulans* (0.02 μm/s vs. 0.04 μm/s) (Trinci, 1974). This difference in growth rates can reflect the fact that in radial growth hyphae located at the colony edge correspond the fastest growing and/or the ones that changed direction little, whereas at the individual hypha level the mean value of extension rate is reported. In addition, growth delays due to branching and other unknown factors in individual hyphae reduce average elongation rates.

3.3. Tracking hyphal growth at increased magnification

To further assess the capabilities of our system, we performed tracking of hyphal growth at a higher microscope magnification (40x). A few technical challenges present in this case. The much-reduced objective working distance (0.6 mm at 40x vs. 5.5 mm at 10x) limited the amount of defocusing of samples, whereas image contrast did not allow efficient auto-focus. We found that the microscope axial drift increased linearly; therefore, the auto-focus routine was disabled and the *Z*-motor advanced by one step every 50 sampling cycles, maintaining the sample at optimal focus. With regard to correction of off-limits events, only one or two *X*,*Y* motor steps (step distance at the sample plane, ~60 μm) was enough to bring the tracked hypha within field of view. From this observation we note that the *X*,*Y* motor step size is thus the main limitation that precludes our system to work at higher magnifications. Finally, as the digital image processing routines were tested to function with wider filament objects, we found that the *Skeletonize* operation was not a required to perform tracking. We can only expect that in research-grade microscopes some of these constraints may not be limiting at all.

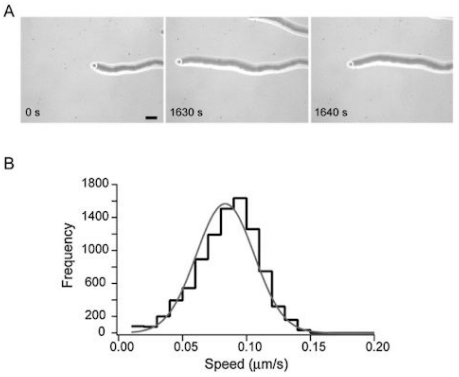

Fig. 8. Tracking hyphal growth at 40x microscope magnification. (A) Sequence of bright field images showing a hypha under tracking at an initial position (left), close to the off-limits range (center), and upon return to the field of view (right). Scale bar, 20 μm. (B) Histogram of hyphal elongation rate obtained from eight different tracking runs (total tracking time, 37.8 h). A Gaussian fit to data (gray line) yields average speed: 0.083 ± 0.014 μm/s (mean ± sd).

Fig. 8A shows images of hyphal tracking at 40x magnification. In this condition, the frequency of off-limits events increases significantly compared to 10x, and the automated routine performs effective correction many times over a number of hours (see Supplementary Video 2). Measurements of growth speed derived from (*x*,*y*) tracking data (Fig. 8B) agree well with measurements at lower magnification. It is interesting to note that at 40x the shape of single hypha can be distinguished. This characteristic can prove useful for future studies aimed at the study of hyphal tip morphology over prolonged times using our automated tracking system.

3.4. Hyphal path tangent angle correlation and persistence length

The availability of (*x*,*y*) coordinates corresponding to hyphal tip elongation provide the opportunity to compute the persistence length associated to the filamentous hypha. The persistence length is a measure often used in polymer mechanics, that indicates "the length of filament over which (…) bending becomes appreciable" (Howard, 2001). In the context of filamentous fungal growth, we propose to use the persistence length as a metric of the characteristic distance before hyphae present changes in direction (see Supplementary Information). This microscopic measure could provide useful information in

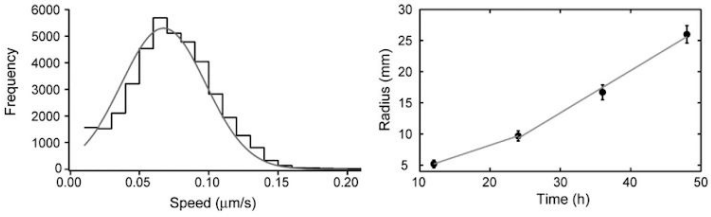

Fig. 7. Microscopic and macroscopic growth rate of *T. atroviride*. Left: Histogram of hyphal elongation rate obtained from 18 different tracking runs. A Gaussian fit to data (gray line) yields the average growth speed of hyphae: 0.072 ± 0.016 μm/s (mean ± sd). Right: Colony radial growth. The first two datapoints define a line (in gray) with slope: 0.104 μm/s. The last three datapoints are adjusted to a line (in gray) of slope 0.189 ± 15 μm/s (error from the fit). $N = 3$.

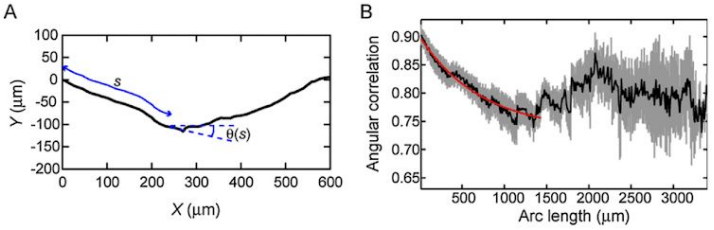

Fig. 9. Angular correlation and persistence length of hyphal growth. (A) The path followed by a hypha is shown (black line) along with an arc length (s) and the angle of the tangent to the path at s. (B) The average angular correlation ($\langle\cos(\theta(s) - \theta(0))\rangle$) shows initial decay followed by asymptotic behavior ($N = 16$, records vary in arc length total extent). Averages (black) and S.E. (gray region) are displayed. An exponential fit to data (red line), limited to values where at least 10 angular correlation records were used to compute averages, yields $L_p = 362 \pm 30$ μm, and the asymptote of the angular correlation for long arc lengths: 0.73 ± 0.01 (errors from the fit). (For interpretation of the references to colour in this figure legend, the reader is referred to the web version of this article.)

understanding how growth direction is set in fungal hyphae (Riquelme et al., 1998) and to build models of macroscopic fungal architecture and organization (Boswell and Hopkins, 2009).

To assess persistence length, the set of (x,y) coordinates associated to the tip of hyphae during growth is recognized as the path that defines the shape of that hypha. The extension of this path is given by the arc length, s. As the arc length increases changes in path direction will dictate changes in the angles of lines tangent to the path (Fig. 9A). This is the main idea behind the analysis that follows.

To quantify changes in direction in the hyphal path, the correlation between tangent angles $\theta(s)$ is computed as the average of: $\cos(\theta(s) - \theta(0))$ (see Materials and Methods and Supporting Information). Fig. 9B shows the average angular correlation as a function of arc length for a set of 16 different tracking records. A fit of the angular correlation to the relation: $Ae^{-(s/2L_p)} + \xi$ yields the persistence length: $L_p = 362 \pm 30$ μm, and the asymptote of the angular correlation for long arc lengths: $\xi = 0.73 \pm 0.01$.

Tangent angle correlation provides information on the characteristic distance of hyphal elongation before changes in direction and the average angle followed during these changes (see Supplementary Information). Based on this notion, we conclude that a growing hypha elongates by ~350 μm before changing direction (by either elongation or branching). Furthermore, the asymptotic value $\xi = 0.73$ corresponds to a mean angle of 43 deg. Interestingly, this value is essentially the same as the branching angle experimentally found in *N. crassa* (45 deg) growing on a surface of agar (Held et al., 2011), suggesting that the main mechanism for hyphae to change direction is branching. Further work should test this inference in *T. atroviride* and other fungi.

The angular correlation analysis presented here is amenable to alternative procedures of microscopic hyphal growth characterization. In particular, the analysis could be applied at the whole-colony scale. Using straightforward image processing procedures, the image of an entire colony can provide the set of (x,y) coordinates that define the path of all hyphae involved. As we described here, these coordinates provide the starting point to compute tangent angle correlation. Therefore, the analysis proposed in our work has the potential to provide information on hyphal morphology for a colony without counting or measuring individual elongating, branching or pausing events.

4. Conclusion

We presented the development of an accessible video microscopy method that allows real-time, continuous tracking of a single filamentous fungi hypha. The system operates in an automated fashion over extended periods of time (up to 14 h) with a sampling time interval of 1.3 s. We tested the quantitative value of our method by obtaining the growth speed and the persistence length associated to hyphae of *T. atroviride*. In particular, we show how tangent angle correlation can provide information on the characteristic distance of hyphal elongation before changes in directions occur and the average angle between parental and branching hyphae. The temporal sampling rate of the developed system allowed us to detect branching dynamics not previously reported. This methodology should prove useful for the analysis of fungal hyphae growth dynamics under different treatments, conditions or strains.

Author contributions

G.S.-O., S.C.-F., and B.G.-M. designed research, performed research, analyzed data; G.S.-O. and B.G.M. wrote the paper.

Acknowledgements

This work was supported by CONACYT (Mexico) grants SEP-CB-2013-01-223377 and IFC-2015-2/1144 to B.G.-M and SEP-CB-2013-01-220791 to S.C.-F. G.S.-O. acknowledges support from a CONACYT graduate scholarship. We thank Nicolás Gómez Hernández and Juan Manuel Martínez Andrade for technical support.

Appendix A. Supplementary material

Supplementary data to this article can be found online at https://doi.org/10.1016/j.fgb.2018.11.006.

References

Oliver, S.G., Trinci, A.P.J., 1985. Modes of growth of bacteria and fungi. Comprehensive Biotechnology: The Principles, Applications, and Regulations of Biotechnology in Industry, Agriculture, and Medicine/Editor-in-Chief, Murray Moo-Young. Pergamon, Oxford.
Samapundo, S., et al., 2007. Growth kinetics of cultures from single spores of Aspergillus flavus and Fusarium verticillioides on yellow dent corn meal. Food Microbiol. 24, 336–345.
Paul, G.C., Thomas, C.R., 1998. Characterisation of mycelial morphology using image analysis. Adv. Biochem. Eng. Biotechnol. 60, 1–59.
Packer, H.L., Thomas, C.R., 1990. Morphological measurements on filamentous micro-organisms by fully automatic image analysis. Biotechnol. Bioeng. 35, 870–881.
Spohr, A., et al., 1998. On-line study of fungal morphology during submerged growth in a small flow-through cell. Biotechnol. Bioeng. 58, 541–553.
Christiansen, T., et al., 1999. On-line study of growth kinetics of single hyphae of Aspergillus oryzae in a flow-through cell. Biotechnol. Bioeng. 63, 147–153.
Diano, A., et al., 2009. Physiology of Aspergillus niger in oxygen-limited continuous cultures: influence of aeration, carbon source concentration and dilution rate. Biotechnol. Bioeng. 103, 956–965.
Lim, J.S., et al., 2006. Effects of morphology and rheology on neofructosyltransferase production by Penicillium citrinum. Biotechnol. Bioprocess Eng. 11, 100.
Ahamed, A., Vermette, P., 2009. Effect of culture medium composition on Trichoderma reesei's morphology and cellulase production. Bioresour. Technol. 100, 5979–5987.
El-Sabbagh, N., et al., 2008. Effects of dissolved carbon dioxide on growth, nutrient consumption, cephalosporin C synthesis and morphology of Acremonium chrysogenum in batch cultures. Enzyme Microb. Technol. 42, 315–324.
Lübbehüsen, T.L., et al., 2003. Characterization of the Mucor circinelloides life cycle by

on-line image analysis. J. Appl. Microbiol. 95, 1152–1160.
Kossen, N.W., 2000. The morphology of filamentous fungi. Adv. Biochem. Eng. Biotechnol. 70, 1–33.
Barry, D., 2010. Development of novel image analysis methods for the morphological quantification of filamentous fungi. Ph.D. Thesis. Dublin Institute of Technology. doi: 10.21427/D7730D.
Lecault, V., et al., 2007. Morphological characterization and viability assessment of Trichoderma reesei by image analysis. Biotechnol. Prog. 23, 734–740.
Brunk, M., et al., 2018. HyphaTracker: an ImageJ toolbox for time-resolved analysis of spore germination in filamentous fungi. Sci Rep. 8, 605.
Riquelme, M., Bartnicki-Garcia, S., 2004. Key differences between lateral and apical branching in hyphae of Neurospora crassa. Fungal Genet. Biol. 41, 842–851.
López-Franco, R., et al., 1994. Pulsed growth of fungal hyphal tips. Proc. Natl. Acad. Sci. USA 91, 12228–12232.
Trinci, A.P.J., 1974. A study of the kinetics of hyphal extension and branch initiation of fungal mycelia. J. Gen. Microbiol. 81, 225–236.
Howard, J., 2001. Mechanics of Motor Proteins and the Cytoskeleton. Sinauer, Sunderland, MA.
Riquelme, M., et al., 1998. What determines growth direction in fungal hyphae? Fungal Genet. Biol. 24, 101–109.
Boswell, G.P., Hopkins, S., 2009. Linking hyphal growth to colony dynamics: spatially explicit models of mycelia. Fungal Ecol. 1, 143–154.
Held, M., Edwards, C., Nicolau, D.V., 2011. Probing the growth dynamics of Neurospora crassa with microfluidic structures. Fungal Biol. 115, 493–505.

Supporting Information for

Automated, continuous video microscopy tracking of hyphal growth

Gamaliel Sánchez-Orellana, Sergio Casas-Flores and Braulio Gutiérrez-Medina*

*corresponding author: bgutierrez@ipicyt.edu.mx

List of Contents:

SI Text

Persistence length. Here we expand on the notion and application of persistence length measurements to hyphal growth. For microscopic filament polymers, thermal fluctuations cause fluctuations in shape. In this context, the persistence length is a measure that indicates "the length of filament over which thermal bending becomes appreciable" [1]. To compute this metric, the correlation between tangent angles is used. It can be shown that:

$$\langle \cos[\theta(s) - \theta(0)] \rangle = e^{-\left(\frac{s}{2L_p}\right)}, \qquad (1)$$

where $\theta(s)$ is the tangent angle at arc length s and L_p is the persistence length [1]. Therefore, the persistence length is the characteristic distance over which tangent angle correlations are preserved.

We propose to borrow the notion of tangent angle correlation to characterize the path followed by fungal hyphae during development, with the expectation that this correlation will show patterns informative of hyphal architecture (see below). Taking the hyphae itself (or equivalently the path followed by the hyphal tip) as the filament under study, we compute the angular correlations: $\langle \cos[\theta(s_2) - \theta(s_1)] \rangle$. To perform this operation in practice, we execute the following steps (see more details in the Materials and Methods section of the main text). (i) Given the set of (*x*,*y*) coordinates corresponding to tracking of a hypha, we compute $\cos[\theta(s_2) - \theta(s_1)]$ for all possible arc lengths s_1 and s_2. (ii) All $\cos[\theta(s_2) - \theta(s_1)]$ values having the same interval $s_2 - s_1$ are averaged. (iii) $\cos[\theta(s_2) - \theta(s_1)]$ values are organized in a histogram, yielding the "individual angular correlation" ($\langle \cos[\theta(s_2) - \theta(s_1)] \rangle$) vs. arc length for that particular (*x*,*y*) record. Finally, we obtain the "angular correlation" as the average of individual correlations $\langle \cos[\theta(s_2) - \theta(s_1)] \rangle$, for all tracking records. In the main text, this "angular correlation" is reported (see Fig. 9).

Figure S1 shows individual angular correlations after application of steps (i)-(iii) of the aforementioned procedure to simple *n*-segment filaments. These examples make evident that high angular correlation corresponds to trajectories presenting little deviations. Figures S2 and S3 show collections of six-segment uniform and random trajectories, respectively, together with their corresponding angular correlations. The average angular correlations (see black curves in Figs. S2 and S3) make evident that two parameters can be recovered from the analysis. First, the angular correlation decays with a characteristic (arc length) distance. Second, the angular correlation decays to an asymptotic value that is just the cosine of the angular distance between consecutive segments.

In our experiment (see Fig. 9), we fit an exponential decay curve to the average correlation. We define persistence length as one-half the decay parameter in the exponential, in analogy with the mechanical filament under thermal bending (see Eq. 1). We interpret this

persistence length as the characteristic distance of hyphal elongation before changes in direction occur (either by branching or by hyphal elongation). Taking branching as the main contributor to direction changes during hyphal growth, the decay curve follows an asymptote whose value informs us on the average angle between parental and branching hyphae.

SI Figures

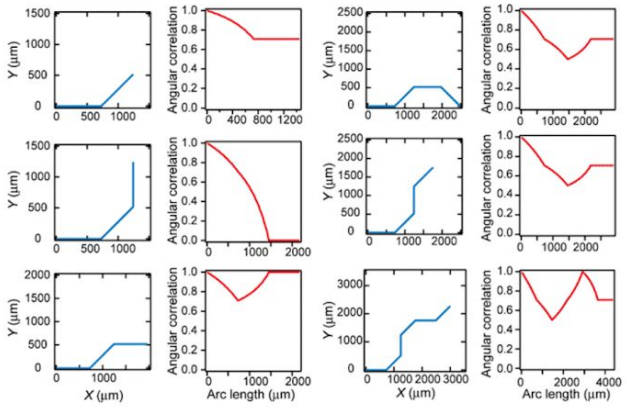

Figure S1. Individual angular correlations for simple mock hyphal trajectories. Hyphal trajectories (blue) were constructed with by joining straight segments of equal length (728 μm) and enforcing angular displacements of ±45 deg between consecutive segments, mimicking hyphal trajectories subject to branching events. Angular correlations (red) quantify changes in direction.

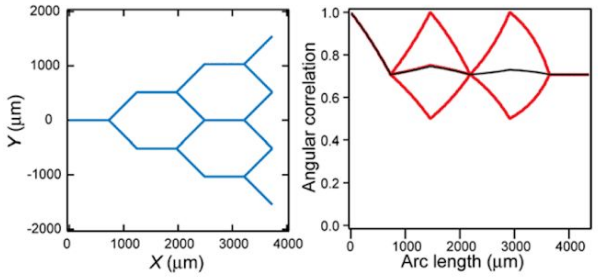

Figure S2. Angular correlation for uniform segment trajectories. Each hyphal trajectory (blue) consists of six straight segments of equal length (728 μm) and angular displacements ±45 deg between adjacent segments. Only forward trajectories (that is, with continuous positive increase in *X*) were considered. All possible trajectories satisfying the above conditions are shown superposed. The corresponding individual angular correlations (red) are also shown superposed. The average angular correlation (black) shows decay after a distance ~730 μm to the constant value 0.707 (= cos[45 deg]), therefore recovering the main morphological aspects of the analyzed trajectories.

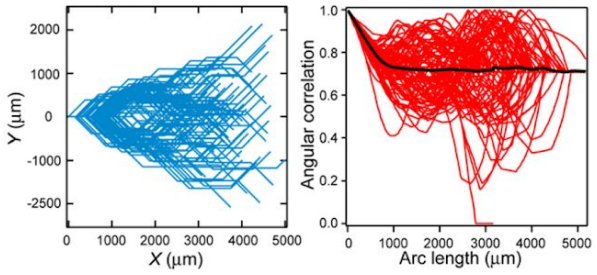

Figure S3. Angular correlation for random segment trajectories. Each hyphal trajectory (blue) consists of six straight segments with ±45 deg angular displacements between adjacent segments. The length of each segment is randomly selected from a Gaussian distribution with mean 728 µm and SD 273 µm. Only forward trajectories were considered. The corresponding individual angular correlations (red) are shown superposed. The average angular correlation (black) shows decay to the constant value 0.7. Number of trajectories, 96.

SI video

Supplementary Video 1. Tracking of hyphal growth in *T. atroviride* at 10x magnification. The video microscopy system automatically tracks the tip of a hypha (white circle) and keeps it within visual field. Frames in this video correspond to raw bright field microscopy images. Total time, 439 min. Field of view, 954 μm × 715 μm. Timestamp (hour, minute, second).

Supplementary Video 2. Tracking of hyphal growth in *T. atroviride* at 40x magnification. The video microscopy system automatically tracks the tip of a hypha (white circle). Automatic correction due to off-limits events is frequent (30 times during the video period). Frames in this video correspond to raw bright field microscopy images. Total time, 304 min. Field of view, 237 μm × 178 μm. Timestamp (hour, minute, second).

SI References

1. Howard, J. 2001. Mechanics of Motor Proteins and the Cytoskeleton (Sinauer, Sunderland, MA).